KINEMATICS OF PARALLEL MANIPULATORS WITH GROUND-MOUNTED ACTUATORS

By

TZU-CHEN WENG

A DISSERTATION PRESENTED TO THE GRADUATE SCHOOL
OF THE UNIVERSITY OF FLORIDA IN
PARTIAL FULFILLMENT OF THE REQUIREMENTS
FOR THE DEGREE OF DOCTOR OF PHILOSOPHY

UNIVERSITY OF FLORIDA

1988

ACKNOWLEDGMENTS

The author wishes to express his sincere appreciation to his committee chairman, Professor George N. Sandor, for years of invaluable guidance, support and encouragement during his graduate studies. The author also gratefully acknowledges the advice and support given by the members of his supervisory committee, Dr. Joseph Duffy, Dr. Ali Seireg, Dr. Gary K. Matthew and Dr. Ralph G. Selfridge.

The author extends his gratitude to Dr. Dilip Kohli of the University of Wisconsin--Milwaukee, for all his help in the development of this work and Dr. Kenneth H. Hunt for his advice during his visit at the University of Florida. Special thanks are also extended to his colleagues and fellow students, especially Mr. Yongxian Xu of the Dalian Railway Institute, for their valuable suggestions.

The financial support of the National Science Foundation under grant DMC-8508029 is gratefully acknowledged.

Most of all, the author wishes to express his sincere appreciation to his parents for their support and encouragement which helped him throughout his graduate studies. Finally, the author extends his deepest appreciation to his wife, Han-Min, for her inspiration and moral support, and for years of patience and encouragement.

TABLE OF CONTENTS

Abstract of Dissertation Presented to the Graduate School of the University of Florida in Partial Fulfillment of the Requirements for the Degree of Doctor of Philosophy

KINEMATICS OF PARALLEL MANIPULATORS WITH GROUND-MOUNTED ACTUATORS

By

TZU-CHEN WENG

December 1988

Chairman: Dr. George N. Sandor
Major Department: Mechanical Engineering

A great deal of research work has been focussed on the theoretical and experimental studies of mechanical manipulators in recent years. Almost all of these works are related to open-loop serial-link mechanisms, but only a few have dealt with multi-degree-of-freedom parallel manipulators such as the Stewart platform or similar mechanisms.

A new type of two-degree-of-freedom Rotary-Linear (R-L) actuator was adapted in this work. Several possible configurations of parallel six-degree-of-freedom manipulators with ground-mounted actuators have been synthesized. With parallel configuration of the manipulators, the computations can be performed simultaneously. Therefore, the computation time will be significantly reduced.

Workspace analysis of a six-degree-of-freedom parallel manipulator has been presented by determining the shapes and boundaries of the subworkspace and root regions in the subworkspace. The workspace of the manipulator is obtained as the common reachable region of the subworkspaces determined by the corresponding subchains. The orientation and the rotatability of the platform are also investigated.

Finally, mechanical error analysis of the manipulator, due to the minor inaccuracies in displacements of the actuators, is studied by using the theory of screws.

CHAPTER 1
INTRODUCTION

1.1 Literature Overview

Robotics has been a very popular subject to study in the last few years. Researchers have developed many advanced concepts and theories in kinematics, dynamics, controls, actuators and sensors for the design of robots. Recent areas of study also involve workspace, obstacle avoidance, full rotational dexterity of the end-effector and the control of flexible manipulator systems recently. With the development of microprocessors, which has played an important role in the rapid growth of industrial robots, multi-degree-of-freedom mechanical systems are now becoming a practical choice for use in automatic machinery. It has been well recognized that, by using multi-degree-of-freedom robotic manipulators with multiple actuators and automatic control systems, we can achieve the goal of improving efficiency, accuracy, reliability and reducing energy consumptions and cost of production in flexible manufacturing systems.

Robotic manipulators currently in use in industry and studied for research purposes are almost all traditional open-loop serial-link manipulators in which the number of degrees of freedom of the end-effector is equal to the sum

of the relative degrees-of-freedom of the joints in the chain. There are only a small number of multi-degree-of-freedom designs which involve multi-loop manipulator linkages, with totally parallel or partially parallel configurations. Since the design techniques for multi-loop robotic manipulators are still in the infancy of their development, investigating and developing the theoretical background for multi-degree-of-freedom multi-loop robotic manipulators may have a significant impact in the near future in manufacturing industry.

For a given set of manipulator linkage dimensions, it is necessary to determine all admissible positions of the end effector. The collection of all such possible positions is called the workspace of the manipulator. Recently several methods have been proposed to determine the workspace of a manipulator by showing possible extreme positions of the end effector. These methods let us calculate directly the boundaries of the workspace of a given point or line on the hand.

Workspace analysis, generally, refers to determining the boundaries of the workspace. Workspace synthesis, on the other hand, consists of determining dimensions of the manipulator linkage and ranges of joint motions for a specified workspace.

One of the primary functions of the manipulator is to have its end-effector reach a set of points in space with prescribed positions and orientations. The manipulators

investigated early were almost all serial kinematic chains, since these manipulators usually have larger workspaces and more dexterous maneuverability than those of parallel kinematic chains. However, serial chains have poor stiffness and undesirable dynamic characteristics in high-speed operation. Also, it is usually difficult to solve their inverse kinematics problem. Therefore, mechanisms based on parallel kinematic chains may have certain advantages when dynamic loading is present and only limited workspace is required.

Serial multi-degree-of-freedom manipulators have been extensively investigated. Roth [1] studied the relationship between the kinematic parameters of a manipulator and its workspace. Shimano and Roth [2] presented the analytical and geometrical conditions for a line on the hand to be at the farthest distance from the base revolute pair. Sugimoto and Duffy [3, 4] developed an algorithm to determine the extreme distances of a robot hand. Kumar and Waldron [5] developed the theory and algorithm for tracing the bounding surfaces of a manipulator workspace. Sugimoto and Duffy [6] and Sugimoto, Duffy and Hunt [7] investigated the singularities in the workspace. Kumar and Waldron [8] presented the algorithm for tracing the bounding surfaces of manipulator workspaces. Tsai and Soni [9] presented the study of determining the accessible region for two and three-link robotic arms with pin-joints. Gupta and Roth [10] presented some basic concepts regarding the workspace

shapes and structures of manipulators. Selfridge [11] presented an algorithm for finding the boundary of reachable volume of an arbitrary revolute-joint, serial-link manipulator. Tsai and Soni [12] developed an algorithm for the workspace of a general n R robot based on a linear optimization technique and on small incremental displacements applied to coordinate transformation equations relating the kinematic parameters on the n R robot. Yang and Lee [13] derived the equations representing the boundaries of the workspace. Existence of holes and voids in the workspace were also investigated. Lee and Yang [14] have made a study of outlining the boundary of the workspace, the quantitative evaluation of the volume, and introduced a manipulator performance index. Hansen, Gupta and Kazerounian [15] used a stable iterative algorithm for inverse kinematic analysis to determine the approach angles and lengths for reaching points in the workspace. Freudenstein and Primrose [16] described the workspace of a three-axis, turning-pair-connected robot arm of general proportions in terms of the volume swept out by the surface of a skew torus rotating about an offset axis in space. Kohli and Spanos [17] studied the workspace analysis of mechanical manipulators by using polynomial displacement equations and their discriminants. Spanos and Kohli [18] performed the study of workspace analysis of a class of manipulators having the last three revolute joint axes intersect orthogonally at a point. Cwiakala and Lee [19]

used an optimization technique to outline the boundary profile of a manipulator workspace and perform quantitative evaluation of the workspace volume. Tsai and Soni [20] illustrated the general procedures to synthesize the workspace of 3R, 4R, 5R and 6R robots. Tsai and Soni [21] also considered the effects of kinematic parameters on the workspace of general 3R robots. Oblak and Kohli [22] used an analytical method, based on displacement equations, to identify the Jacobian surface or a D-shaped surface which the workspace of a regional structure is bounded by. Davidson and Hunt [23] had a study of the rigid body location and robot workspaces by using an enumeration procedure. Davidson and Hunt [24] described plane workspaces for robots by using a sweeping process and the necessary equations for computer generation of plane-workspace envelops and boundaries. Davidson and Pingail [25] continued to generate envelope-surfaces for plane-workspace of generally proportioned manipulators. Chen [26, 27] presented an analytical method for workspace analysis of robot arms by using differential geometry. Kohli and Hsu [28] studied the Jacobian analysis of workspaces of mechanical manipulators by determining the maximum reach of the manipulator within the intersection of the boundary with a specified plane. Hsu and Kohli [29] dealt with closed-form workspace analysis and used the Jacobian surfaces to separate inaccessible regions, two- and four-way accessible regions in both manipulator coordinates and Cartesian

coordinates. Palmquist [30] studied the reachable workspace common to two planar RRR robots, dexterous relationship between them and the kinematic motion capabilities of them.

There are few works that have dealt with parallel multi-degree-of-freedom manipulators. The Stewart platform [31] is a kind of parallel manipulator which has two plates connected by six adjustable legs and is a six-degree-of-freedom mechanism. It was originally used for flight simulators and was suggested for applications on machine tools and on space vehicle simulators. Asada and Ro [32] applied a direct-drive arm to a closed-loop five-link mechanism to overcome the problems encountered in open-loop arrangements. Trevelyan, Kovesi and Ong [33] applied such a mechanism to a sheep shearing robot. Bajpai and Roth [34] studied the workspace and mobility of such a closed-loop planar five-link mechanism. Yang and Lee [35] presented a feasibility study of the Stewart platform as a robot manipulator. The extreme ranges of motion, rotatability and workspace were investigated and the workspace and the maneuverability were found to be relatively restricted. Fichter [36] also studied Stewart platform-based manipulators, theoretical aspects of the generalized Stewart platform, and practical considerations for building a working machine. Again, Cwiakala [37] used the optimum path search technique to find the section of the workspace of the Stewart platform mechanism. Recently, Kohli, Lee, Tsai and Sandor [38] investigated manipulator configurations

with ground-mounted rotary-linear actuators; their direct and inverse kinematics were also derived.

The majority of current industrial robots are used for body guidance. One of the criteria in the control steps is to reduce the positioning error to a limited range. The techniques needed to solve such problems have been developed in the study of closed-loop spatial linkages. Hartenberg and Denavit [39] used a deterministic method to analyze the mechanical error. Garrett and Hall [40] used a statistical approach for mechanical error analysis. Dhande and Chakraborty [41] presented a stochastic model of the planar four-bar function generating linkage mechanism for error analysis and synthesis for specified maximum of mechanical error. Chakraborty [42] presented a probabilistic model of linkage mechanisms considering tolerances on the link lengths and clearances in the hinges, which may cause mechanical error. Dhande and Chakraborty [43] studied the effect of random error in the joint of spatial linkages and developed a synthesis procedure to allocate tolerances and clearances on different members of linkages to restrict the output error within specified limits.

1.2 Serial and Parallel Manipulators

Open-loop serial-link manipulators have been the subject of numerous investigations and have found considerable applications in industry. In recent years, there has been considerable increase in research in the

area of robotics and multi-degree-of-freedom programmable automation devices. For being competitive in international markets, the use of flexible manufacturing systems in industries is becoming more and more important.

The heart of the flexible manufacturing system consists of computer controlled multi-degree-of-freedom devices such as robots and N.C. machines. The configurations which have been widely used for these machines are serial-link (open-chain type) arrangements, where one link is connected to adjacent links by single-degree-of-freedom joints, each with its separate actuator. Similarly, although N.C. machines are also serial-link devices, the several degrees of freedom are distributed between the work piece and the tool, which decouples the motions associated with various groups of several degrees of freedom. This simplifies kinematic, dynamic, and control computations. The manipulator mechanism generally consists of six links serially connected via six single-degree-of-freedom separately actuated revolute or prismatic joints. The end effector, which is attached to the most distal link, imparts motion of six degrees of freedom to the work piece. The motion and/or force associated with these six degrees of freedom may be controlled.

Although the mechanism may appear simple, the motion of the end effector is related to joint motions by mathematical transformations which are generally not easy to visualize.

Duffy [44] developed the theory which is applied to the analysis of single-loop mechanisms, which are movable polygons or open chains with one end fixed to the ground, closed by an imaginary link between ground and a free end where there is a mechanical hand or gripping device.

Hunt [45] has discussed all possible single- and multi-degree-of-freedom kinematic pairs and used screw theory, kinematic geometry and the techniques of linear algebra to systematize in-parallel-actuated robot-arms. Mohamed and Duffy [46] also applied screw theory to study the instantaneous kinematics of the end-effector platform of fully parallel robot-type device. Sugimoto [47] derived the kinematic and dynamic model for a parallel manipulator by using motor algebra and Newton-Euler formulation.

A comparison between the serial and parallel devices in terms of some necessary and desirable performance and control characteristics was presented by Cox [48]. There are eight performance characteristics chosen as follows:

i. Range of motion
ii. Rigidity or stiffness and strength
iii. Complexity of end-effector positioning formulation (computability)
iv. Complexity of system dynamics (computability)
v. Precision positioning
vi. Load carrying distribution through system
vii. Fabrication (economics)
viii. Compactness

Hunt [45, 49] also showed some possible alternative designs for manipulators using parallel kinematic chains, and pointed out that there are many intermediate possibilities between purely serial and purely parallel kinematic structures.

It is well recognized that more investigations in the study of parallel manipulators are needed and they may have potential usefulness in the manufacturing industry.

1.3 Summary

Conventional serial-linkage manipulators have each of their up-to 6 actuators mounted on the joint they actuate. This means that the mass of these actuators is added to the link masses, which greatly increases the inertia seen by actuators and links closer to the ground.

On the other hand, multi-loop manipulators with ground-mounted actuators need to consider only the masses of the links themselves. Also, the links can be lighter for the same payload.

In Table 1.1, a comparison between serial and parallel kinematic chains is shown, where X means more favorable performance.

The successful completion of the study of parallel manipulators would open up a new direction in the design of robotic manipulators with advantages over present practice, such as improved payload capacities, increased positioning accuracy, greater economy in energy consumption, better

dynamic performance, increased speed with improved precision, and reduced first cost.

Table 1.1 Performance characteristic between serial and parallel kinematic chains

Performance characteristic	Serial structure	Parallel structure
Compactness	X	
Computation time		X
Dexterous maneuverability	X	
Direct kinematics	X	
Inertia		X
Inverse kinematics		X
Payload capacity		X
Power/weight		X
Precision positioning		X
Stiffness		X
Workspace	X	

CHAPTER 2
TYPE SYNTHESIS AND INVERSE KINEMATICS OF THE MANIPULATORS

2.1 Introduction

Industrial robots are available in a wide variety of shapes, sizes and physical configurations. Generally, the first three degrees of freedom (links) of the majority of today's available robots are primarily used to achieve a desired position for the origin of the wrist. These differ considerably from one another and can be classified as cartesian, cylindrical, spherical and revolute which are shown in Fig. 2.1. The remaining degrees of freedom are subsequently employed to achieve desired tool frame orientations. For this purpose, almost all arrangements use revolute pairs with their axes intersecting at a point. For such geometries, the position of the common point of intersection (wrist center) depends only on the first three joint variables of the structure. Once these are computed, the orientation of the hand can be attained by rotating the last three joints only. However, the number of links can be reduced by using joints with larger degrees of freedom such as cylindric and spherical pairs.

A novel geometry of a ground-mounted two-degree-of-freedom self-actuated joint connecting a manipulator link to

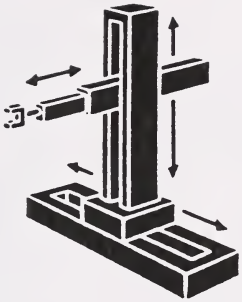

CARTESIAN

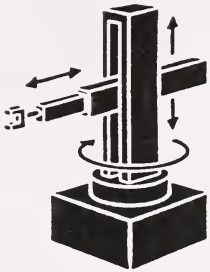

CYLINDRICAL

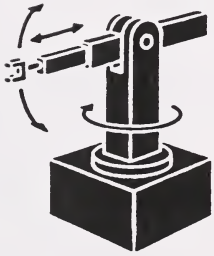

SPHERICAL

REVOLUTE

Figure 2.1 Four basic manipulator configurations

the ground is presented by Kohli, Lee, Tsai and Sandor [38]. It combines a rotary actuator and a linear actuator in such a way that it imparts cylindrical (two-degree-of-freedom, combined rotational and translational) relative motion to the manipulator link with respect to ground. The rotary and the linear actuators are independent of each other and do not "see" each other's inertias. Based on this new arrangement, several possible manipulator linkage configurations with six degrees of freedom are described in this chapter.

2.2 R-L (Rotary-Linear) Actuator

Two different configurations of R-L actuators are shown in Figs. 2.2 and 2.3. In Fig. 2.2, C is a splined shaft, and link E is mounted on the shaft and contains internal splines in its hub. Therefore, link E can be translated on shaft C and be rotated when shaft C rotates. A is a linear actuator and is connected to bracket B which is not splined and can freely slide on shaft C and makes the link E slide on shaft C. The rotary actuator D rotates the shaft C. The rotary and linear actuators thus rotate and translate link E on shaft C without seeing each others' inertia. The motion of link E is the same as that provided by a cylinder pair with an axis which is the same as that of shaft C. In such configuration, link E cannot rotate by 360 degrees due to interference between link E and bracket B. In Fig. 2.3, the linear actuator is connected to link E

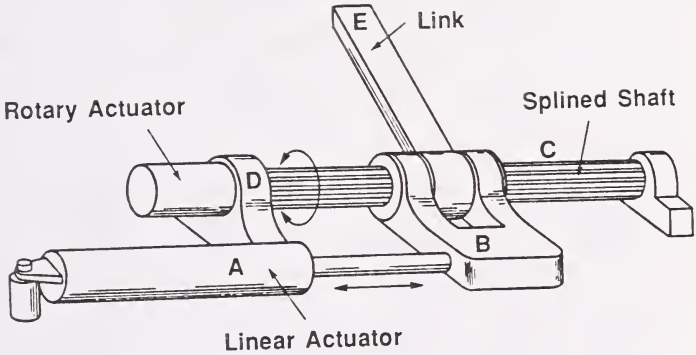

Figure 2.2 (R-L) actuator

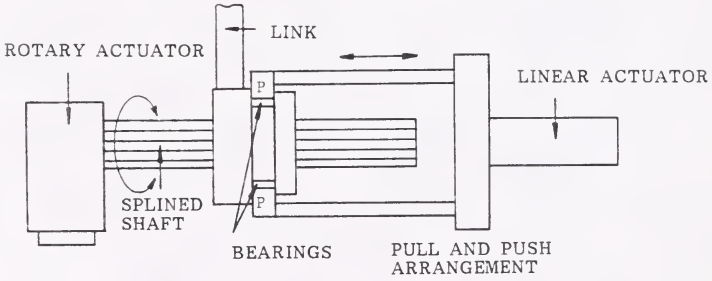

Figure 2.3 (R-L) actuator with 360° rotatability

through grooved hub B by means of pins or split ring P. In this configuration link E can rotate a full 360 degrees.

The R-L actuator controls a rotation around and a translation along the axis of a cylinder pair and is used in type synthesis of parallel manipulators. The principal advantages of using this type of actuator in the structure of parallel manipulators are that, first, R-L actuators can all be mounted on the ground. This reduces the necessary load capacities of the joints which need support only the mechanism links and the payload, whereas serial open-loop robot manipulators must have joints that carry not only the links and the payload, but also the actuators, their controls and power conduits of all subsequent joints. Secondly, with all three R-L actuators mounted on the ground, the computations required for inverse kinematics and thus the Jacobian matrix are significantly simplified.

In a manipulator configuration where all the actuators could be mounted on the ground, the rotary and linear actuators that form the R-L actuator could be off-the-shelf items, since the power to weight ratio is not a major concern in this situation. Thus the cost of the R-L actuators can be considerably less than the actuators currently being designed especially for and used in serial link manipulators.

2.3 Type Synthesis

The earliest study of parallel manipulators is that of Stewart's platform, as shown in Fig. 2.4, which has six degrees of freedom. The actuators are mounted on the floating links. Hunt [45] shows a three-degree-of-freedom and a six-degree-of-freedom parallel manipulator, as shown in Figs. 2.5 and 2.6 respectively, whose actuators are mounted on the floating links and on the ground, respectively. However, Hunt's six-degree-of-freedom manipulator, as shown in Fig. 2.6, has additional six redundant degrees of freedom: the axial rotation of the six S-S links which causes uncontrolled wear in the S joints. By using ground-mounted R-L actuators, we can reduce the number of links of the mechanisms and still have six degrees of freedom of the end effector, without any redundant degrees of freedom in the mechanism.

With the R-L actuator ground-mounted, we can have several possible configurations for each subchain of the parallel manipulators with six degrees of freedom. These configurations are as follows:

Dyads	(R-L)-S-R	(R-L)-R-S	(R-L)-P-S
	(R-L)-S-P	(R-L)-C-C	
Triads	(R-L)-R-R-C	(R-L)-C-R-R	(R-L)-R-C-R
	(R-L)-R-P-C	(R-L)-R-C-P	(R-L)-P-R-C
	(R-L)-P-C-R	(R-L)-C-R-P	(R-L)-C-P-R
	(R-L)-P-P-C	(R-L)-P-C-P	(R-L)-C-P-P

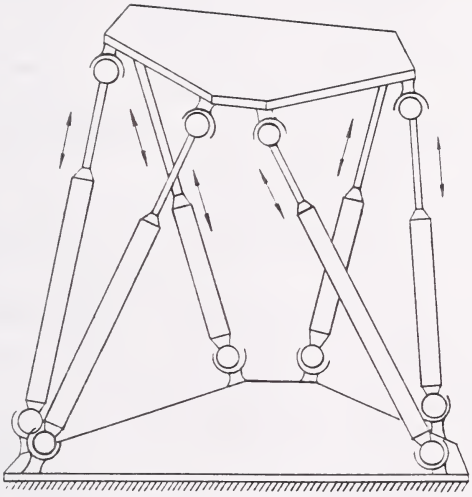

Figure 2.4 Stewart platform mechanism

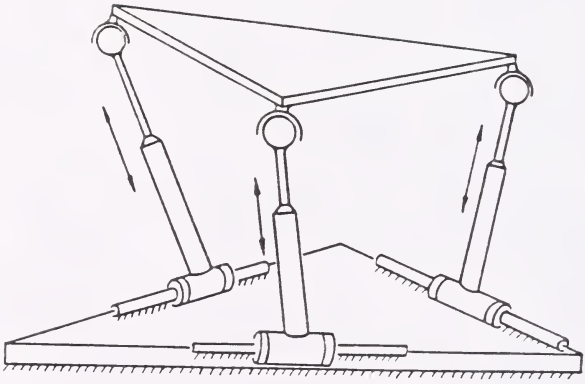

Figure 2.5 Parallel platform-type manipulator with three degrees of freedom

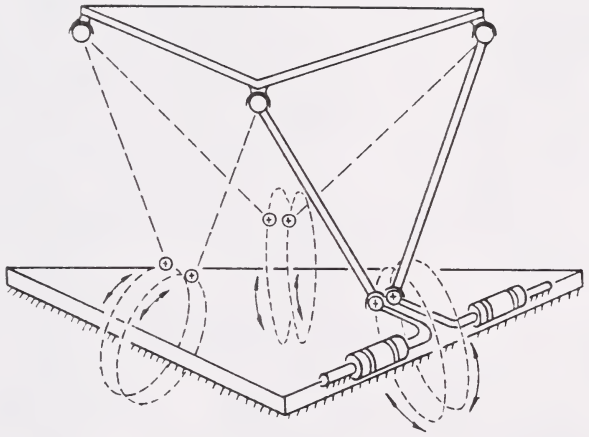

Figure 2.6 Parallel platform-type manipulator with six degrees of freedom

These chains are shown in Figs. 2.7 and 2.8, where the order of (R-L) can be reversed as (L-R).

2.4 Technical Discussion

Actuator. One of the major concerns in the design of serial open-loop manipulators is to maximize the actuator power/weight ratio, since some of the actuators must be mounted on the moving links, as shown in Fig. 2.9, which adds to the inertia of the actuators to the links' inertia and decreases payload capacity. Therefore, the actuator size increases from the distal joint to the proximal joint. The manipulator becomes a massive linkage requiring bigger actuator sizes and resulting in smaller payloads. If one-degree-of-freedom actuators are to be used, this will result in a five-loop linkage for a six-degree-of-freedom robot manipulator. Further, if only one-degree-of-freedom joints are used, the number of links in the linkage becomes quite large. The number of links can, however, be reduced by using joints with more than one degree of freedom, such as cylinder and spherical pairs. The number of loops can also be reduced, thereby reducing the number of links further by devising and using two- or more-degree-of-freedom self-actuated joints. A six-degree-of-freedom parallel manipulator, where all actuators are ground-mounted, is shown in Fig. 2.10.

Computation. The computation of inverse kinematics and dynamics requires considerable time for serial-link

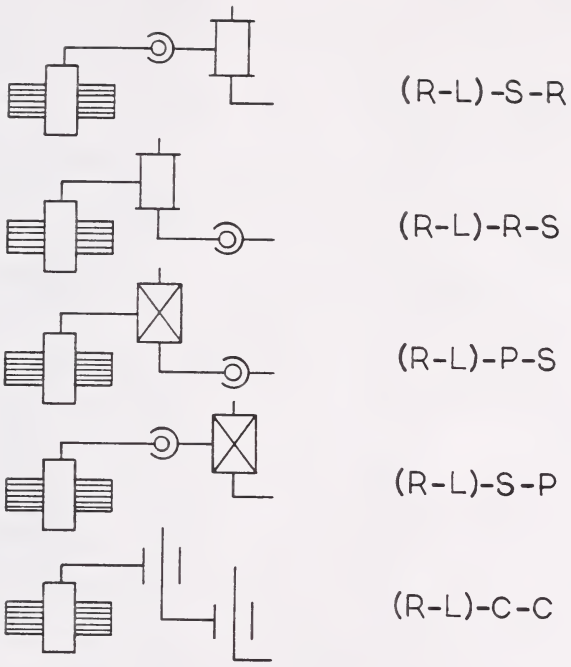

Figure 2.7 Possible configurations of dyads with six degrees of freedom

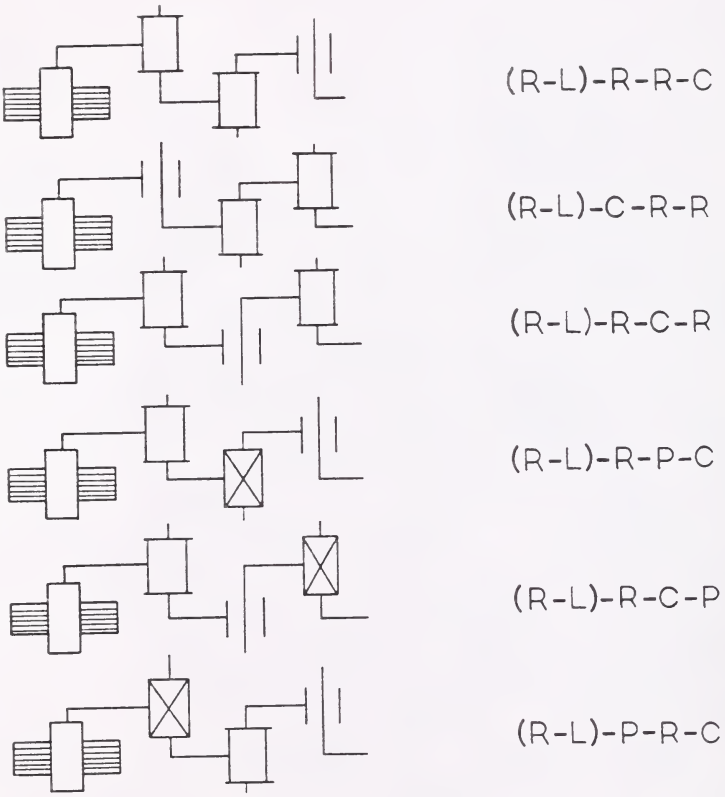

Figure 2.8 Possible configurations of triads with six degrees of freedom

(continued)

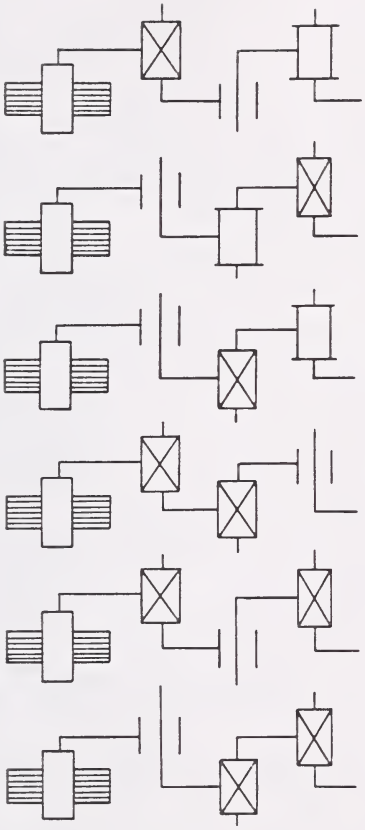

(R-L)-P-C-R

(R-L)-C-R-P

(R-L)-C-P-R

(R-L)-P-P-C

(R-L)-P-C-P

(R-L)-C-P-P

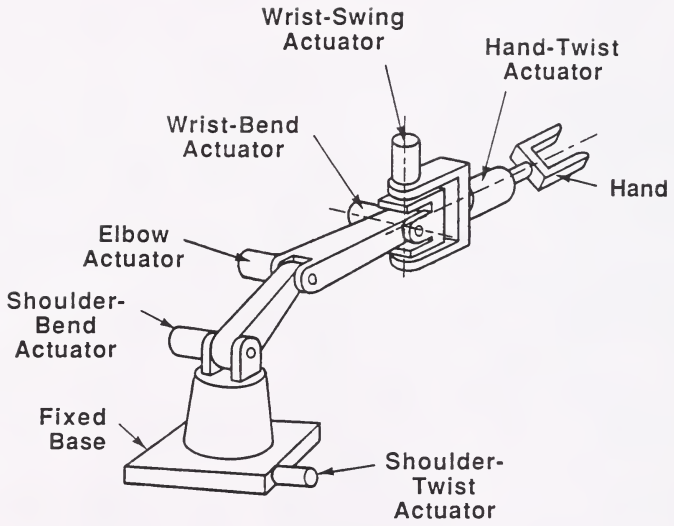

Figure 2.9 Actuators in a serial manipulator

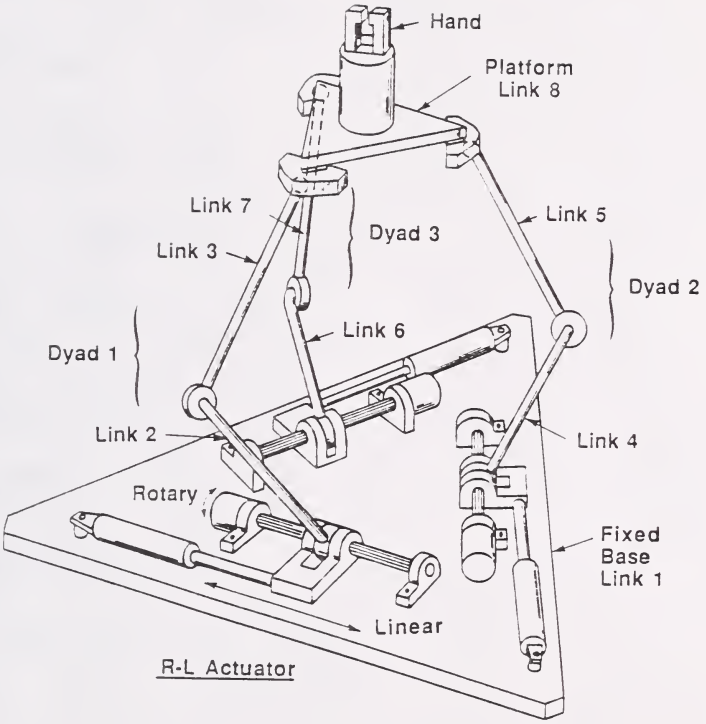

Figure 2.10 Actuators in a parallel manipulator

manipulators. Generally, computations of one link depend upon other links. These computations must be done serially, thus making parallel processing difficult and ineffective in reducing computation time. With parallel-type configuration in the manipulators, the computation can be performed in parallel. Therefore, the computation time will be significantly reduced. In general, the computations required for inverse kinematics and Jacobian matrices will be less complicated than those of serial open-loop manipulators, but the computations for direct kinematics are much involved.

Based on this new possibility, we describe possible manipulator configuration linkages with six degrees of freedom. Then we identify possible configurations in which all actuators for actuating the manipulator linkage are ground-mounted. The distinct advantage of being able to put many actuators on the ground makes these manipulator topologies appealing.

Degrees of freedom. In general, the mobility of a kinematic chain can be obtained from the Kutzbach criterion. The six-dimensional form of the criterion is given as

$$m = 6(n - 1) - 5j_1 - 4j_2 - 3j_3 - 2j_4 - j_5 \qquad (2.1)$$

where m = mobility of mechanism,

n = number of links,

j_i = number of joints having i degrees of freedom.

Freudenstein and Maki [50] also show that a general form of the degree-of-freedom equation for both planar and spatial mechanisms can be written as

$$F = d(n - j - 1) + \sum_{i}^{j} f_i - I_d \qquad (2.2)$$

where F = the effective degree of freedom of the assembly or mechanism,

d = the degree of freedom of the space in which the mechanism operates (for spatial motion $d = 6$, and for planar motion and motion on a surface $d = 3$),

n = number of links,

j = number of joints,

f_i = degree of freedom of i-th joint,

I_d = idle or passive degrees of freedom.

The number of degrees of freedom that a manipulator possesses is the number of independent position variables which would have to be specified in order to locate all parts of the mechanism. In the case of serial manipulators, each joint displacement is usually defined with a single variable; the number of joints equals the number of degrees of freedom.

The number of degrees of freedom of multi-loop manipulator linkages containing multi-degree-of-freedom self-actuated joints can be determined simply by the following equation:

$$F_c = \sum_{i=1}^{n} F_i - 6(n - 1) \tag{2.3}$$

where F_c = the number of degrees of freedom of the multi-loop mechanism,

F_i = the number of degrees of freedom of the i-th subchain (leg),

n = the number of subchains (legs)

As shown in Fig. 2.10, there are three identical subchains and each subchain has six degrees of freedom. Therefore, the number of degrees of freedom of this type of parallel manipulator can be calculated from Eq. (2.3) as

$$F_c = (6 + 6 + 6) - 6(3 - 1) = 6$$

2.5 Inverse Kinematics

When the position of one link, generally the hand, is specified and it is required to determine the position of all other links, including the joint variables of actuated joints which will move the hand to the specified position, the method is called inverse kinematics. The determination of the actuated joint variables for a specified position of the hand is conducted by obtaining a set of equations relating the actuated joint variables and constant parameters of the manipulator linkages to the hand position variables. In general, this set of equations is also

reduced to one equation of polynomial form in only one joint variable. For a specified hand position, one proceeds to find the roots of this displacement polynomial to determine the joint variable. The degree of this polynomial also determines the number of possible ways the desired hand position can be reached.

Generally, the methods employed in solving the inverse kinematics in robotics are either analytical or numerical. An analytical solution is one that produces a particular mathematical equation or formula for each joint variable (rotation or translation) in terms of known configuration values (length of the link, twist angle and offset), whereas a numerical solution generally pertains to the determination of appropriate joint displacements as the result of an iterative computational procedure. It is noted that the equations associated with the inverse kinematic problem are nonlinear and coupled, and this nonlinear dependence is basically trigonometric.

As shown in Figs. 2.7 and 2.8, there are five possible dyads with six degrees of freedom and twelve possible triads with six degrees of freedom. In order to reduce the number of links in forming the mechanism and avoid the number of translational joints greater than three in a loop, we only consider subchains (R-L)-R-S, (R-L)-P-S, (R-L)-S-R and (R-L)-S-P as shown in Fig. 2.7 in the following sections.

2.5.1 Subchain (R-L)-R-S

A schematic diagram of subchain (R-L)-R-S is shown in Fig. 2.11. Since the position and orientation of the hand, which is embedded in the platform, is known, we can find the position and orientation of the coordinate system $Cx_3y_3z_3$ embedded in the sphere at point C with respect to the local fixed coordinate system $ox_0y_0z_0$ through systems $Hx_4y_4z_4$ and OXYZ by coordinate transformations. Also, we can write the following equation to describe the position of point C with respect to the local fixed coordinate system $ox_0y_0z_0$ through systems $Bx_2y_2z_2$ and $Ax_1y_1z_1$ as follows:

$$\underset{\sim}{C}^{O} = A_1A_2\underset{\sim}{C}^{3} \tag{2.4}$$

or

$$\begin{bmatrix} C_x \\ C_y \\ C_z \\ 1 \end{bmatrix} = \begin{bmatrix} C\Theta_a & -S\Theta_a & 0 & 0 \\ S\Theta_a & C\Theta_a & 0 & 0 \\ 0 & 0 & 1 & d_a \\ 0 & 0 & 0 & 1 \end{bmatrix} \begin{bmatrix} 1 & 0 & 0 & a \\ 0 & C\alpha_b & -S\alpha_b & 0 \\ 0 & S\alpha_b & C\alpha_b & 0 \\ 0 & 0 & 0 & 1 \end{bmatrix}$$

$$\begin{bmatrix} C\Theta_b & -S\Theta_b & 0 & bC\Theta_b \\ S\Theta_b & C\Theta_b & 0 & bS\Theta_b \\ 0 & 0 & 1 & s_b \\ 0 & 0 & 0 & 1 \end{bmatrix} \begin{bmatrix} 0 \\ 0 \\ 0 \\ 1 \end{bmatrix} \qquad \text{(continued)}$$

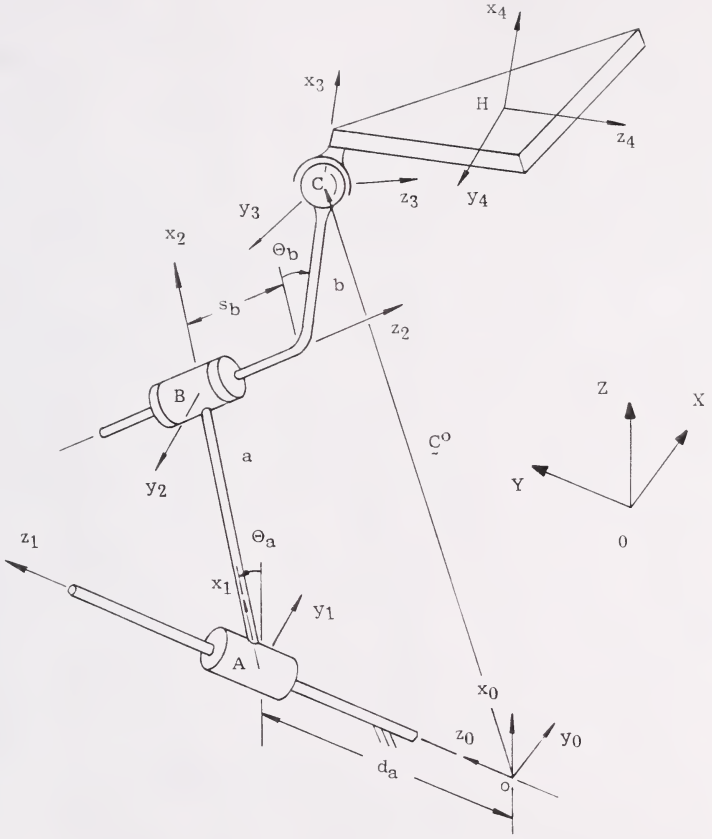

Figure 2.11 Subchain (R-L)-R-S

$$= \begin{bmatrix} C\Theta_a(bC\Theta_b + a) - S\Theta_a(bS\Theta_bC\alpha_b - s_bS\alpha_b) \\ S\Theta_a(bC\Theta_b + a) + C\Theta_a(bS\Theta_bC\alpha_b - s_bS\alpha_b) \\ bS\Theta_bS\alpha_b + s_bC\alpha_b + d_a \\ 1 \end{bmatrix} \qquad (2.5)^*$$

where the vector $\underset{\sim}{C}^o$ or its components C_k^o (k= x, y and z) denote the coordinates of point C with respect to the local fixed coordinate system $ox_0y_0z_0$; the vector $\underset{\sim}{C}^3$ denotes the location of point C with respect to the coordinate system $Cx_3y_3z_3$; Θ_a and Θ_b are the rotation angles from x_o to x_1 and from x_2 to x_3, respectively; d_a is the translation of cylindric joint A along the fixed axis z_1 form the origin of the local fixed coordinate system $ox_0y_0z_0$; a and b are the perpendicular distance between successive joint axes z_1, z_2 and z_3, respectively; s_b is the offset along the z_2 axis; α_b is the twist angle between the axes z_1 and z_2, and A_i, i = 1 and 2, represent the Hartenberg and Denavit [39] 4 x 4 homogeneous transformation matrices which relate the kinematic properties of link i to link i-1 and can be derived as

$$A_i = \begin{bmatrix} C\Theta_i & -S\Theta_iC\alpha_i & S\Theta_iS\alpha_i & a_iC\Theta_i \\ S\Theta_i & C\Theta_iC\alpha_i & -C\Theta_iS\alpha_i & a_iS\Theta_i \\ 0 & S\alpha_i & C\alpha_i & d_i \\ 0 & 0 & 0 & 1 \end{bmatrix} \qquad (2.6)$$

---

* $\underset{\sim}{C}^o$ can also be obtained by using the method in [44], which is presented in Appendix A.1.

where $C\Theta$ and $S\Theta$ are shorthand for $\cos(\Theta)$ and $\sin(\Theta)$, respectively. Similarly, Θ_c denotes the relative rotation angle of joint C, d_b and d_c denote the translations of joints B and C along the moving axes z_2 and z_3, respectively, and c denotes the length of link c. It is noted that d_b, d_c and c are zero for this subchain, but all these notations are used throughout the following sections.

Premultiplying both sides of Eq. (2.4) by $A_2^{-1}A_1^{-1}$ yields

$$bC\Theta_b = C_xC\Theta_a + C_yS\Theta_a - a \tag{2.7}$$

$$bS\Theta_b = -C_xS\Theta_aC\alpha_b + C_yC\Theta_aC\alpha_b + C_zS\alpha_b - d_aS\alpha_b \tag{2.8}$$

$$s_b = C_xS\Theta_aS\alpha_b - C_yC\Theta_aS\alpha_b + C_zC\alpha_b - d_aC\alpha_b \tag{2.9}$$

Squaring and adding Eqs. (2.7), (2.8) and (2.9) yields

$$b^2 + s_b^2 = C_x^2 + C_y^2 + C_z^2 + d_a^2 - 2C_zd_a - 2aC_xC\Theta_a - 2aC_yS\Theta_a + a^2 \tag{2.10}$$

From Eq. (2.9), we have

$$d_a = \frac{1}{C\alpha_b}(C_xS\Theta_aS\alpha_b - C_yC\Theta_aS\alpha_b + C_zC\alpha_b - s_b)$$

Substituting d_a into Eq. (2.10) yields

$$E_1X^4 + E_2X^3 + E_3X^2 + E_4X + E_5 = 0 \tag{2.11}$$

where

$$X = \tan(\Theta_a/2)$$

$$D_1 = C_zC\alpha_b - s_b$$

$$D_2 = C_x^2 + C_y^2 + C_z^2 + a^2 - b^2 - s_b^2$$

$$E_1 = D_2C^2\alpha_b + 2aC_xC^2\alpha_b - 2C_yC_zS\alpha_bC\alpha_b - 2D_1C_zC\alpha_b + C_y^2S^2\alpha_b + D_1^2 + 2D_1C_yS\alpha_b$$

$$E_2 = -4(aC_yC^2\alpha_b + C_xC_zS\alpha_bC\alpha_b - D_1C_xS\alpha_b - C_xC_yS^2\alpha_b)$$

$$E_3 = 2(D_2C^2\alpha_b - 2D_1C_zC\alpha_b + 2C_x^2S^2\alpha_b - C_y^2S^2\alpha_b + D_1^2)$$

$$E_4 = -4(aC_yC^2\alpha_b + C_xC_zS\alpha_bC\alpha_b - D_1C_xS\alpha_b + C_xC_yS^2\alpha_b)$$

$$E_5 = D_2C^2\alpha_b - 2aC_xC^2\alpha_b + 2C_yC_zS\alpha_bC\alpha_b - 2D_1C_zC\alpha_b + C_y^2S^2\alpha_b + D_1^2 - 2D_1C_yS\alpha_b$$

Since Eq. (2.11) is a fourth-degree polynomial equation, there are up to four possible solutions for variable X (or Θ_a). Back substituting Θ_a into Eqs. (2.7) and (2.9), we can obtain up to four possible sets of solutions of Θ_b and d_a, respectively. Therefore, the subchain (R-L)-R-S has a fourth-degree polynomial equation in inverse kinematics.

Numerical example. The given parameters are as follows:

$a = 2"$, $b = 12"$, $s_b = 8"$, $\alpha_b = 72°$ and $\underset{\sim}{C}^o = [-4.86, -11.60, 3.97]^T$

The four possible solutions are computed as

Solutions	Θ_a (deg.)	d_a (in.)	Θ_b (deg.)
1	29.932	1.557	180.299
2	-50.609	12.297	-71.132
3	17.534	7.618	212.427
4	-87.785	-5.592	38.407

2.5.2 Subchain (R-L)-P-S

Figure 2.12 shows a subchain (R-L)-P-S. The inverse kinematics is similar to that of the subchain (R-L)-R-S. We can write the equation to express the location vector of point C with respect to the local fixed coordinate system $ox_0y_0z_0$ as follows:

$$\underset{\sim}{C}^{o} = A_1A_2\underset{\sim}{C}^{3} \tag{2.12}$$

or

$$\begin{bmatrix} C_x \\ C_y \\ C_z \\ 1 \end{bmatrix} = \begin{bmatrix} C\Theta_a & -S\Theta_a & 0 & 0 \\ S\Theta_a & C\Theta_a & 0 & 0 \\ 0 & 0 & 1 & d_a \\ 0 & 0 & 0 & 1 \end{bmatrix} \begin{bmatrix} 1 & 0 & 0 & a \\ 0 & C\alpha_b & -S\alpha_b & 0 \\ 0 & S\alpha_b & C\alpha_b & 0 \\ 0 & 0 & 0 & 1 \end{bmatrix}$$

$$\begin{bmatrix} 1 & 0 & 0 & b \\ 0 & 1 & 0 & 0 \\ 0 & 0 & 1 & d_b \\ 0 & 0 & 0 & 1 \end{bmatrix} \begin{bmatrix} 0 \\ 0 \\ 0 \\ 1 \end{bmatrix}$$

$$= \begin{bmatrix} C\Theta_a(a + b) + S\Theta_aS\alpha_bd_b \\ S\Theta_a(a + b) - C\Theta_aS\alpha_bd_b \\ d_a + S\alpha_bd_b \\ 1 \end{bmatrix} \tag{2.13}**$$

Premultiplying both sides of Eq. (2.12) by $A_2^{-1}A_1^{-1}$ yields

$$b = C_xC\Theta_a + C_yS\Theta_a - a \tag{2.14}$$

** $\underset{\sim}{C}^{o}$ can also be obtained by using the method in [44], which is presented in Appendix A.2.

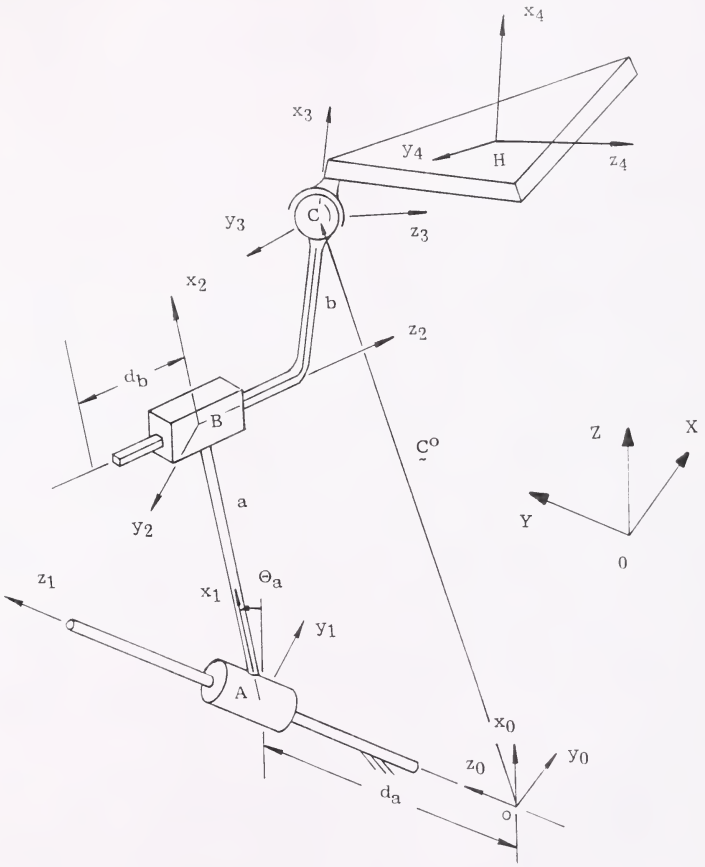

Figure 2.12 Subchain (R-L)-P-S

$$0 = -C_x S\Theta_a C\alpha_b + C_y C\Theta_a C\alpha_b + C_z S\alpha_b - d_a S\alpha_b \quad (2.15)$$

$$d_b = C_x S\Theta_a S\alpha_b - C_y C\Theta_a S\alpha_b + C_z C\alpha_b - d_a C\alpha_b \quad (2.16)$$

Let $\tan(\Theta_a/2) = X$, and then substituting $C\Theta_a = (1 - X^2)/(1 + X^2)$ and $S\Theta_a = 2X/(1 + X^2)$ into Eq. (2.14), we obtain

$$(a + b + C_x)X^2 - 2C_y X + a + b - C_x = 0 \quad (2.17)$$

There are up to two possible solutions of X in Eq. (2.17), or up to two possible solutions for Θ_a. Back substituting these two possible solutions of Θ_a into Eqs. (2.15) and (2.16), we will have up to two possible solutions of d_a and d_b from each equation. Thus it is seen that this subchain has a second-degree polynomial equation in inverse kinematics.

Numerical example. The given parameters are as follows:

$a = 3"$, $b = 2"$, $\alpha_b = 60°$ and $\underset{\sim}{C}^o = [5.85, -0.13, 4.25]^T$

The two possible solutions are computed as

Solutions	Θ_a (deg.)	d_a (in.)	d_b (in.)
1	30.024	2.495	3.510
2	-32.570	6.005	-3.510

2.5.3 Subchain (R-L)-S-R

In Fig. 2.13, a schematic diagram of the subchain (R-L)-S-R is shown. The spherical pair is kinematically

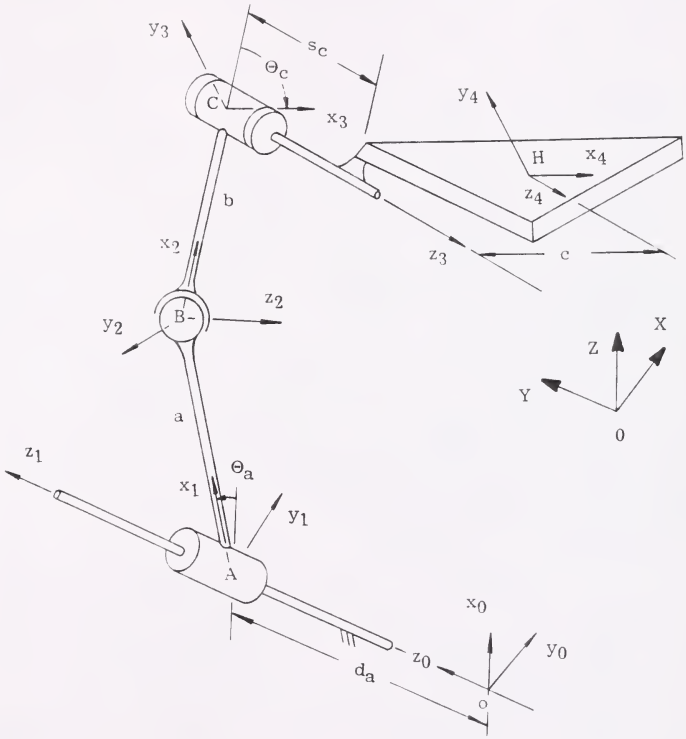

Figure 2.13 Subchain (R-L)-S-R

equivalent to three revolute joints with three mutually perpendicular concurrent axes. Since the orientation and position of the hand, H, is given, we thus can obtain the following equations with the assumption that z_3 is parallel to z_4:

$$
{}^{H}_{0} = \begin{bmatrix} n_x & s_x & a_x & p_x \\ n_y & s_y & a_y & p_y \\ n_z & s_z & a_z & p_z \\ 0 & 0 & 0 & 1 \end{bmatrix}
$$

$$
= \begin{bmatrix} C\theta_a & -S\theta_a & 0 & aC\theta_a \\ S\theta_a & C\theta_a & 0 & aS\theta_a \\ 0 & 0 & 1 & d_a \\ 0 & 0 & 0 & 1 \end{bmatrix} \begin{bmatrix} C\theta_{b1} & 0 & S\theta_{b1} & 0 \\ S\theta_{b1} & 0 & -C\theta_{b1} & 0 \\ 0 & 1 & 0 & 0 \\ 0 & 0 & 0 & 1 \end{bmatrix}
$$

$$
\begin{bmatrix} C\theta_{b2} & 0 & S\theta_{b2} & 0 \\ S\theta_{b2} & 0 & -C\theta_{b2} & 0 \\ 0 & 1 & 0 & 0 \\ 0 & 0 & 0 & 1 \end{bmatrix} \begin{bmatrix} C\theta_{b3} & -S\theta_{b3} & 0 & bC\theta_{b3} \\ S\theta_{b3} & -C\theta_{b3} & 0 & bS\theta_{b3} \\ 0 & 0 & 1 & 0 \\ 0 & 0 & 0 & 1 \end{bmatrix}
$$

$$
\begin{bmatrix} C\theta_c & -S\theta_c & 0 & cC\theta_c \\ S\theta_c & C\theta_c & 0 & cS\theta_c \\ 0 & 0 & 1 & s_c \\ 0 & 0 & 0 & 1 \end{bmatrix} \qquad (2.18)
$$

where components of the position (p_x, p_y and p_z) and orientation (n_x, n_y, n_z, s_x, s_y, s_z, a_x, a_y and a_z) of system $Hx_4y_4z_4$ with respect to the local fixed coordinate system $ox_0y_0z_0$ are all specified; and θ_{b1}, θ_{b2} and θ_{b3} are

the three rotational variables of the spherical joint B, which play no part in the manipulation of the platform.

Equation (2.18) can be rewritten as

$$H_o = A_1 A_2 A_3 \tag{2.19}$$

where

$$A_1 = \begin{bmatrix} C\Theta_a & -S\Theta_a & 0 & aC\Theta_a \\ S\Theta_a & C\Theta_a & 0 & aS\Theta_a \\ 0 & 0 & 1 & d_a \\ 0 & 0 & 0 & 1 \end{bmatrix}$$

$$A_2 = \begin{bmatrix} C\Theta_{b1} & 0 & S\Theta_{b1} & 0 \\ S\Theta_{b1} & 0 & -C\Theta_{b1} & 0 \\ 0 & 1 & 0 & 0 \\ 0 & 0 & 0 & 1 \end{bmatrix} \begin{bmatrix} C\Theta_{b2} & 0 & S\Theta_{b2} & 0 \\ S\Theta_{b2} & 0 & -C\Theta_{b2} & 0 \\ 0 & 1 & 0 & 0 \\ 0 & 0 & 0 & 1 \end{bmatrix}$$

$$A_3 = \begin{bmatrix} C\Theta_{b3} & -S\Theta_{b3} & 0 & bC\Theta_{b3} \\ S\Theta_{b3} & -C\Theta_{b3} & 0 & bS\Theta_{b3} \\ 0 & 0 & 1 & 0 \\ 0 & 0 & 0 & 1 \end{bmatrix} \begin{bmatrix} C\Theta_c & -S\Theta_c & 0 & cC\Theta_c \\ S\Theta_c & C\Theta_c & 0 & cS\Theta_c \\ 0 & 0 & 1 & s_c \\ 0 & 0 & 0 & 1 \end{bmatrix}$$

Postmultiplying both sides of Eq. (2.19) by $A_3^{-1}A_2^{-1}$ yields Eq. (2.20). Premultiplying both sides of Eq. (2.19) by A_1^{-1} and then postmultiplying both sides by A_3^{-1} yields Eq. (2.21).

$$A_1 = H^o A_3^{-1} A_2^{-1} \tag{2.20}$$

$$A_2 = A_1^{-1} H^o A_3^{-1} \tag{2.21}$$

Since $([A_1]_{(1,4)})^2 + ([A_1]_{(2,4)})^2 = ([H^0A_3^{-1}A_2^{-1}]_{(1,4)})^2 + ([H^0A_3^{-1}A_2^{-1}]_{(2,4)})^2$ is true, we can obtain the following equation:

$$a^2 = [-n_x(c + bC\Theta_c) + bS_xS\Theta_c - a_xS_c + p_x]^2 + [-n_y(c + bC\Theta_c) + bS_yS\Theta_c - a_yS_c + p_y]^2 \quad (2.22)$$

Equation for Θ_a is obtained since $[A_1]_{(2,4)} / [A_1]_{(1,4)} = [H^0A_3^{-1}A_2^{-1}]_{(2,4)} / [H^0A_3^{-1}A_2^{-1}]_{(1,4)}$ holds, and can be expressed as

$$\Theta_a = \tan^{-1}\left(\frac{-n_y(c + bC\Theta_c) + s_ybS\Theta_c - a_ys_c + p_y}{-n_x(c + bC\Theta_c) + s_xbS\Theta_c - a_xs_c + p_x}\right) \quad (2.23)$$

It is observed that $[A_1]_{(3,4)} = [H^0A_3^{-1}A_2^{-1}]_{(3,4)}$ directly implies the translation of joint A as

$$d_a = -n_z(c + bC\Theta_c) + s_zbS\Theta_c - a_zs_c + p_z \quad (2.24)$$

Let $\tan(\Theta_c/2) = X$; then substituting $C\Theta_c = (1 - X^2)/(1 + X^2)$ and $S\Theta_c = 2X/(1 + X^2)$ into Eqs. (2.22) yields

$$E_1X^4 + E_2X^3 + E_3X^2 + E_4X + E_5 = 0 \quad (2.25)$$

where

$$D_1 = (n_x^2 + n_y^2)b^2$$

$$D_2 = (s_x^2 + s_y^2)b^2$$

$$D_3 = 2b(n_x^2c + n_y^2c + n_xa_xs_c + n_ya_ys_c - p_xn_x - p_yn_y)$$

$$D_4 = -2b(n_xs_xc + n_ys_yc + s_xa_xs_c + s_ya_ys_c - s_xp_x - s_yp_y)$$

$$D_5 = -2b^2(n_x s_x + n_y s_y)$$

$$D_6 = n_x^2 c^2 + n_y^2 c^2 + a_x^2 s_c^2 + a_y^2 s_c^2 + p_x^2 + p_y^2 + 2n_x a_x s_c c + 2n_y a_y s_c c - 2p_x n_x c - 2p_y n_y c - 2a_x s_c p_x - 2a_y s_c p_y - a^2$$

$$E_1 = D_1 - D_3 + D_6$$

$$E_2 = 2(D_4 - D_5)$$

$$E_3 = -2(D_1 - 2D_2 - D_6)$$

$$E_4 = 2(D_4 + D_5)$$

$$E_5 = D_1 + D_3 + D_6$$

It is seen that there is a maximum of four solutions of X (or Θ_c) in Eq. (2.25). Back substituting the values of Θ_c into Eq. (2.23) and (2.24) yields up to four sets of solutions for Θ_a and d_a.

From Eq. (2.21), we can find certain relationships by equating corresponding elements of the two matrices on either side of the equation. Thus we obtain the following equations:

$$\Theta_{b1} = \tan^{-1}\left(\frac{-a_x S\Theta_a + a_y C\Theta_a}{a_x C\Theta_a + a_y S\Theta_a}\right) \tag{2.26}$$

$$\Theta_{b2} = \tan^{-1}\left(\frac{a_x C\Theta_a + a_y S\Theta_a}{-a_z C\Theta_{b1}}\right) \tag{2.27}$$

$$\Theta_{b3} = \tan^{-1}\left(\frac{n_z S\Theta_c + s_z C\Theta_c}{s_z S\Theta_c + n_z C\Theta_c}\right) \tag{2.28}$$

Since the subchain of (R-L)-S-R has a fourth-degree polynomial equation in inverse kinematics, there are up to four possible solutions in Eq. (2.25). However, the possible solutions may be reduced due to special dimensions of the subchain as shown in the following example.

Numerical example. The given parameters are as follows:

$a = 5"$, $b = 3"$, $\alpha_c = 0°$, $c = 0.75"$, $s_c = 1.50"$ and

$$H^o = \begin{bmatrix} 0.9300 & -0.3323 & -0.1574 & 8.3382 \\ -0.3466 & -0.9352 & -0.0734 & 0.2201 \\ -0.1228 & 0.1228 & -0.9848 & -1.5205 \\ 0 & 0 & 0 & 1 \end{bmatrix}$$

Since two of the solutions of Eq. (2.25) are complex numbers, the remaining two possible real solutions are computed as

Solutions	Θ_c (deg.)	Θ_a (deg.)	d_a (in.)	Θ_{b1} (deg.)	Θ_{b2} (deg.)	Θ_{b3} (deg.)
1	33.435	-1.008	0.559	26.009	-10.002	11.565
2	14.988	10.009	0.500	14.992	-10.002	30.012

2.5.4 Subchain (R-L)-S-P

The procedure of inverse kinematics of the subchain (R-L)-S-P, as shown in Fig. 2.14, is similar to that of the

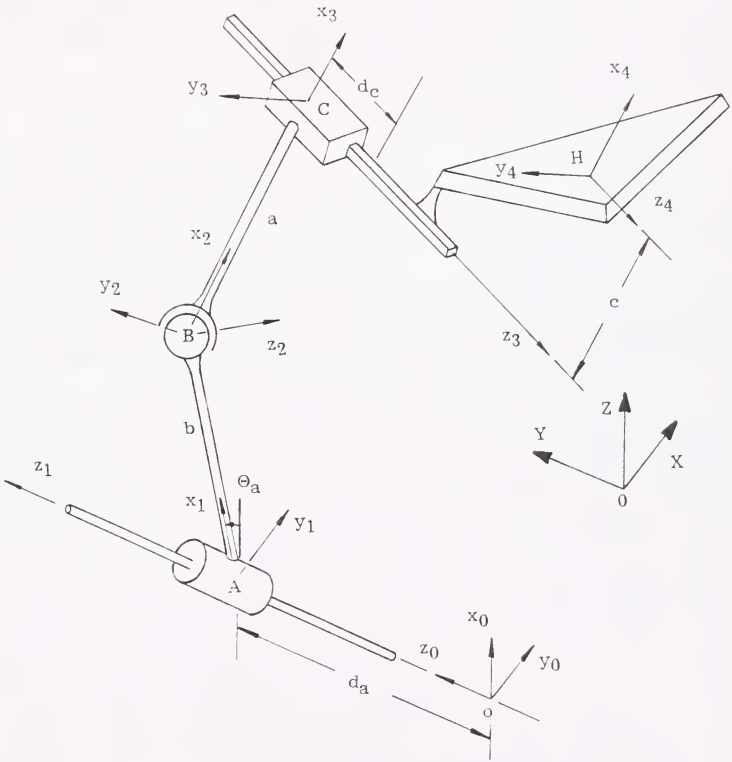

Figure 2.14 Subchain (R-L)-S-P

subchain (R-L)-S-R in 2.5.3. Therefore, we can obtain the following equation:

$$H_o = A_1 A_2 A_3 \tag{2.29}$$

where

$$H^o = \begin{bmatrix} n_x & s_x & a_x & p_x \\ n_y & s_y & a_y & p_y \\ n_z & s_z & a_z & p_z \\ 0 & 0 & 0 & 1 \end{bmatrix}$$

$$A_1 = \begin{bmatrix} C\Theta_a & -S\Theta_a & 0 & aC\Theta_a \\ S\Theta_a & C\Theta_a & 0 & aS\Theta_a \\ 0 & 0 & 1 & d_a \\ 0 & 0 & 0 & 1 \end{bmatrix}$$

$$A_2 = \begin{bmatrix} C\Theta_{b1} & 0 & S\Theta_{b1} & 0 \\ S\Theta_{b1} & 0 & -C\Theta_{b1} & 0 \\ 0 & 1 & 0 & 0 \\ 0 & 0 & 0 & 1 \end{bmatrix} \begin{bmatrix} C\Theta_{b2} & 0 & S\Theta_{b2} & 0 \\ S\Theta_{b2} & 0 & -C\Theta_{b2} & 0 \\ 0 & 1 & 0 & 0 \\ 0 & 0 & 0 & 1 \end{bmatrix}$$

$$A_3 = \begin{bmatrix} C\Theta_{b3} & -S\Theta_{b3} & 0 & bC\Theta_{b3} \\ S\Theta_{b3} & -C\Theta_{b3} & 0 & bS\Theta_{b3} \\ 0 & 0 & 1 & 0 \\ 0 & 0 & 0 & 1 \end{bmatrix} \begin{bmatrix} 1 & 0 & 0 & c \\ o & 1 & 0 & 0 \\ 0 & 0 & 1 & d_c \\ 0 & 0 & 0 & 1 \end{bmatrix}$$

where components of the position (p_x, p_y and p_z) and orientation (n_x, n_y, n_z, s_x, s_y, s_z, a_x, a_y and a_z) of system $Hx_3y_3z_3$ with respect to the local fixed coordinate system $ox_0y_0z_0$ are all specified; and Θ_{b1}, Θ_{b2} and Θ_{b3} are

the three rotational variables of the spherical joint B, which play no part in the manipulation of the platform.

Postmultiplying both sides of Eq. (2.29) by $A_3^{-1}A_2^{-1}$ yields Eq. (2.30). Premultiplying both sides of Eq. (2.29) by A_1^{-1} and then postmultiplying both sides by A_3^{-1} yields Eq. (2.31).

$$A_1 = H^oA_3^{-1}A_2^{-1} \tag{2.30}$$

$$A_2 = A_1^{-1}H^oA_3^{-1} \tag{2.31}$$

Since $([A_1]_{(1,4)})^2 + ([A_1]_{(2,4)})^2 = ([H^oA_3^{-1}A_2^{-1}]_{(1,4)})^2 + ([H^oA_3^{-1}A_2^{-1}]_{(2,4)})^2$ is true, we can obtain the following equation:

$$\begin{aligned}(a_x^2 + a_y^2)d_c^2 + 2[(c+b)n_xa_x + (c+b)n_ya_y - a_xp_x \\ -a_yp_y]d_c + (c+b)^2(n_x^2 + n_y^2) + p_x^2 + p_y^2 - \\ 2(c+b)(n_xp_x + n_yp_y) - a^2 = 0\end{aligned} \tag{2.32}$$

Equation for Θ_a is obtained since $[A_1]_{(2,4)} / [A_1]_{(1,4)} = [H^oA_3^{-1}A_2^{-1}]_{(2,4)} / [H^oA_3^{-1}A_2^{-1}]_{(1,4)}$ holds, and can be expressed as

$$\Theta_a = \tan^{-1}\left[\frac{-(c+b)n_y - a_yd_c + p_y}{-(c+b)n_x - a_xd_c + p_x}\right] \tag{2.33}$$

It is observed that $[A_1]_{(3,4)} = [H^oA_3^{-1}A_2^{-1}]_{(3,4)}$ directly implies the translation of joint A as

$$d_a = -(c+b)n_z - a_zd_c + p_z \tag{2.34}$$

From Eq. (2.31), we can find certain relationships by equating corresponding elements of the two matrices on either side of the equation. Thus we obtain the following equations:

$$\Theta_{b1} = \tan^{-1}\left(\frac{-a_x S\Theta_a + a_y C\Theta_a}{a_x C\Theta_a + a_y S\Theta_a}\right) \tag{2.35}$$

$$\Theta_{b2} = \tan^{-1}\left(\frac{a_x C\Theta_a + a_y S\Theta_a}{-a_z C\Theta_{b1}}\right) \tag{2.36}$$

$$\Theta_{b3} = \tan^{-1}\left(\frac{s_z}{-n_z}\right) \tag{2.37}$$

There are two possible solutions for d_c in Eq. (2.32), since it is a quadratic polynomial equation. Back substituting these solutions of d_c into Eqs. (2.33) - (2.37), respectively, we can obtain two possible sets of solutions for Θ_a, d_a, Θ_{b1}, Θ_{b2} and Θ_{b3} from each equation. Therefore, the subchain (R-L)-S-P has a second-degree polynomial equation in inverse kinematics.

Numerical example. The given parameters are as follows:

$a = 3"$, $b = 2"$, $\alpha_c = 0°$, $c = 0.25"$ and

$$H^o = \begin{bmatrix} 0.7259 & 0.5900 & 0.3536 & 5.1151 \\ 0.4803 & -0.8027 & 0.3536 & 3.4645 \\ 0.4924 & -0.0868 & -0.8660 & 0.4428 \\ 0 & 0 & 0 & 1 \end{bmatrix}$$

The two possible solutions are computed as

Solutions	d_c (in.)	Θ_a (deg.)	d_a (in.)	Θ_{b1} (deg.)	Θ_{b2} (deg.)	Θ_{b3} (deg.)
1	2.499	30.001	1.499	14.999	30.004	9.997
2	14.089	239.999	11.536	-14.999	-30.004	189.997

2.6 Summary

The equations of inverse kinematics have been derived for the dyads (R-L)-R-S, (R-L)-P-S, (R-L)-S-R and (R-L)-S-P as shown in Fig. 2.7, each of which has six degrees of freedom. Numerical examples have been shown to illustrate the possible solutions for each subchain. The degrees of polynomial equations in inverse kinematics for the dyads with six degrees of freedom are summarized in Table 2.1.

Table 2.1 Degree of polynomial equation in inverse kinematics

Type of dyads	Degree of polynomial equation
(R-L)-R-S	4
(R-L)-P-S	2
(R-L)-S-R	4
(R-L)-S-P	2

The detailed analysis and polynomial equation occurring in inverse kinematics can be obtained using several methods. The reader is advised to see the literature on kinematic

analysis of spatial mechanisms, particularly the work by Duffy [44].

Hunt [45] pointed out that a serially-actuated arm accumulates errors from the shoulder out to the end-effector; also, such arms often suffer from lack of rigidity and, in the absence of sophisticated techniques of computer-control compensation, are subject to load-dependent error. They also suffer relatively low-frequency oscillations. With in-parallel-actuation by ground-mounted actuators, there are the advantages of both greater rigidity and lightness of the linkage, but at the expense of more limited workspace and dexterity. Since actuator-error is not cumulative, greater precision is likely to be attainable without excessive control complications. There should surely be a future for in-parallel-actuation by ground-mounted actuators in robotic devices.

CHAPTER 3
WORKSPACE ANALYSIS OF THE MANIPULATORS

3.1 Introduction

This chapter deals with the workspace of a parallel manipulator having three rotary-linear (R-L) actuators on grounded cylindric joints, three revolute and three spherical pairs as shown in Fig. 3.1. The workspace is defined as the reachable region of the origin of the moving coordinate system embedded in the six-degree-of-freedom platform of the manipulator. Since the mechanism consists of three subchains, the workspace is the common reachable region of three subworkspaces determined by the corresponding subchains. The subworkspace described in this chapter is defined as the workspace of the center of the platform determined by a subchain regardless of the constraints imposed by the other subchains. The dimensions of the platform are considered to be infinitesimal and therefore the workspace is determined without considering the orientation of the platform in this chapter[1]. When the R joint rotates about the C joint without translation and the spherical joint rotates about R joint, the locus of the spherical joint at the end of a dyadic subchain is the

[1]Workspaces with finite-size platform are derived in Chapter 4.

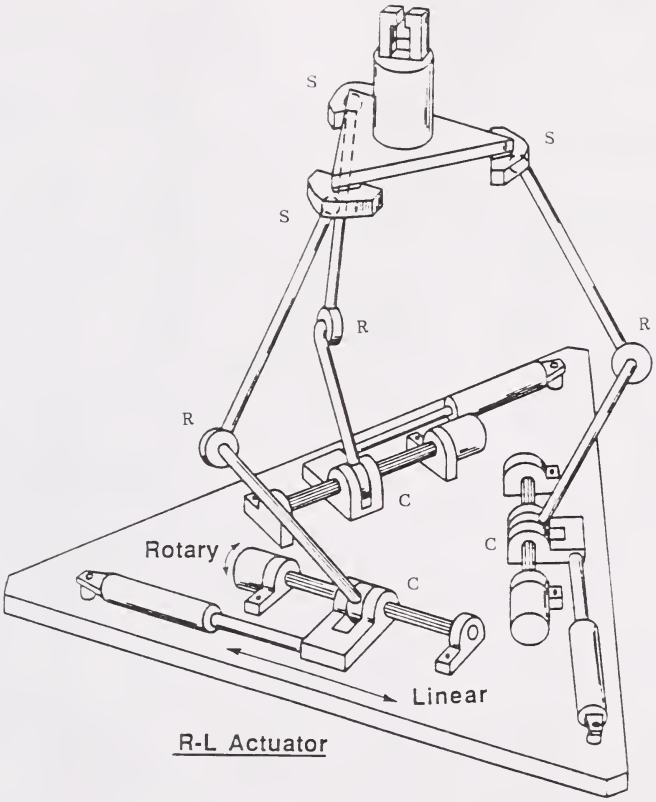

Figure 3.1 Six-degree-of-freedom closed-loop manipulator. C: Cylindric joint, R: Revolute joint, S: Spherical joint.

surface of a torus. The subworkspace of each open subchain is the volume swept by this torus translated along the axis of each ground-mounted (R-L) joint. In this chapter, the shapes of the above-described torus of the subchain are studied for different dimensions of the links. The conditions on the dimensions of the links, for which the subworkspace has no hole, are presented. Of course, an infinitesimally small platform is not practical, because the three spherical pairs supporting the platform coincide. Therefore the platform has no controllability of its orientation. To have controlled orientation, the platform requires three controllable rotational degrees of freedom with concurrent non-coplanar axes. This is attained by placing the three spherical joints at finite distances from one another. Nevertheless, the workspace study with infinitesimally small platform is a useful step toward more practical workspace studies with finite-size platforms having controllable orientation, which will be covered in Chapter 4.

One basic need in the design of mechanical manipulators is to determine the shape of the workspace. Workspace analysis of mechanical manipulators has been investigated by many authors. Almost all the studies are related to open-loop multi-degree-of-freedom serial-link mechanical manipulators. Little work has been done in the area of mechanical manipulators with parallel kinematic chains.

Therefore, theories for the workspace of such parallel mechanical manipulators are needed.

3.2 Configuration of a Parallel Manipulator with R-L Actuators

A six-degree-of-freedom parallel manipulator, where all actuators are ground-mounted, is considered in this chapter. It has three six-degree-of-freedom subchains, each of which has a two-degree-of-freedom R-L actuator, which controls both the rotation and the translation of a ground-supported cylindrical joint. For reducing the number of links in the subchains, spherical joints, which are three-degree-of-freedom kinematic pairs, are used in the subchains. A Cylindric-Revolute-Spherical ((R-L)-R-S) triad may then be used as the subchain with the C joint (R-L actuator) connected to the ground, and the S joint connected to the end-effector platform of the manipulator. The axes of the C joints (R-L joints) on the frame may be arranged in several different configurations, such as star form, triangle form, or parallel to each other, as shown in Fig. 3.2. Furthermore, they need not be coplanar, even if they are not parallel to one other.

The lengths from the center of the platform, H, to the centers of the spherical joints, C_1, C_2 and C_3, affect the volume of the workspace, and more significantly, the rotatability of the platform about the center H. Thus, to get a workspace of the manipulator with rotatability of the end effector as large as possible, the lengths between H and

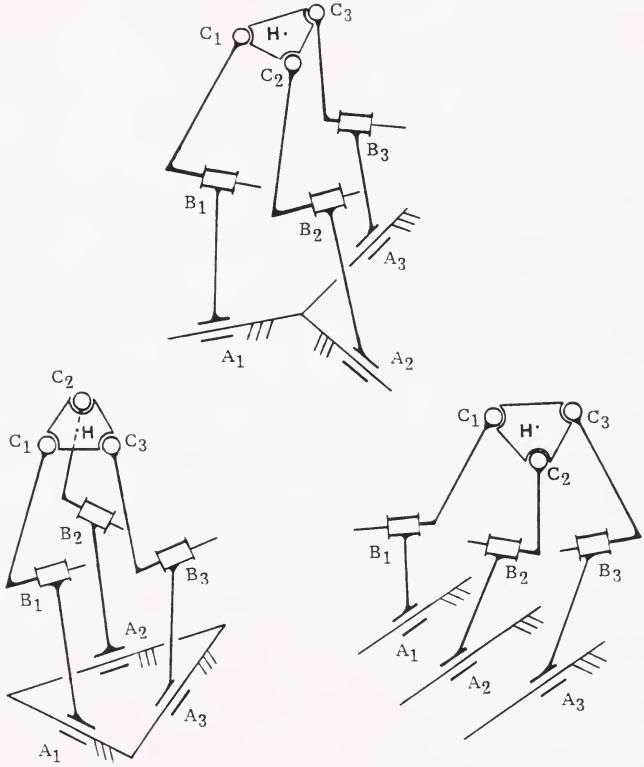

Figure 3.2 Three possible configurations of the arrangements of the R-L actuators on the base. Also, the R-L actuators need not be either parallel or coplanar.

C_i (i = 1, 2 and 3) should be as small as possible, which is consistent with controllability of end-effector orientation. When the lengths are infinitesimal or, in the limit, zero, the largest possible workspace with complete, but uncontrollable rotatability of the platform results. In this chapter, the equations of the workspace of the manipulator with infinitesimal dimensions of the platform are derived, i.e., with joints C_1, C_2 and C_3 infinitesimally close to each other. In chapter 4, the workspace of a similar parallel manipulator with a finite size platform will be determined. Of course, controllability of the orientation of the platform is reduced sharply as the spherical joints approach one another. Therefore it must be realized that there must be a practical trade-off between the distances of the spherical joints from one another and the controllability of platform orientation.

3.3 The Subworkspace Analysis of the Manipulator

The toroidal surface (torus) is the locus of a point attached to a body that is jointed back to the reference system through a dyad of two serially connected revolute pairs. A general R-R dyad with a point C which traces the surface of a general form of torus is shown in Fig. 3.3. It is similar to the subchain (R-L)-R-S when the platform is assumed to be infinitesimal and without the consideration of translation along the axis of the cylindric (R-L) joint. The shapes of the torus are illustrated first, then the

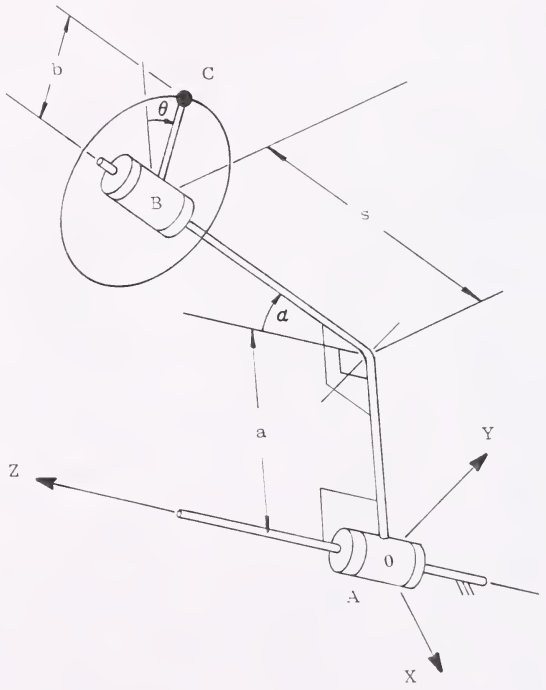

Figure 3.3 An R-R (Revolute - Revolute) dyad with a point C tracing a general form of torus. Note that a is the common perpendicular of the axes of the revolutes A and B.

equations of the boundaries of the subworkspace, which is the volume swept by this torus as the R-L joint translates, will be derived.

3.3.1 Shapes of the subworkspace

Fichter and Hunt [51] have geometrically described and analyzed four forms of the torus, which are common, flattened, symmetrical-offset and general forms as shown in Fig. 3.4. They also introduced two types of bitangent-plane[2], A-type, whose quartic curve intersection with the torus always encircles the OZ axis and B-type, whose points of tangency are both on one side of the OZ axis. Any bitangent-plane to any form of torus cuts the torus in two circles of the same radius which intersect one another at the two points of tangency. The curve of intersection of the bitangent-plane and the torus can be obtained by the simultaneous solution of the equations of the bitangent-plane and the torus. The curve of intersection of A-type bitangent-plane and a common torus ($a > b$) is shown in Fig. 3.5.

The equation of the surface of a completely general form of torus can be expressed as follow:

---

[2] A bitangent-plane has two points of tangency with a toroidal surface.

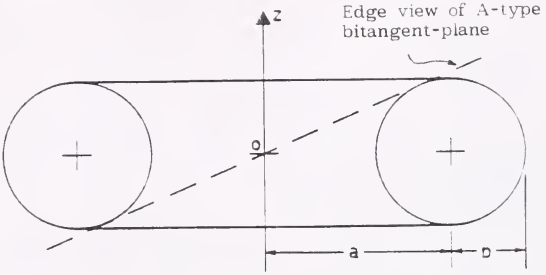

(a) Common torus

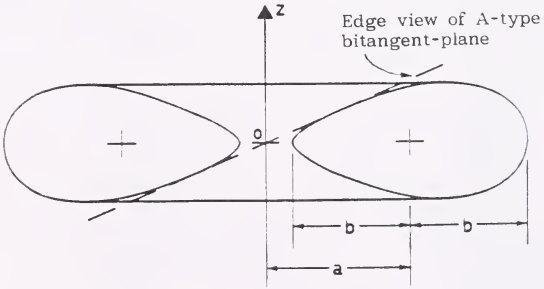

(b) Flattened torus

Figure 3.4 Diametral sections through tori: (a) common, (b) flattened, (c) symmetrical-offset and (d) general types.

(continued)

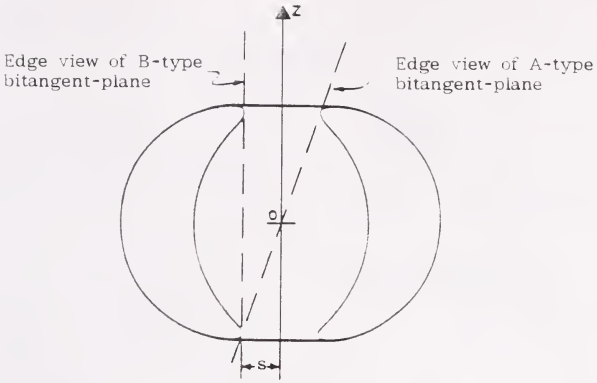

(c) Symmetrical-offset torus

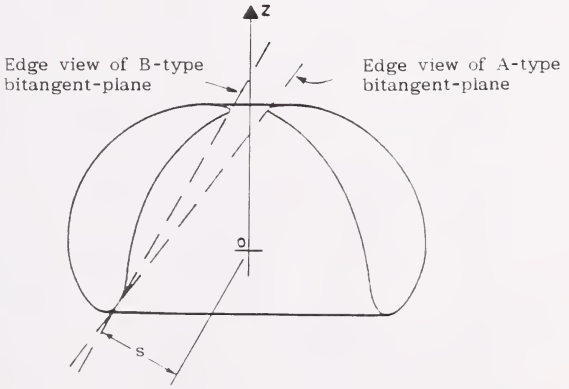

(d) General torus

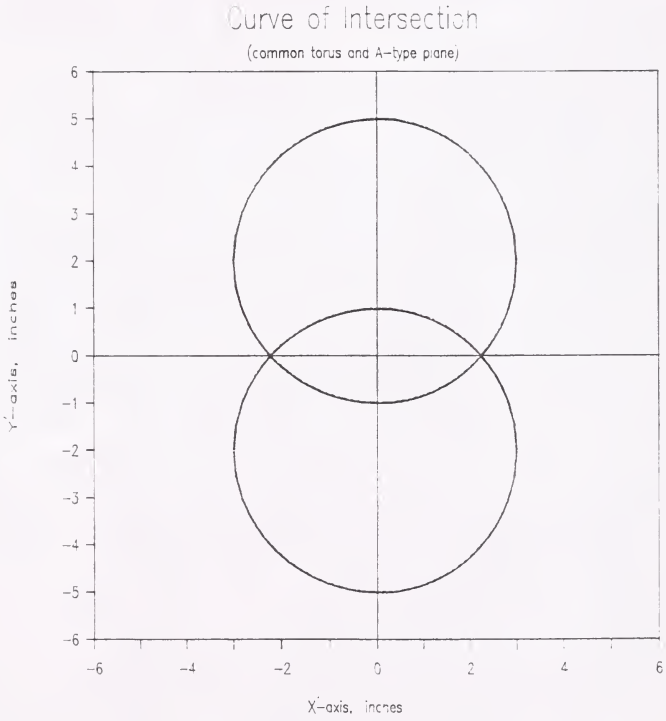

Figure 3.5 Intersection of the A-type bitangent-plane and the right circular torus (a = 3", b= 2")

$$\{(x^2 + y^2 + z^2) - (a^2 + b^2 + s^2)\}^2$$

$$= 4a^2\{b^2 - (\frac{z - s\cos\alpha}{\sin\alpha})^2\} \qquad (3.1)^3$$

Common form. The common form of torus (right circular), sometimes called the anchor-ring, is shown in diametral section in Fig. 3.4(a). The axes of the two revolute pairs are at right angle ($\alpha = 90°$). Their common perpendicular is a and the offset between them is zero ($s = 0$) (see Fig. 3.3). The equation of the torus can be expressed as

$$\{(x^2 + y^2 + z^2) - (a^2 + b^2)\}^2 = 4a^2(b^2 - z^2) \qquad (3.2)$$

The difference between the lengths of the links affects the shape of the torus, which is illustrated in Fig. 3.6. As $a > b$ shown in Fig. 3.6(a), the two circles in the diametral section are separated by a distance of $2(a - b)$. This kind of torus is also shown in Fig. 3.7. When the two circles in the diametral section are tangent at a point, the origin 0, then $a = b$ as shown in Fig. 3.6(b). The torus will intersect itself when $a < b$ as shown in Fig. 3.6(c). There is a void in this kind of torus when $a < b$ exists.

Flattened form. The flattened form of torus has no offset ($s = 0$) either, but the axes of the two revolute

---

[3] The equation of the general form of torus is derived in Appendix B.

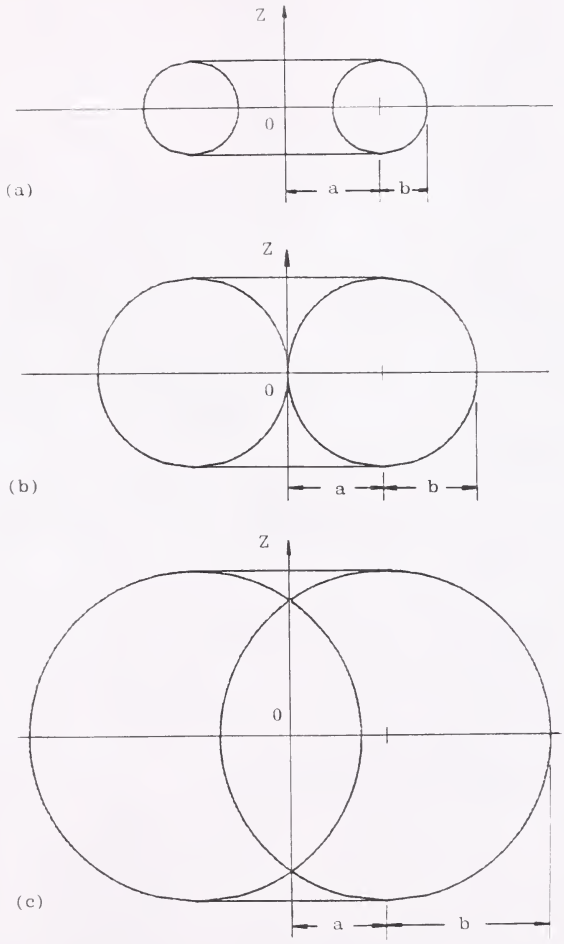

Figure 3.6 Diametral section of the common form of torus: (a) a > b, (b) a = b and (c) a < b

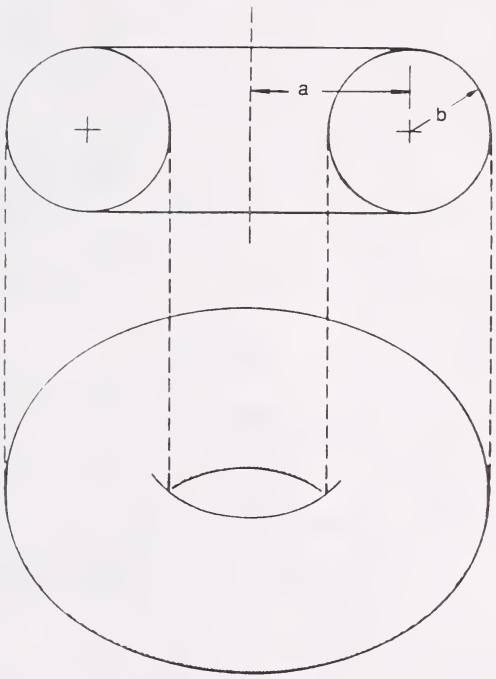

Figure 3.7 A right circular torus, a > b.

pairs are not at right angle ($\alpha \neq 90°$). The equation of this form of torus can be expressed as

$$\{(x^2 + y^2 + z^2) - (a^2 + b^2)\}^2 = 4a^2(b^2 - \frac{z^2}{\sin^2\alpha}) \tag{3.3}$$

The diametral plane cuts the torus in egg-shaped curves as shown in Fig. 3.4(b). For different twist angles (30°, 45° and 75°) and dimensions of the links ($a > b$, $a = b$, and $a < b$) with each specified twist angle, the shapes of the torus are shown in Figs. 3.8 - 3.10, respectively. It is noticed that the diametral sections of these tori are similar to those of the common form when $a > b$ and $a = b$, but flattened and egg-shaped. But the tori in Figs. 3.8 - 3.10 do not intersect themselves when $a < b$, which differs from the schematic shown in Fig. 3.6(c).

Symmetrical-offset form. The symmetrical-offset form has the axes of the two revolute pairs at right angle ($\alpha = 90°$) and with offset ($s \neq 0$). The equation of this form of torus can be expressed as

$$\{(x^2 + y^2 + z^2) - (a^2 + b^2 + s^2)\}^2 = 4a^2(b^2 - z^2) \tag{3.4}$$

The diametral section of this kind of torus is shown in Fig. 3.4(c). For $a > b$ and small s, the shape of the torus as shown in Fig. 3.11(a) is slightly different from that in Fig. 3.6(a). As shown in Fig. 3.11(b), the inner walls of the anchor-ring become flatter when $a = b$. The two closed

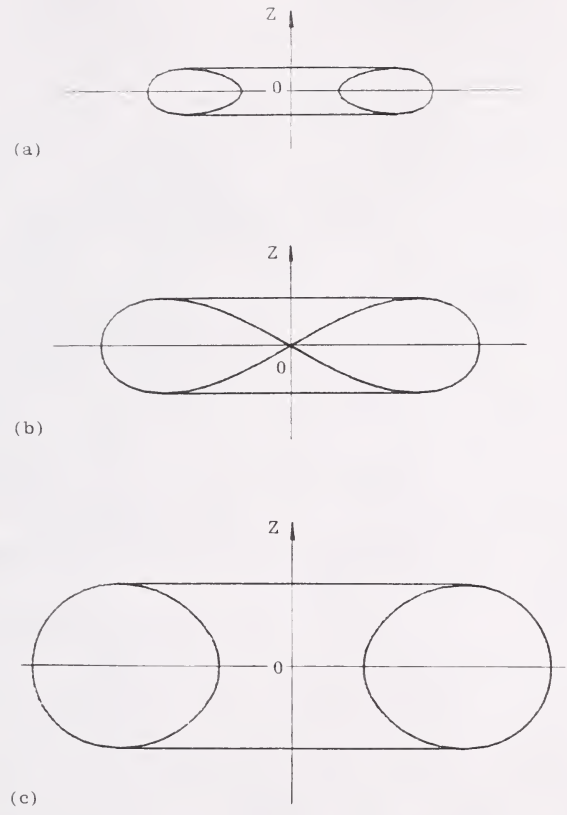

Figure 3.8 Diametral section of the flattened form of torus ($\alpha = 30°$): (a) a > b, (b) a = b and (c) a < b

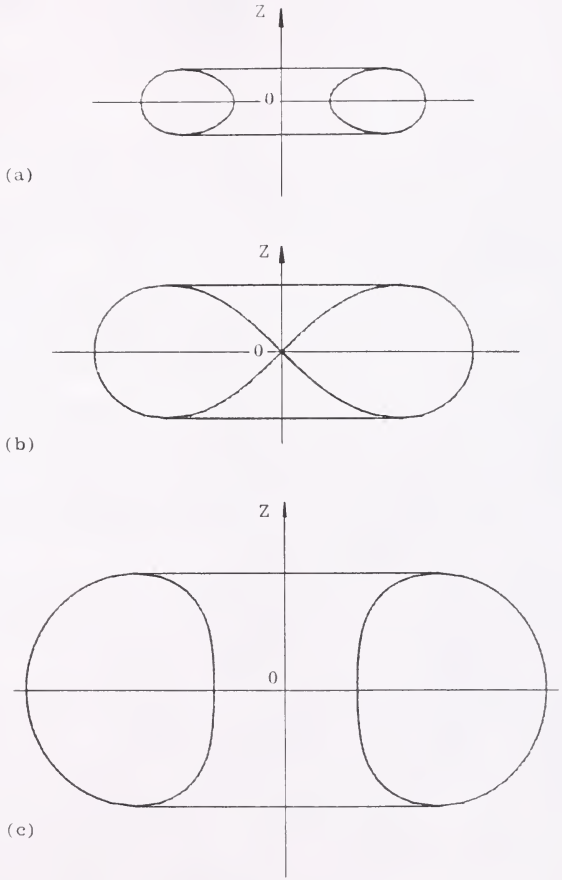

Figure 3.9 Diametral section of the flattened form of torus ($\alpha = 45°$): (a) a > b, (b) a = b and (c) a < b

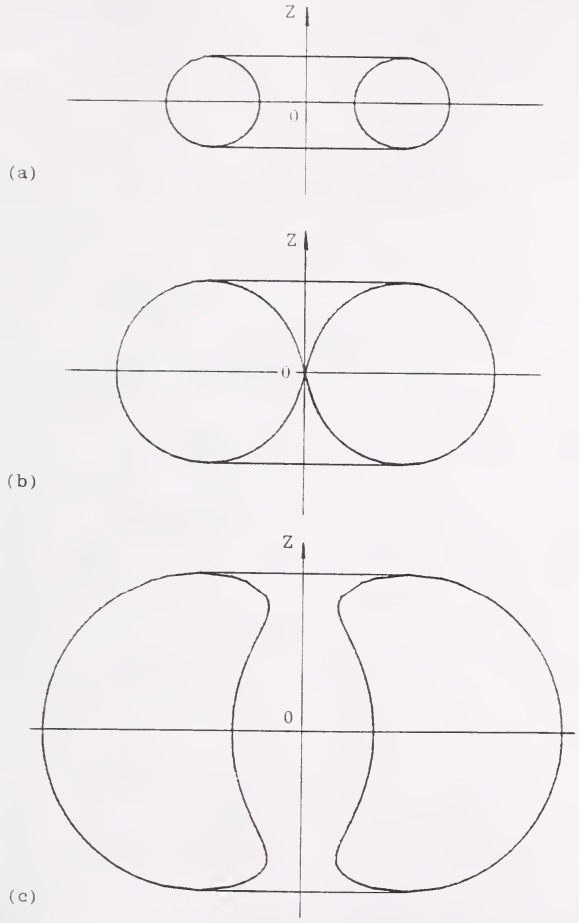

Figure 3.10 Diametral section of the flattened form of torus ($\alpha = 75°$): (a) $a > b$, (b) $a = b$ and (c) $a < b$

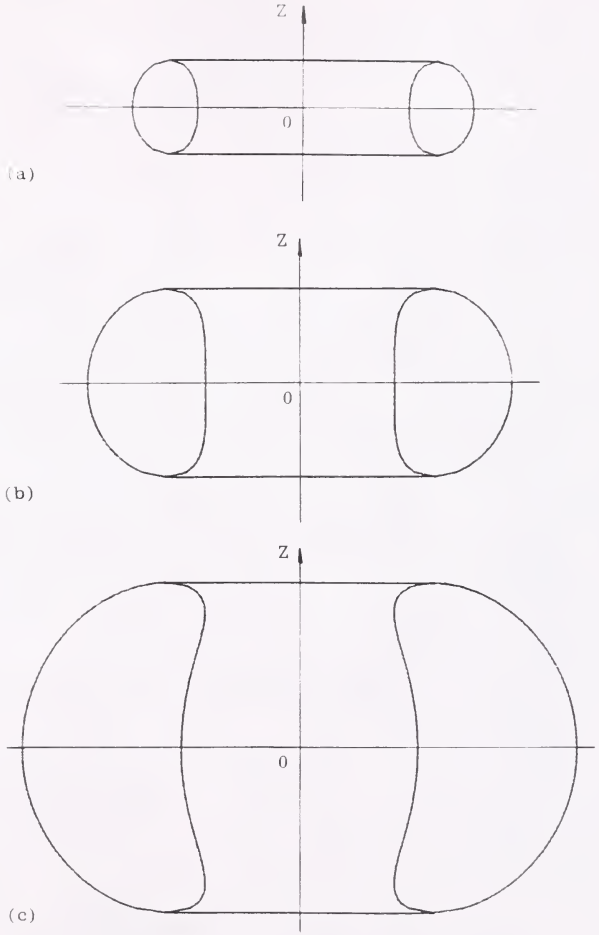

Figure 3.11 Diametral section of the symmetrical-offset form of torus: (a) a > b, (b) a = b and (c) a < b

curves in the diametral section become banana-shaped, as shown in Fig. 3.11(c), when a < b.

General Form. The diametral section of the torus is shown in Fig. 3.4(d). For different twist angles (30°, 45° and 75°) and dimensions of the links (a > b, a = b, and a < b) with each specified twist angle, the shapes of the torus are shown in Figs. 3.12 - 3.14, respectively. The closed curves in the diametral section, while still more or less banana-shaped, but now they are tilted over.

Equations (3.1) - (3.4) are all of the fourth degree and all forms of torus are thus quartic surfaces. The curve of intersection between a torus and a general plane is a quartic; also, in general, a straight line cuts any torus in four points (real, imaginary, or coincident).

The volume and shape of the workspace are very important for applications since they determine capabilities of the robot. In order to obtain the optimum workspace, the volume of the subworkspace of the corresponding subchain generally should be as large as possible. Since most of today's available industry robots have 0° or ±90° twist angles, we will discuss the following two cases with the conditions of s = 0 and twist angle α = 0° or ±90° applied, respectively.

Case 1: s = 0 and α = 0° (or ± π)

Since the axes of the two revolute pairs are parallel and there is no offset, the toroidal surface degenerates

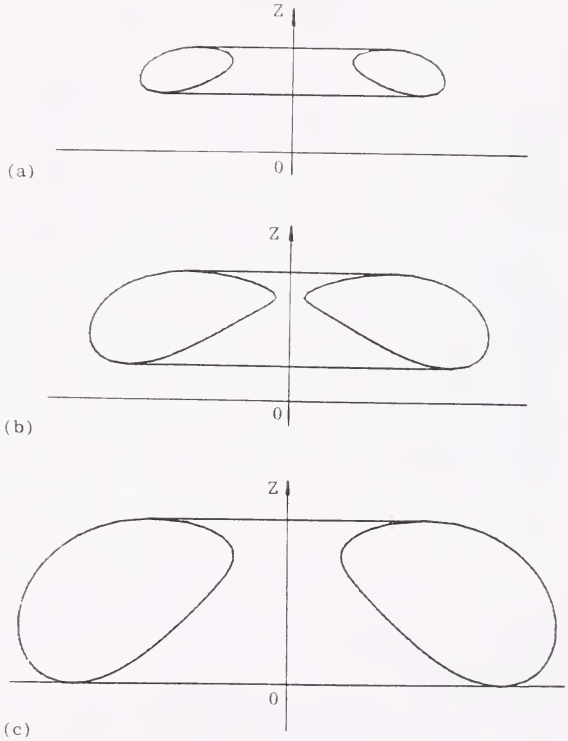

Figure 3.12 Diametral section of the general form of torus ($\alpha = 30°$): (a) $a > b$, (b) $a = b$ and (c) $a < b$

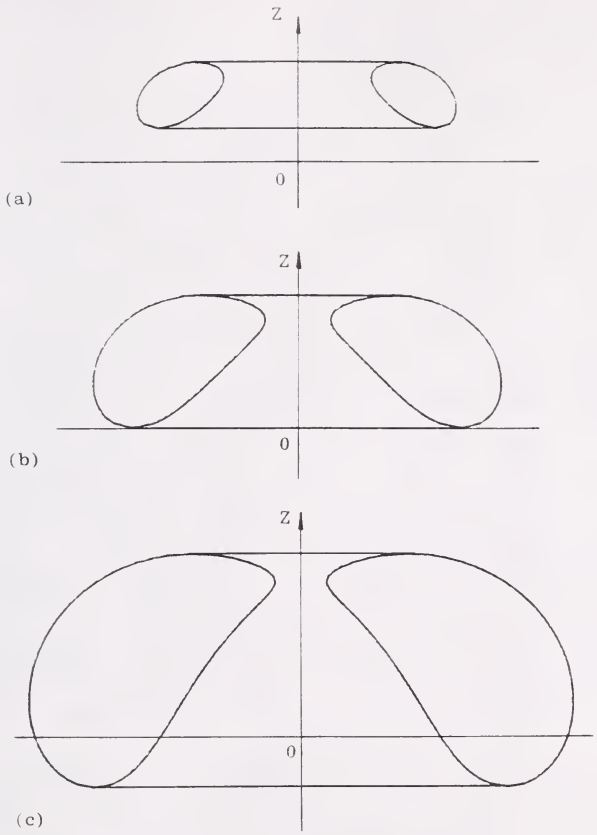

Figure 3.13 Diametral section of the general form of torus ($\alpha = 45°$): (a) $a > b$, (b) $a = b$ and (c) $a < b$

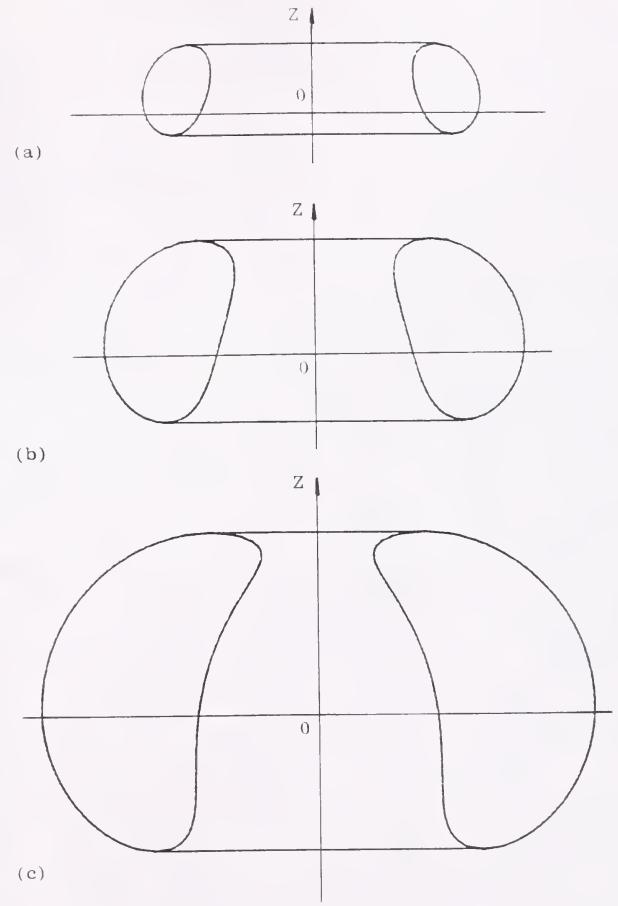

Figure 3.14 Diametral section of the general form of torus ($\alpha = 75°$): (a) a > b, (b) a = b and (c) a < b

into a plane. For different dimensions of the links a and b, the shapes of the now planar toroidal surface are illustrated in Fig. 3.15. The workspace resulting when this surface is translated along the Z axis has no hole only when a = b as shown in Fig. 3.15(b).

The workspace of this kind of subchain is generally the volume between two coaxial cylinders when the translation along the Z axis is in effect. Due to the limitation of the rotation of the first revolute joint which is ground-mounted, the workspace of this subchain is actually reduced to the upper half ($X \geq 0$) of the volume between the two coaxial cylinders. Whenever the condition a = b exists, the inner boundary disappears and there is no hole in the workspace.

Case 2: $s = 0$ and $\alpha = \pm 90°$

Since the two axes of the two revolute pairs are perpendicular to each other and there is no offset, the locus of point C is a torus, which is defined as the common form of torus shown in Fig. 3.6. When the translation along the Z axis is in effect, the workspace of the subchain can be described as shown in Figs. 3.16 - 3.18, respectively.

In Fig. 3.16(a), the torus has a hole because of a > b. When the translation d along the Z axis is in effect, we obtain the workspace as the volume between the two coaxial cylinders with radii of (a + b) and (a - b), respectively and height d, plus the volume of a half torus at each end.

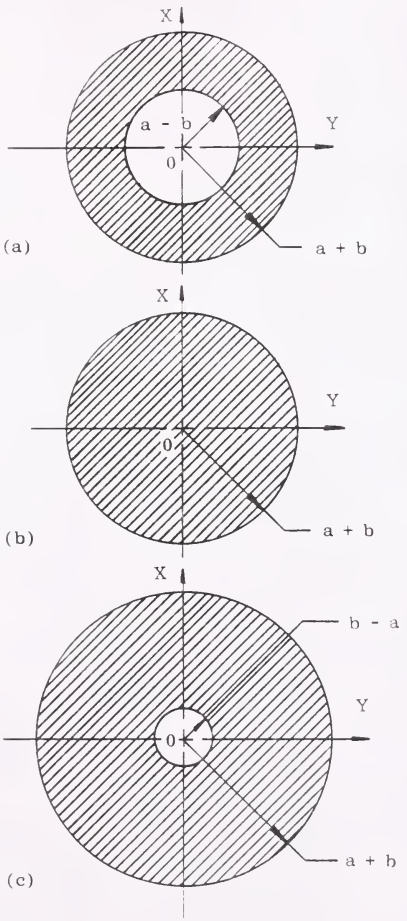

Figure 3.15 Cross sections of the Workspace generated by the planar R-R dyad: (a) a > b, (b) a = b and (c) a < b (infinitesimal platform)

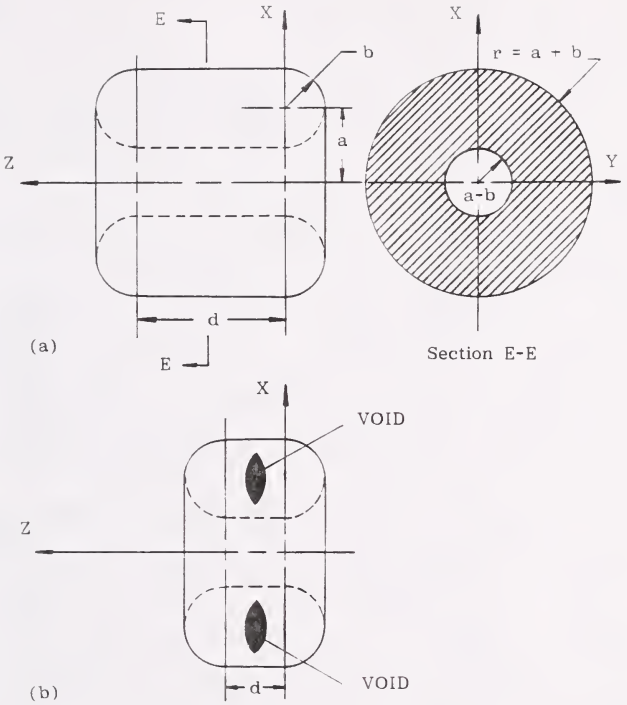

Figure 3.16 Workspace with the common form of torus ($a > b$); Along the Z axis: (a) $d \geq 2b$ and (b) $0 < d < 2b$ (infinitesimal platform)

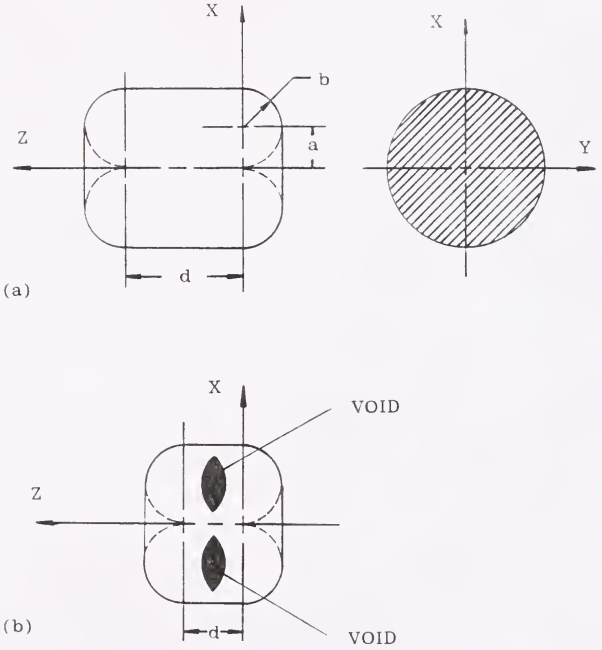

Figure 3.17 Workspace with the common form of torus (a = b); Along the Z axis: (a) d ≥ 2b and (b) 0 < d < 2b (infinitesimal platform)

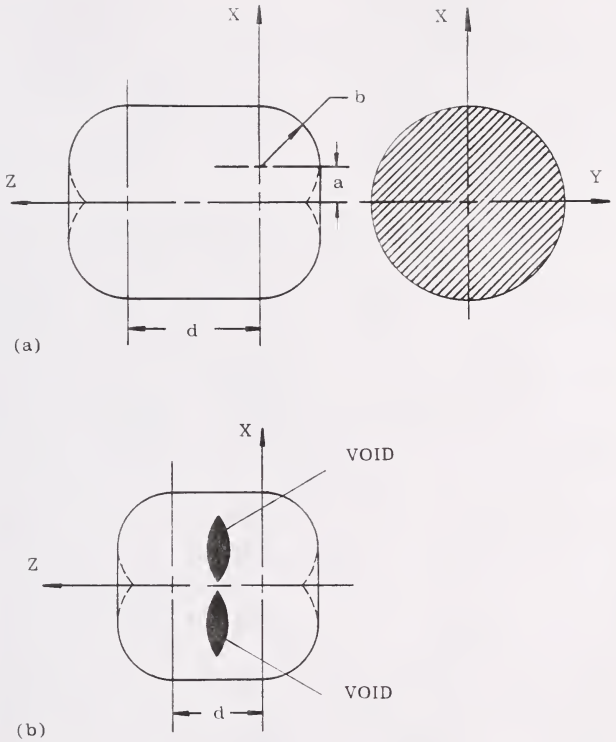

Figure 3.18 Workspace with the common form of torus (a < b); Along the Z axis: (a) d ≥ 2b and (b) 0 < d < 2b (infinitesimal platform)

However, this is true only when the translation along the Z axis, d, is greater than or equal to 2b. Otherwise, there are additional voids that can be found as shaded areas shown in Fig. 3.16(b). When the translation along the Z axis is less than 2b, there is a void inside the workspace, shown with a lentil-shaped cross section in Fig. 3.16(b). When a = b as shown in Fig. 3.6(b), there is no hole as the translation along the Z axis is in effect and $d \geq 2b$. The workspace is the volume of the cylinder with radius of (a + b), height d, plus the volume of this kind of half torus at each end, as shown in Fig. 3.17(a). If the translation along the Z axis is less than 2b, voids can be found even if the torus has no hole at all. The lentil-shaped cross sections of the void can be shown as shaded areas in Fig. 3.17(b). Finally, when the torus intersect itself as shown in Fig. 3.6(c), there is a void inside in this torus. As the translation d along the Z axis is in effect and is greater than or equal to 2b, we obtain the workspace as the volume of the cylinder with radius of (a + b) and height d, plus the volume of this kind of half torus at each end as shown in Fig. 3.18(a). Similarly, voids can be found if the translation along the Z axis is less than 2b, which is shown in Fig. 3.18(b).

3.3.2 Boundaries of the subworkspace and root regions in the subworkspace (infinitesimal platform)

In order to calculate the volume of the subworkspace, we must find the boundaries (external and internal) of the

subworkspace. From the inverse kinematics of subchain (R-L)-R-S solved in section 2.5.1, we know it has up to four possible solutions for a given position of the S joint. Once the orientation and position of the hand is given, we may have up to 64 solutions for the manipulator. Therefore, the study of root regions in the subworkspace is also important.

A manipulator with R-L actuators in the subchains whose axes are arranged in triangle form on the base can be represented as shown in Fig. 3.19. The notation is as follows:

OXYZ — global fixed coordinate system.

i — i-th subchain.

A_i, B_i — R-L actuator joint and revolute joint in the i-th subchain.

$o_i x_i y_i z_i$ — local fixed coordinate systems with the z_i axis along the axis of the cylindric joint A_i.

$A_i x_{ai} y_{ai} z_{ai}$, $B_i x_{bi} y_{bi} z_{bi}$ — moving coordinate systems embedded in joints A_i and B_i, respectively.

Θ_{ai}, Θ_{bi} — relative rotation angle between successive links.

d_i — translation along the axis z_i of cylindric joint A_i from the origin of the local fixed coordinate system $o_i x_i y_i z_i$.

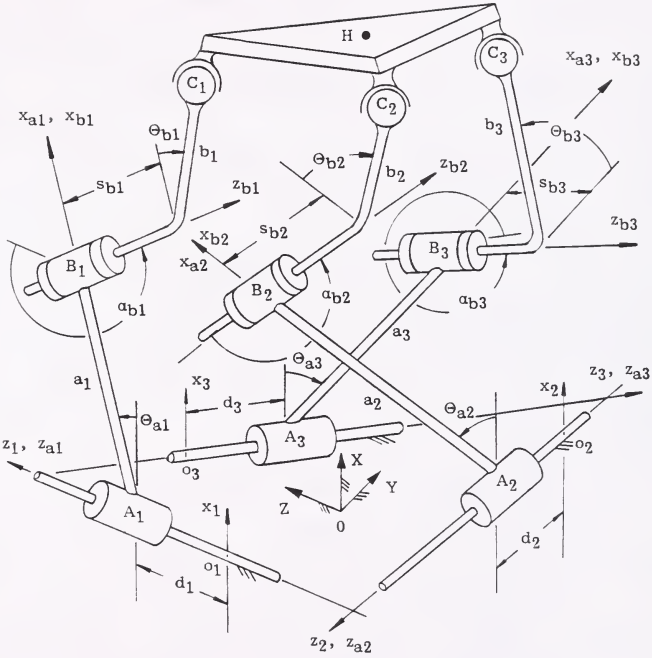

Figure 3.19 Notation of the manipulator with ground-mounted R-L actuators arranged in triangle configuration

a_i, b_i — perpendicular distance between successive joint axes z_1, z_2 and z_3, respectively.

s_{bi}, α_{bi} — offset along axis z_{bi} and twist angle between z_{ai} and z_{bi}, respectively.

$\overline{HC}_i$ — approaching zero for infinitesimal platform.

As shown in Figs. 3.20 and 3.21 when $s_{bi} \neq 0$ or $s_{bi} = 0$ respectively, if the revolute joint B_i makes a complete rotation, the locus of the point C_i is a circle with respect to the moving coordinate system $B_i x_{bi} y_{bi} z_{bi}$. It can also be expressed with respect to the coordinate system $A_i x_{ai} y_{ai} z_{ai}$ from Eq. (2.5) as follows:

$$x_{ai} = b_i C\theta_{bi} + a_i \tag{3.5}$$

$$y_{ai} = b_i S\theta_{bi} C\alpha_{bi} - s_{bi} S\alpha_{bi} \tag{3.6}$$

$$z_{ai} = b_i S\theta_{bi} S\alpha_{bi} + s_{bi} C\alpha_{bi} \tag{3.7}$$

The locus, generated by the point C_i turning around the revolute joint B_i and the cylindric joint A_i, without translating along the axis of the cylindric joint, can be obtained by turning the circle, now represented by Eqs. (3.5) and (3.6), about the z_{ai} axis. The shape of this locus is the surface of a general form of torus as described in section 3.3.1. The subworkspace of this subchain is the volume swept by this toroidal surface as it translates along the axis of the cylindric joint.

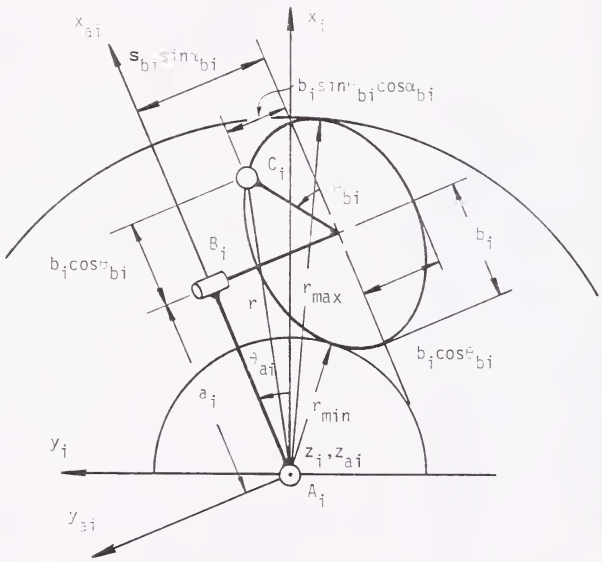

Figure 3.20 Subworkspace element of the i-th dyad of the manipulator as the offset at joint B_i, $s_{bi} \neq 0$ (infinitesimal platform)

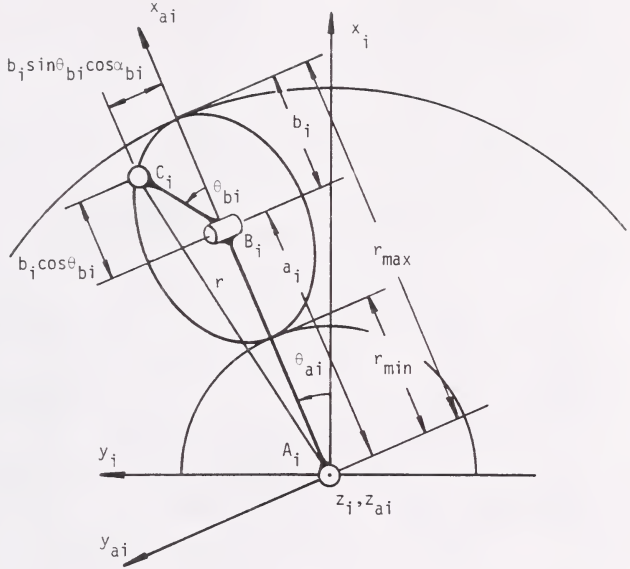

Figure 3.21 Subworkspace element of the i-th dyad of the manipulator as the offset at joint B_i, $s_{bi} = 0$ (infinitesimal platform)

Since the manipulator's workspace with infinitesimal platform is the common intersection of the three subworkspaces of the three dyads that support the platform, in general the ends of these subworkspaces need not be considered. Therefore, only the projection of the subworkspace onto the xy plane is of interest. For this reason, henceforth r will designate only the xy projection of the vector from the center A_i to the cylindric boundary of the subworkspace. Accordingly:

$$r^2 = x_{ai}^2 + y_{ai}^2 = x_i^2 + y_i^2$$

$$= (b_i C\Theta_{bi} + a_i)^2 + (b_i S\Theta_{bi} C\alpha_{bi} - s_{bi} S\alpha_{bi})^2 \qquad (3.8)$$

Subworkspace with offset $s_{bi} = 0$[4] (infinitesimal platform). For the sake of simplicity and ease of visualization, we will discuss the subworkspace with infinitesimal platform and with offset $s_{bi} = 0$ first. Eq. (3.8) becomes

$$r^2 = (b_i C\Theta_{bi} + a_i)^2 + b_i^2 S^2\Theta_{bi} C^2\alpha_{bi} \qquad (3.9)$$

The projections on the $o_i x_i y_i$ plane of the circles described by C_i, which are ellipses, can be represented by Eqs. (3.8) and (3.9) in terms of the parameter Θ_{bi}. Figs. 3.20 and 3.21 show these ellipses when $a_i > b_i$. When

---

[4]See page 102 for subworkspace with offset $s_{bi} \neq 0$.

cylindric joint A_i translates along its fixed axis z_i, the subworkspace with respect to the system $A_i x_i y_i z_i$ is the volume between two concentric cylinders without considering the two ends of the subworkspace. The radii of the external and the internal cylinders are respectively the maximum and the minimum radii of the torus described by C_i without translation. Taking the derivative of r expressed by Eq. (3.9) with respect to Θ_{bi} and making the resulting expression equal zero, we can obtain the maximum and minimum radii of the torus from the following equation

$$r \frac{dr}{d\Theta_{bi}} = -b_i S\Theta_{bi}(b_i C\Theta_{bi} S^2\alpha_{bi} + a_i) = 0 \qquad (3.10)$$

Then we obtain the following two equations

$$S\Theta_{bi} = 0 \qquad (3.11)$$

and

$$C\Theta_{bi} = - \frac{a_i}{b_i S^2\alpha_{bi}} \qquad (3.12)$$

When $S\alpha_{bi} = 0$ ($\alpha_{bi} = 0$ or π) (the circles described by B_i and C_i are coplanar), or $a_i > b_i S^2\alpha_{bi}$, no real roots of Θ_{bi} can be found in Eq. (3.12). Hence we only have two roots of Θ_{bi} from Eq. (3.11), i.e. $\Theta^1_{bi} = 0$ and $\Theta^2_{bi} = \pi$. In this case, the values of r corresponding to Θ^1_{bi} and Θ^2_{bi} are respectively the maximum and minimum values of r. Therefore, substituting the value of Θ^1_{bi} and Θ^2_{bi} into Eq. (3.9) yields the maximum and minimum values of r as follows:

$$r_{max}^2 = (a_i + b_i)^2 = r_{1i}^2 \tag{3.13}$$

and

$$r_{min}^2 = (a_i - b_i)^2 = r_{2i}^2, \tag{3.14}$$

which are intuitively correct.

The relationship between r and Θ_{bi} can be expressed in a Cartesian coordinate system as shown in Fig. 3.22. It is obvious that in the subworkspace where $r_{2i} < r (= \sqrt{x_i^2 + y_i^2}) < r_{1i}$, for a given position of point C_i, which implies a given value of r, there are two corresponding solutions of Θ_{bi}. The subworkspace is a two-root region or two-way accessible region. In other words, there are two sets of Θ_{ai} and Θ_{bi}, or two kinematic branches of the i-th dyad for reaching a given position of C_i. On the boundaries where $\sqrt{x_i^2 + y_i^2} = r_{1i}$ or r_{2i}, there is only one solution for Θ_{bi}. Thus the boundary surfaces are one-root regions. (Recall that this is a planar R-R case).

In another case, when $S\alpha_{bi} \neq 0$ ($\alpha_{bi} \neq 0$ or π) and $a_i \leq b_i S^2\alpha_{bi}$, two additional roots of Θ_{bi} are found from Eq. (3.12). Therefore in addition to r_{1i} and r_{2i} there are another two values of r, say r_{3i} and r_{4i}, which are also limiting values of Eq. (3.9).

Substituting Eq. (3.12) into Eq. (3.9) yields

$$r_{3i}^2 = r_{4i}^2 = \cot^2\alpha_{bi}(b_i^2 S^2\alpha_{bi} - a_i^2) \tag{3.15}$$

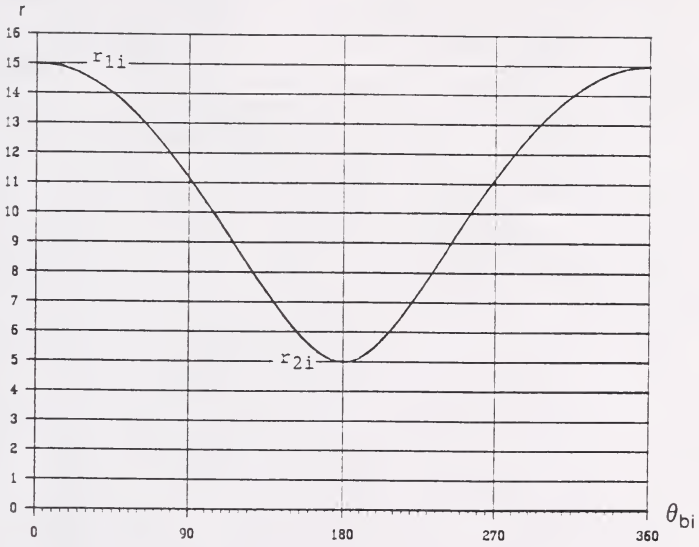

Figure 3.22 Two solutions of Θ_{bi} corresponding to $r_2 < r < r_1$ ($a_i = 10$, $b_i = 5$, $s_{bi} = 0$ and $\alpha_{bi} = 0$ or π) (circles described by B_i and C_i without translation of A_i are coplanar)

Thus, r_{1i}, r_{2i}, r_{3i} and r_{4i} are the local minima or local maxima of r expressed by Eq. (3.9). In order to find the global minimum and maximum values, we take the second derivative of r with respect to Θ_{bi} of Eq. (3.10), which yields

$$r\frac{d^2r}{d\Theta_{bi}^2} + \left(\frac{dr}{d\Theta_{bi}}\right)^2 = -b_i[b_iS^2\alpha_{bi}(2C^2\Theta_{bi} - 1) + a_iC\Theta_{bi}] \qquad (3.16)$$

At the position of local minima or maxima, the first derivatives equal zero, and then

$$r\frac{d^2r}{d\Theta_{bi}^2}\Bigg|_{\Theta_{bi} = 0} = -b_i(b_iS^2\alpha_{bi} + a_i) < 0 \qquad (3.17)$$

$$r\frac{d^2r}{d\Theta_{bi}^2}\Bigg|_{\Theta_{bi} = \pi} = -b_i(b_iS^2\alpha_{bi} - a_i) < 0 \qquad (3.18)$$

At the position of r_3 or r_4,

$$r\frac{d^2r}{d\Theta_{bi}^2}\Bigg|_{\Theta_{bi} = \arccos\left(\frac{-a_i}{b_iS^2\alpha_{bi}}\right)} = -\frac{a_i^2 - b_i^2S^4\alpha_{bi}}{S^2\alpha_{bi}} > 0 \qquad (3.19)$$

According to Eqs. (3.17) - (3.19), r_{1i} and r_{2i} are local maxima, and r_{3i} and r_{4i} are equal local minima of r. Since

$r_{1i} > r_{2i}$, the global maximum is r_{1i}, and there are two equal global minima, namely r_{3i} and r_{4i}. The external and internal cylinders of the subworkspace are then the cylinders of radii of r_{1i} and r_{3i}, respectively.

Figure 3.23 shows the relationship between r and Θ_{bi} in a Cartesian coordinate system in this case. It is seen that in the portion of the subworkspace where $r_{2i} < r < r_{1i}$, for a given position of point C_i, which implies for a given value of r, there are two corresponding solutions of Θ_{bi}. Thus this is the two-root region of the subworkspace. The other portion of the subworkspace is the four-root region of the subworkspace since four solutions of Θ_{bi} can be found in that region for a given translation d_i (see Fig. 3.19) and a given position of C_i. The cylinder of radius $r = r_{2i}$ inside the subworkspace divides the subworkspace into a two-root region and a four-root region, and the surface of the cylinder of radius r_{2i} itself is a three-root region. It can also be seen that the external boundary (the surface of the cylinder of radius $r = r_{1i}$) is a one-root region, and the internal boundary (the surface of the cylinder of radius $r = r_{3i}$) is a two-root region. Since the offset is zero and the twist angle is not 90°, without the translation of A_i, the locus of the positions of point C_i is the surface of a flattened form of torus. The diametral section of this kind of torus is shown in Fig. 3.24 and the root regions can also be visualized easily from the figure.

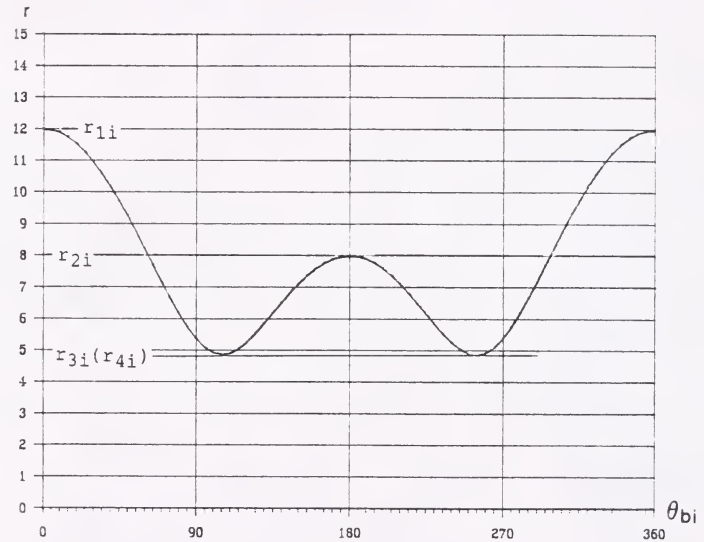

Figure 3.23 Two solutions of Θ_{bi} corresponding to $r_2 < r < r_1$ and four solutions of Θ_{bi} corresponding to $r_3 < r < r_2$ ($a_i = 2$, $b_i = 10$, $s_{bi} = 0$ and $\alpha_{bi} = \pi/3$)

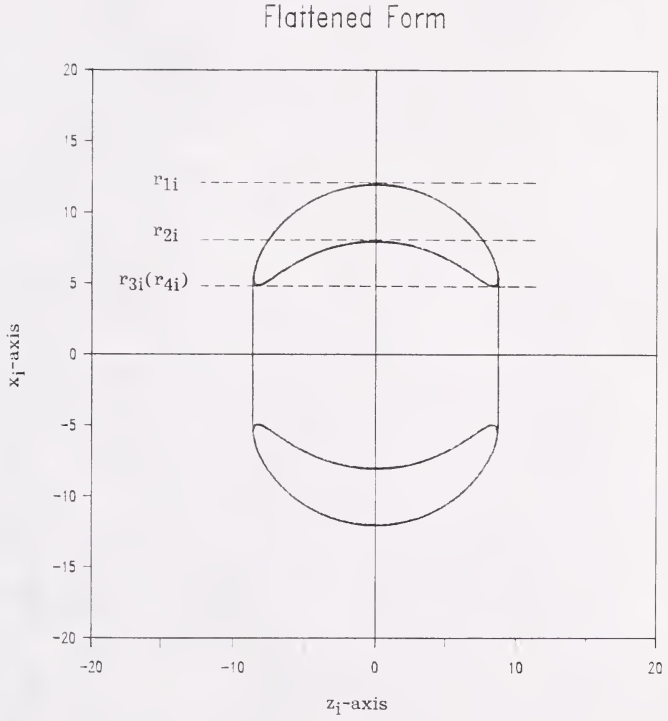

Figure 3.24 Diametral section of flattened form of torus ($a_i = 2$, $b_i = 10$, $s_{bi} = 0$ and $\alpha_{bi} = \pi/3$)

Furthermore, in the case when $a_i = b_i s^2 \alpha_{bi}$, the roots of θ_{bi} of Eq. (3.12) are coincident and equal, i.e., $\theta_{bi}^3 = \theta_{bi}^4 = \theta_{bi}^2 = \pi$. Thus, $r_{3i} = r_{4i} = r_{2i}$, and their value is the minimum of r, and is the radius of the internal cylinder of the subworkspace.

The results derived are illustrated in Figs. 3.25 - 3.31, where the projections of the configurations of the subchain are presented.

Figures 3.25 and 3.26 are shown for the case of $\alpha_{bi} = 0$ or π, i.e., $s\alpha_{bi} = 0$. The projection of the circle generated by point C_i on the $A_i x_i y_i$ plane is also a circle. The radii of the external and internal cylinders of the boundary are the maximum and minimum radii r of the torus. It is also shown that the subchain can take two branches for point C_i to reach the same position in the subworkspace, illustrating a two-root region.

Figures 3.27 and 3.28 are shown as the case of $\alpha_{bi} \neq 0$ or π and $a_i > b_i s^2 \alpha_{bi}$. The results are the same as in the case shown in Figs. 3.25 and 3.26, except that the projection of the circle of point C_i on the $A_i x_i y_i$ plane is an ellipse now.

Figures 3.29 and 3.30 are shown as the case of $\alpha_{bi} \neq 0$ or π and $a_i < b_i s^2 \alpha_{bi}$. The internal boundary is the cylinder of radius r_{3i}. The circle of radius r_{3i} on the plane $o_i x_i y_i$ is tangent to the ellipse at two points showing the values of r_{3i} and r_{4i} (at the points of tangency), which are both the equal limiting values of the radius r of the

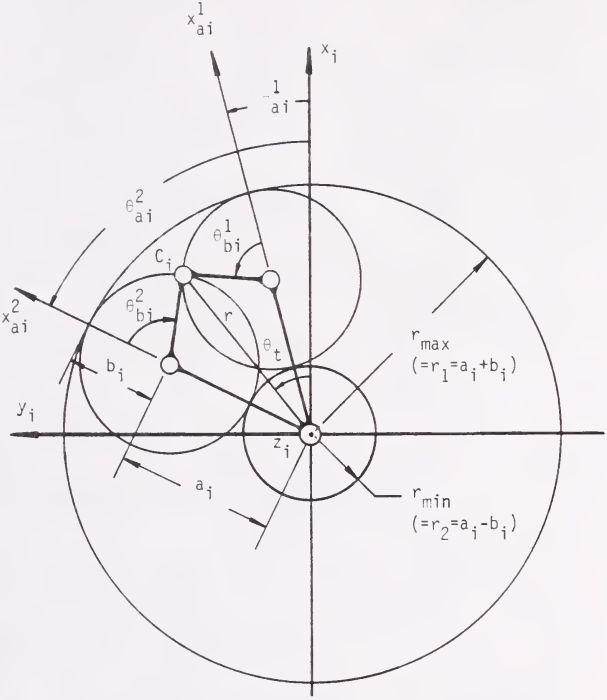

Figure 3.25 Two-root subworkspace as $\alpha_{bi} = 0$ or π and $a_i > b_i$

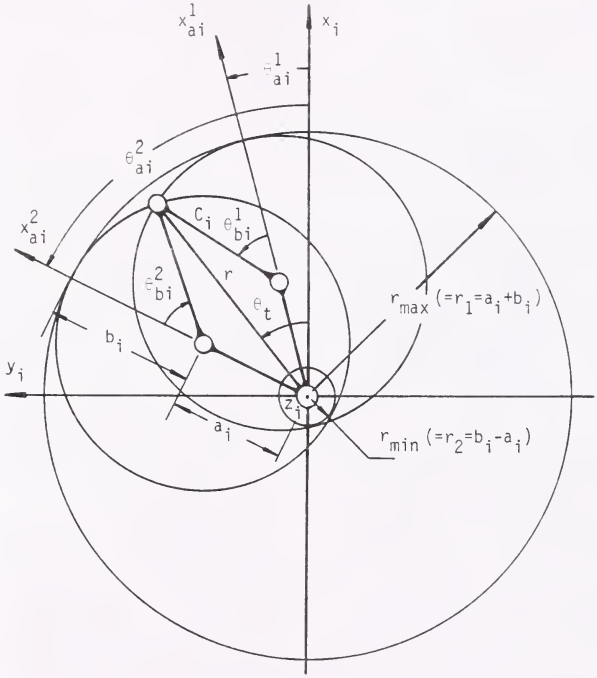

Figure 3.26 Two-root subworkspace as $\alpha_{bi} = 0$ or π and $a_i < b_i$

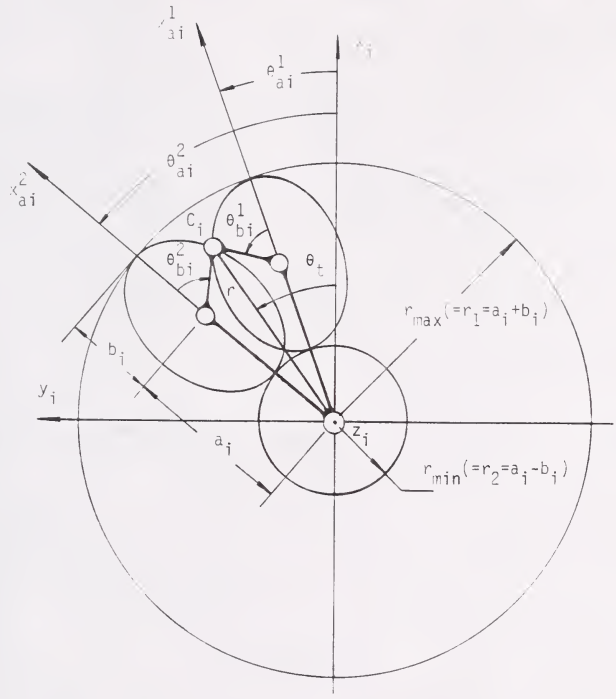

Figure 3.27 Two-root subworkspace as $a_i > b_i s^2\alpha_{bi}$ and $a_i > b_i$

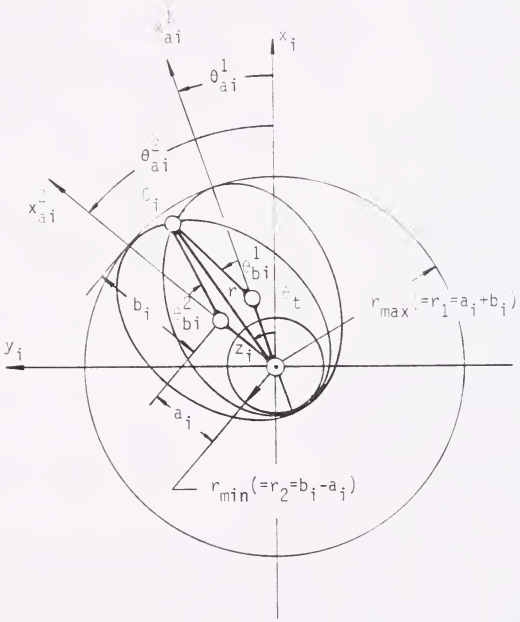

Figure 3.28 Two-root subworkspace as $a_i > b_i S^2 \alpha_{bi}$ and $a_i < b_i$

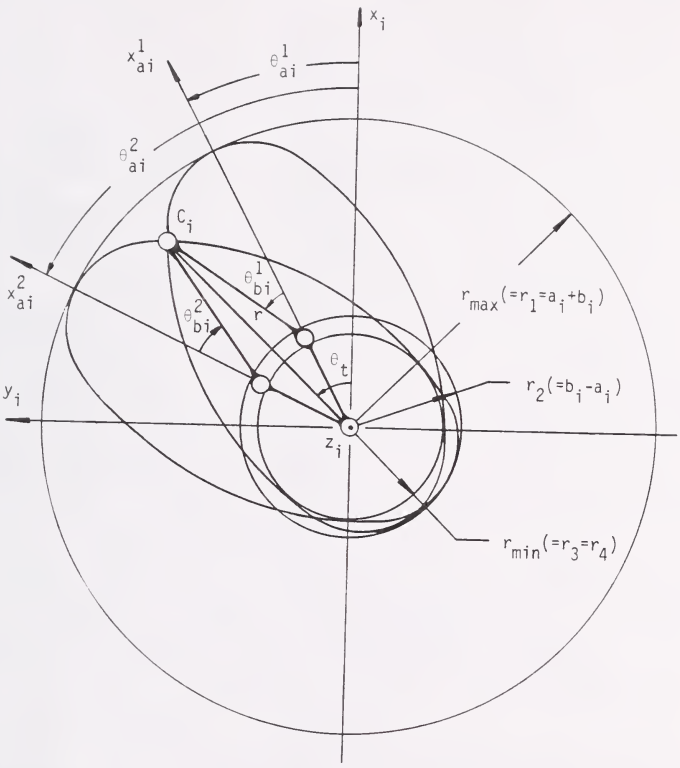

Figure 3.29 Two-root subworkspace as $a_i < b_i S^2\alpha_{bi}$ and $r_2 < r < r_1$

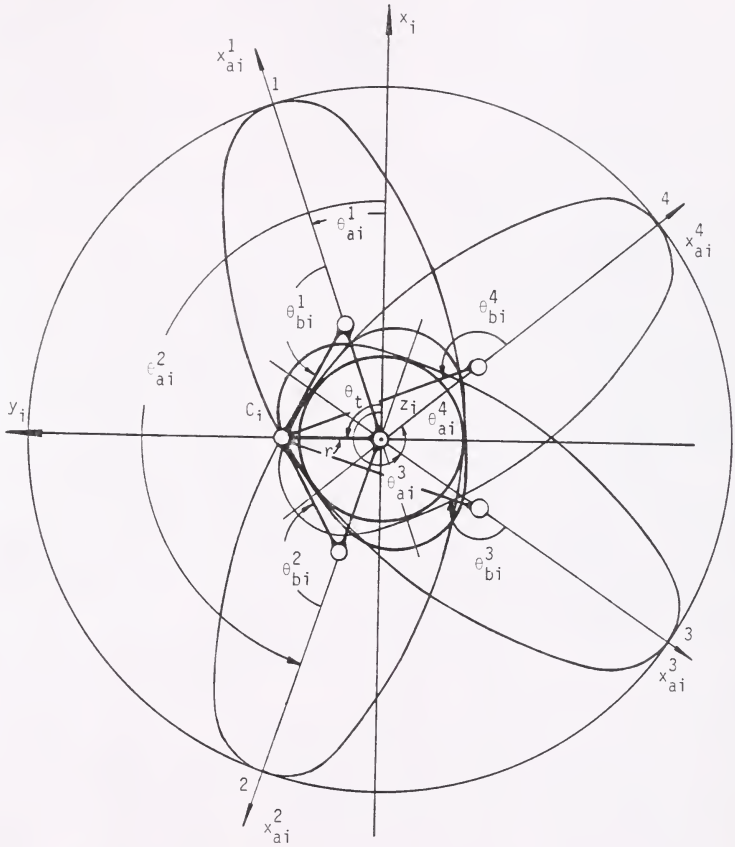

Figure 3.30 Four-root subworkspace as $a_i < b_i s^2 \alpha_{bi}$ and $r_3 < r < r_2$

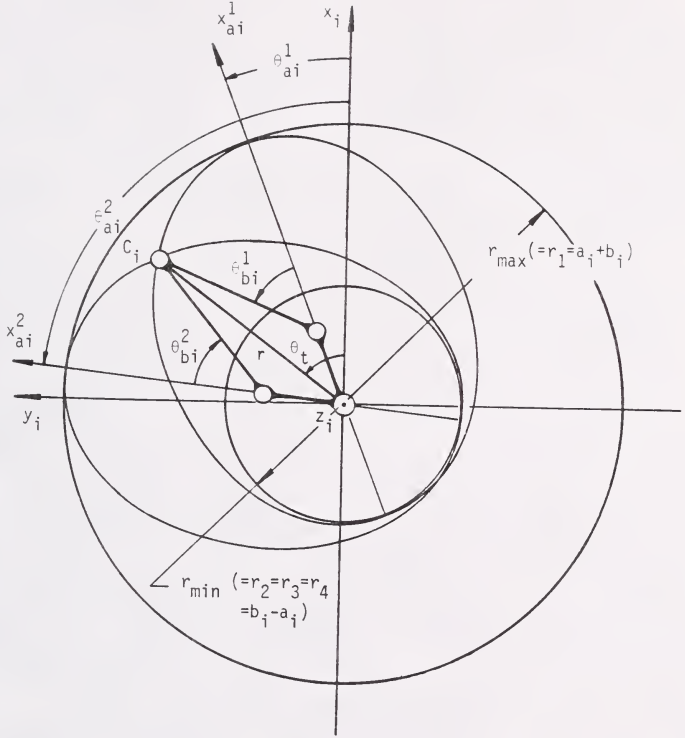

Figure 3.31 Two-root subworkspace as $a_i = b_i s^2 \alpha_{bi}$

torus. In Fig. 3.29, the subchain can take two branches for point C_i to reach a certain position in the region of $r_{2i} < r < r_{1i}$. In Fig. 3.30, the subchain can take four branches for the point C_i to reach a certain position in the region of r_{3i} (or r_{4i}) $< r < r_{2i}$. These figures illustrate that these two regions are the two-root and four-root regions of the subworkspace, respectively.

Figure 3.31 describes the case of $\alpha_{bi} \neq 0$ or π, and $a_i = b_i S^2\alpha_{bi}$. In this case, the circles of radii r_{2i} and r_{3i} (or r_{4i}) shown in Figs. 3.29 and 3.30 are coincident. Thus the four-root region of the subworkspace degenerates to a one-root cylindrical surface.

Subworkspace with Offset $s_{bi} \neq 0$. Taking the derivative of both sides of Eq. (3.8) with respect to Θ_{bi} and letting the resulting expression equal zero, yields

$$-S\Theta_{bi}(b_i C\Theta_{bi} + a_i) + C\Theta_{bi}C\alpha_{bi}(b_i S\Theta_{bi}C\alpha_{bi} - s_{bi}S\alpha_{bi}) = 0 \qquad (3.20)$$

Expanding $S\Theta_{bi}$ and $C\Theta_{bi}$ in terms of tan-half-angle, $X = \tan(\Theta_{bi}/2)$, Eq. (3.20) can be rewritten in the form of a quartic equation in X:

$$X^4 + BX^3 + CX^2 + DX + E = 0 \qquad (3.21)$$

where

$$B = 4\,\frac{a_i + b_i(1 - C\alpha_{bi})}{s_{bi}S^2\alpha_{bi}}$$

$$C = 0$$

$$D = 4\,\frac{a_i - b_i(1 - Ca_{bi})}{s_{bi}s^2a_{bi}}$$

$$E = 1$$

Solving the quartic equation Eq. (3.21), we can obtain up to four real roots for X, and then of Θ_{bi}. Back substituting the roots of Θ_{bi} into Eq. (3.8), up to four limiting values of the radius r of the torus are obtained.

In the case where only two limiting values of r exist, one is the maximum r_{max}, and the other is the minimum r_{min} in the range of $0 \leq \Theta_{bi} \leq 2\pi$. Hence the subworkspace can be expressed as

$$x_i^2 + y_i^2 \leq r^2_{max} \tag{3.22}$$

and

$$x_i^2 + y_i^2 \geq r^2_{min} \tag{3.23}$$

In the case where four limiting values of r exist, we need to compare the four values and find the maximum and the minimum which are respectively the radii of the external and internal cylinders of the boundaries of the subworkspace.

Furthermore, the relationship between r and Θ_{bi}, in the two cases, are shown schematically in Figs. 3.32 and 3.33 in Cartesian coordinate systems, respectively. In the first case (Fig. 3.32) for a given value of r in the region

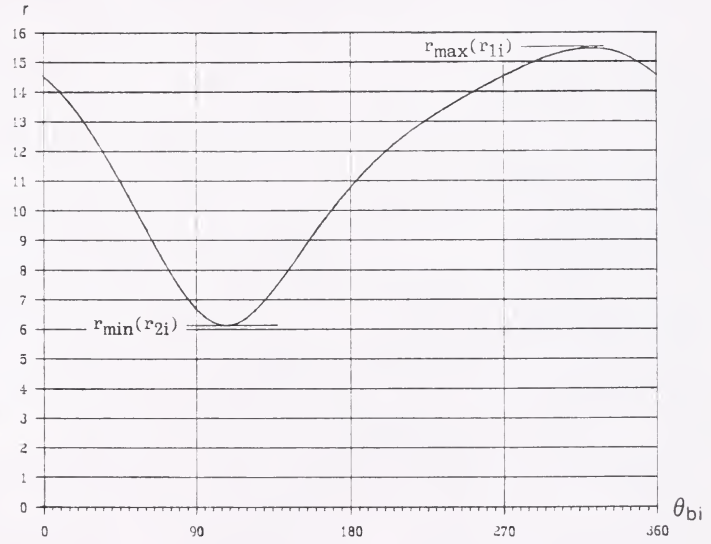

Figure 3.32 Schematics showing the relationship between r and Θ_{bi} as $s_{bi} \neq 0$. Two limit values of r exist as $a_i = 2$, $b_i = 12$, $\alpha_{bi} = \pi/6$ and $s_{bi} = 8$

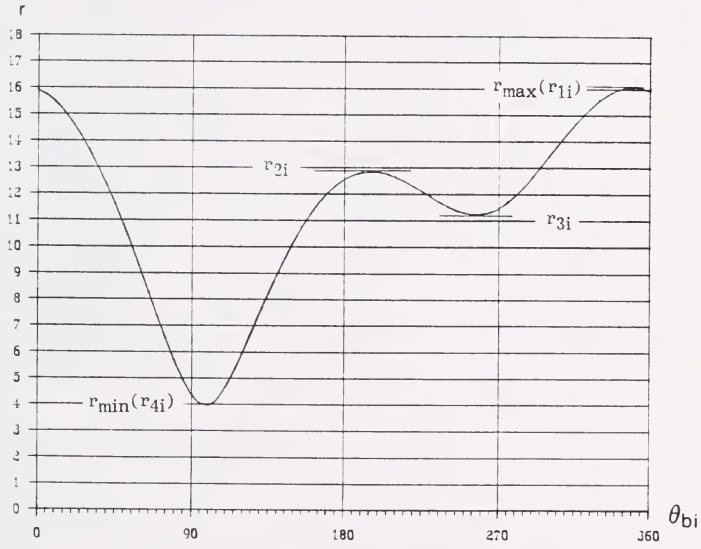

Figure 3.33 Schematics showing the relationship between r and Θ_{bi} as $s_{bi} \neq 0$. Four limit values of r exist as $a_i = 2$, $b_i = 12$, $\alpha_{bi} = \pi/2.5$ and $s_{bi} = 8$.

$r_{min} < r < r_{max}$, two corresponding values of Θ_{bi} are found. Hence, the subworkspace is a two-root region. In the other case (Fig. 3.33), r reaches limiting values at four positions in the range of $0 \leq \Theta_{bi} \leq 2\pi$. We find that for given values of r in the region of $r_2 < r < r_{max}$, $r_3 < r < r_2$, and $r_{min} < r < r_3$, the numbers of corresponding Θ_{bi} are two, four and two, respectively. Hence these regions in the subworkspace are respectively two-, four- and two-root regions. Since these involve the general form of torus, the diametral sections of the torus are shown in Figs. (3.34) and (3.35), respectively. The root regions in the subworkspace can also be visualized easily from the figures.

The procedure of finding the root regions in the subworkspace can be summarized as shown in Fig. (3.36).

3.4 Conditions for No-Hole Workspace

Since the workspace of the manipulator is the common region of the three subworkspaces, if none of the subworkspaces has any holes, the workspace has no hole. Subworkspaces in general, as described in the above sections, have cylindrical internal boundaries. Under some conditions of the dimensions of the manipulator, the radii of the internal cylinders are zero. Thus the internal boundaries disappear and the subworkspaces have no hole. These conditions are listed in Table 3.1.

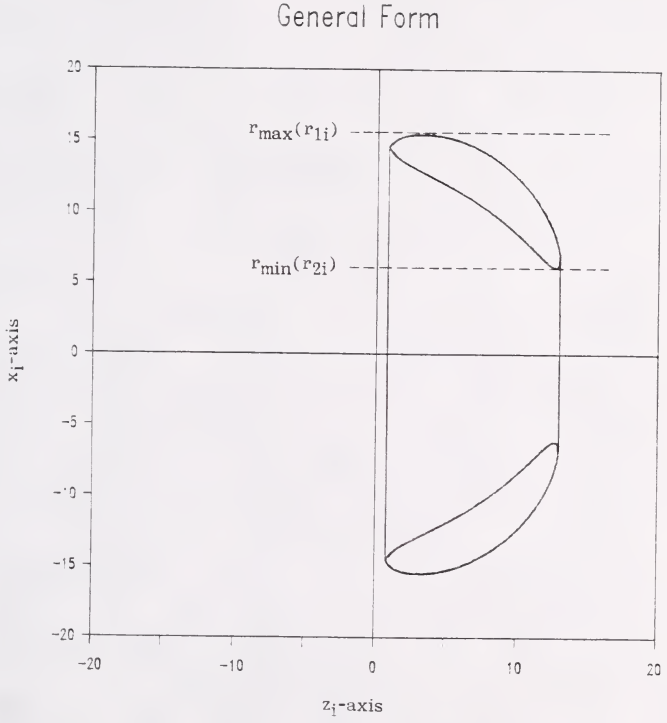

Figure 3.34 Diametral section of general form of torus (a_i = 2, b_i = 12, α_{bi} = $\pi/6$ and s_{bi} = 8)

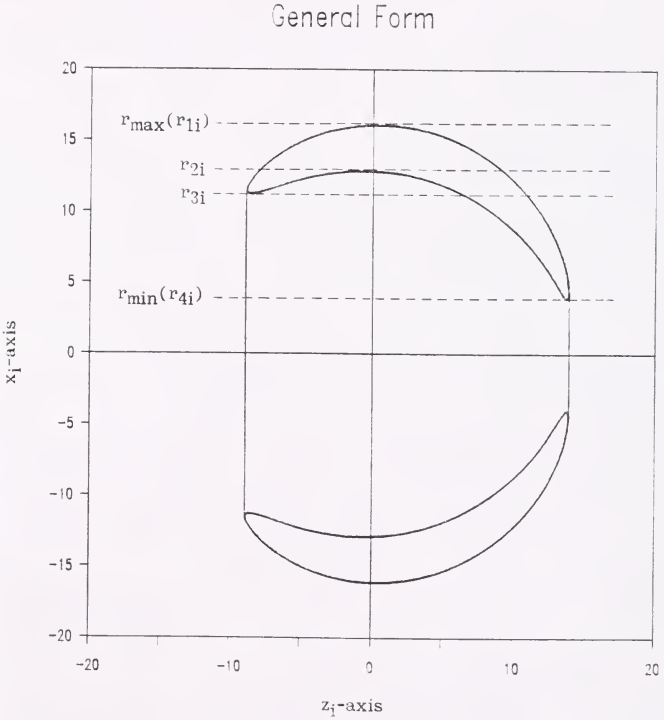

Figure 3.35 Diametral section of general form of torus (a_i = 2, b_i = 12, α_{bi} = $\pi/2.5$ and s_{bi} = 8)

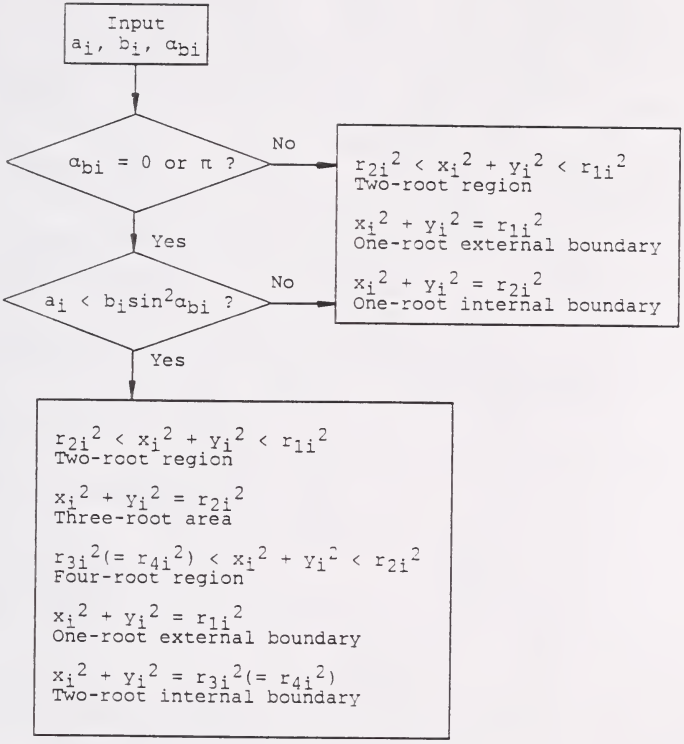

Figure 3.36 Procedure of finding the root regions in the subworkspace as $s_{bi} = 0$

Table 3.1 Conditions for No-Hole Workspace ($i = 1, 2, 3$)

Case		Radius of internal cylinder	Condition for no-hole
$\alpha_{bi} = 0$ or π		$r_{2i}^2 = (b_i - a_i)^2$	$b_i = a_i$
$\alpha_{bi} \neq 0$ or π	$a_i \geq b_i s^2\alpha_{bi}$		
	$a_i < b_i s^2\alpha_{bi}$	$r_{3i}^2 = \cot^2\alpha_{bi}(b_i^2 s^2\alpha_{bi} - a_i^2)$	$\alpha_{bi} = \pm \pi/2$

3.5 Workspace of the Manipulator

The subworkspace analysis results in the equations of the subworkspace i ($i = 1, 2, 3$) with respect to the local fixed coordinate system $o_i x_i y_i z_i$. Using coordinate transformation matrix A_{gi} from the global fixed system OXYZ to the above-mentioned system, $o_i x_i y_i z_i$, we transform these equations to be expressed with respect to the global system OXYZ.

$$\begin{bmatrix} x_i \\ y_i \\ z_i \\ 1 \end{bmatrix} = A_{gi} \begin{bmatrix} X \\ Y \\ Z \\ 1 \end{bmatrix} \tag{3.24}$$

In the case, for example, where the axes of the three R-L actuator joints are arranged in equilateral triangle form on the base as shown in Fig. 3.37, the matrices A_{gi} ($i = 1, 2, 3$) are as follows:

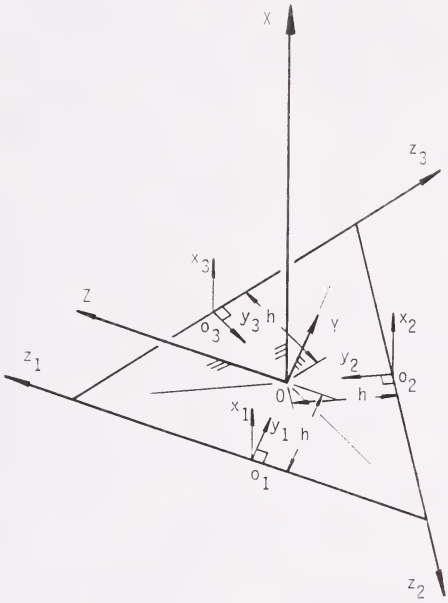

Figure 3.37 Coordinate systems of the ground-mounted R-L actuators in the arrangement of equilateral triangle form

$$A_{g1} = \begin{bmatrix} 1 & 0 & 0 & 0 \\ 0 & 1 & 0 & h \\ 0 & 0 & 1 & 0 \\ 0 & 0 & 0 & 1 \end{bmatrix}$$

$$A_{g2} = \begin{bmatrix} 1 & 0 & 0 & 0 \\ 0 & \cos(-120) & -\sin(-120) & h \\ 0 & \sin(-120) & \cos(-120) & 0 \\ 0 & 0 & 0 & 1 \end{bmatrix}$$

$$= \begin{bmatrix} 1 & 0 & 0 & 0 \\ 0 & -1/2 & \sqrt{3}/2 & h \\ 0 & -\sqrt{3}/2 & -1/2 & 0 \\ 0 & 0 & 0 & 1 \end{bmatrix}$$

$$A_{g3} = \begin{bmatrix} 1 & 0 & 0 & 0 \\ 0 & \cos(-240) & -\sin(-240) & h \\ 0 & \sin(-240) & \cos(-240) & 0 \\ 0 & 0 & 0 & 1 \end{bmatrix}$$

$$= \begin{bmatrix} 1 & 0 & 0 & 0 \\ 0 & -1/2 & -\sqrt{3}/2 & h \\ 0 & \sqrt{3}/2 & -1/2 & 0 \\ 0 & 0 & 0 & 1 \end{bmatrix}$$

With the substitution of these matrices into Eq. (3.24), we obtain

$$x_1 = X$$
$$y_1 = Y + h$$
$$z_1 = Z$$

$$x_2 = X$$
$$y_2 = -(1/2)Y + (\sqrt{3}/2)Z + h$$
$$z_2 = -(\sqrt{3}/2)Y - (1/2)Z$$

$$x_3 = X$$
$$y_3 = -(1/2)Y - (\sqrt{3}/2)Z + h$$
$$z_3 = (\sqrt{3}/2)Y - (1/2)Z$$

Thus the equations of the subworkspace can be expressed as follows:

$$F_{Ei} = x_i^2 + y_i^2 - (a_i + b_i)^2 \leq 0$$

and

$$F_{Ii} = x_i^2 + y_i^2 - r_{Ii}^2 \geq 0$$

where r_{Ii}^2 denotes r_{2i}^2 or r_{3i}^2 (see Fig. 3.36), can be respectively transformed to be expressed with respect to the global OXYZ system as follows:

$$F_{E1} = X^2 + (Y + h)^2 - (a_1 + b_1)^2 \leq 0 \qquad (3.25)$$

$$F_{E2} = X^2 + [-Y/2 + (\sqrt{3}/2)Z + h]^2 - (a_2 + b_2)^2 \leq 0 \qquad (3.26)$$

$$F_{E3} = X^2 + [-Y/2 - (\sqrt{3}/2)Z + h]^2 - (a_3 + b_3)^2 \leq 0 \qquad (3.27)$$

$$F_{I1} = X^2 + (Y + h)^2 - r_{I1}^2 \geq 0 \qquad (3.28)$$

$$F_{I2} = X^2 + [-Y/2 + (\sqrt{3}/2)Z + h]^2 - r_{I2}^2 \geq 0 \qquad (3.29)$$

$$F_{I3} = X^2 + [-Y/2 - (\sqrt{3}/2)Z + h]^2 - r_{I3}^2 \geq 0 \qquad (3.30)$$

where subscripts E and I denote the external and internal boundary, respectively.

The workspace of the platform of the manipulator with infinitesimal platform is the common reachable region of the three subworkspaces. Therefore the workspace of the manipulator is the region where Eqs. (3.25) - (3.30) are satisfied simultaneously.

The workspace can be expressed graphically by plotting the cross sections of the workspace on the planes normal to the axes of the system OXYZ. For the cross sections, Eqs. (3.25) - (3.27) are rewritten respectively as follows:

On plane OYZ, X = constant

$$Y = \pm \sqrt{(a_1 + b_1)^2 - X^2} - h \qquad (3.31)$$

$$Y = (\sqrt{3})Z + 2h \pm 2\sqrt{(a_2 + b_2)^2 - X^2} \qquad (3.32)$$

$$Y = -(\sqrt{3})Z + 2h \pm 2\sqrt{(a_3 + b_3)^2 - X^2} \qquad (3.33)$$

On plane OZX, Y = constant

$$X = \pm \sqrt{(a_1 + b_1)^2 - (Y + h)^2} \qquad (3.34)$$

$$X = \pm \sqrt{(a_2 + b_2)^2 - [-Y/2 + (\sqrt{3}/2)Z + h]^2} \qquad (3.35)$$

$$X = \pm \sqrt{(a_3 + b_3)^2 - [-Y/2 - (\sqrt{3}/2)Z + h]^2} \qquad (3.36)$$

On plane OXY, Z = constant

$$X = \pm \sqrt{(a_1 + b_1)^2 - (Y + h)^2} \qquad (3.37)$$

$$X = \pm \sqrt{(a_2 + b_2)^2 - [-Y/2 + (\sqrt{3}/2)Z + h]^2} \qquad (3.38)$$

$$X = \pm \sqrt{(a_3 + b_3)^2 - [-Y/2 - (\sqrt{3}/2)Z + h]^2} \qquad (3.39)$$

Similarly, Eqs. (3.28) - (3.30) can be rewritten by way of replacing the terms $(a_i + b_i)^2$ in Eqs. (3.31) - (3.39) by r_{Ii}^2, and are not listed.

Numerical example. The given parameters are as follows:

$a_1 = a_2 = a_3 = 3"$, $b_1 = b_2 = b_3 = 3"$, $h = 2"$ and $L = 4"$

The workspace of the manipulator is the common reachable region of three subworkspaces determined by the corresponding subchains. We thus can plot the cross section of the workspace on the plane, say OYZ, X = 4, plane, which is shown in Fig. 3.38. There are three pairs of parallel lines which denote the intersections of the external boundaries of subchains 1, 2 and 3, respectively, with the X = 4 plane. The areas between those parallel lines are the intersections of the workspaces of those subchains with the X = 4 plane. It is noted that the lengths of link a and b are equal, the radius of internal cylinder thus is zero, and there is no hole in the subworkspace. In Fig. 3.39, the cross section of the workspace on the plane OXY, Z = 0, is shown. The contour of the external boundary of the first subchain is a half circle and the contours of the second and third subchains are coincident half ellipses. The shaded

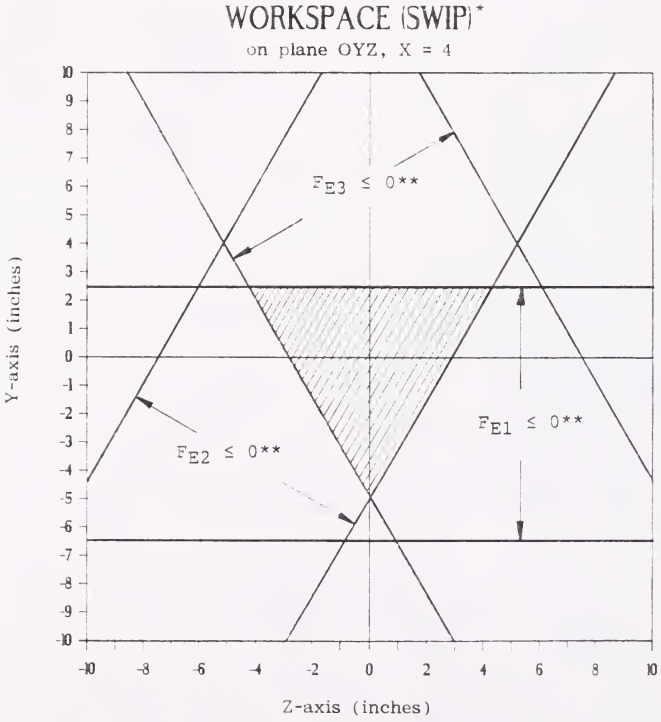

Figure 3.38 Workspace of the manipulator on plane OYZ as X = 4. *SubWorkspace, Infinitesimal Platform. **See Eqs. (3.25) - (3.27).

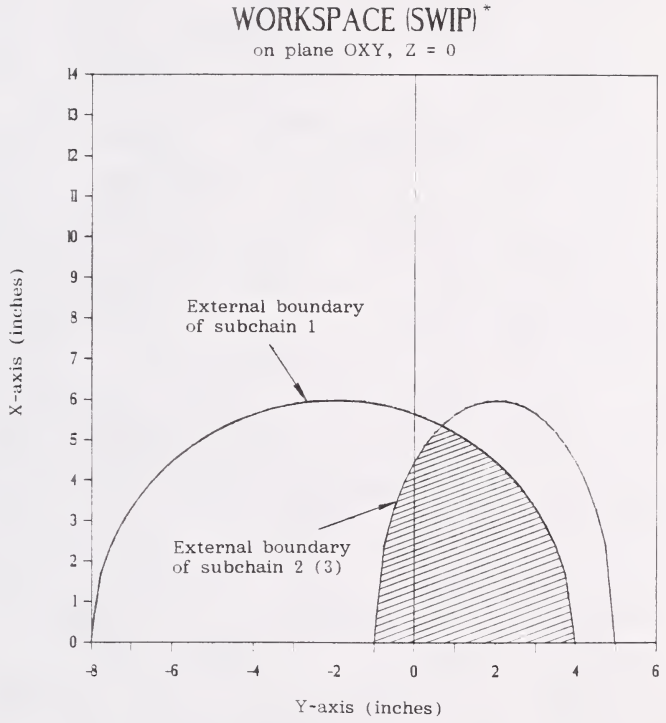

Figure 3.39 Workspace of the manipulator on plane OXY as Z = 0. *SubWorkspace, Infinitesimal Platform

area is the intersection of the workspace of the manipulator with infinitesimal platform with plane OXY, Z = 0.

3.9 Summary

A general approach for the workspace analysis of a parallel manipulator (shown in Fig. 3.1), which is a new area to be developed, has been presented in this chapter, considering the platform to be infinitesimally small.

In order to get the workspace of the manipulator, the shapes of the subworkspaces are illustrated first, then the boundaries of the subworkspaces and the root regions in the subworkspaces are determined.

Different combinations of joints in a chain create different surfaces. Torfason and Crossley [52] showed the surfaces generated by all closed spatial pairs. Jenkins, Crossley and Hunt [53] used the generated surface method to analyze the gross motion of the generating mechanism.

According to the equations derived in this chapter, the workspace of the manipulator depends on the length of the links, twist angles, offsets and the arrangements of the R-L actuators on the base (Fig. 3.2). As to the design requirements, the methods presented may help decide how to choose those parameters to achieve a desired workspace. The ground-mounted R-L actuators are initially assumed to have no limits on translation along their axes; but the actually needed maximum translations will be determined by the required boundaries.

The dimensions of the end-effector-carrying platform, on which the hand is mounted, are neglected in this chapter in order that the workspace of this type of parallel manipulator be more readily visualized at first. In Chapter 4, the workspace analysis in case of finite-size platform will be discussed. One of the problems that will be encountered in connection with the workspace is the interference between the links, which will affect the workspace. This is regarded as a subject for further study.

CHAPTER 4
THE WORKSPACE OF THE MANIPULATOR WITH FINITE SIZE PLATFORM

4.1 Introduction

This chapter deals with the workspace determined by the geometric method which was developed in Chapter 3 as well as the consideration of finite size platform of the manipulator. The lengths from the center of the platform, H, to the centers of the spherical joints, C_1, C_2 and C_3, affect the volume of the workspace, and more significantly, the rotatability of the platform about the center H. Thus, to get a workspace of the manipulator with rotatability of the end effector as large as possible, the lengths between H and C_i (i = 1, 2, 3) should be as small as possible, consistent with controllability of end-effector orientation. When, in the limit, the lengths are infinitesimal or zero, we get the largest theoretical workspace with complete, but uncontrollable rotatability of the platform.

The workspace of the parallel manipulator is defined here as the region within which every point can be reached by the center of the platform, H, of the manipulator (Fig. 3.19). The volume of the workspace is correlated with the orientation and the rotatability of the platform, because it is often important for a designer to know the rotatability

of the platform about its center in various regions of the workspace.

The surface where the platform can not rotate about H in any direction, when the center H is on that surface, is called the nonrotatability surface (NRS). The platform thus cannot assume an arbitrary prescribed orientation when H is on the NRS. The complete rotatability workspace (CRW) refers to the workspace within which or on whose boundary the platform can theoretically rotate in any direction. The region between the nonrotatability surface and the external boundary of the complete rotatability workspace can be called the partial rotatability workspace (PRW). The contours of the NRSS and CRSW of a subchain are shown schematically in Fig. 4.1.

4.2 Workspace of the Manipulator with Infinitesimal Platform

The workspace of the parallel manipulator is the common region of the three subworkspaces which are, respectively, the reachable regions of H, determined by subchain i (i = 1, 2 or 3), regardless of the constraints imposed by the other two subchains. In the case of the manipulator with hypothetically infinitesimal platform, point H is coincident with the three centers of the spherical joints, C_i at the corners of a finite size platform. The subworkspace of infinitesimal platform (SWIP) contains the reachable region of point C_i. Symbolically, they can be expressed in the form of the following inequalities:

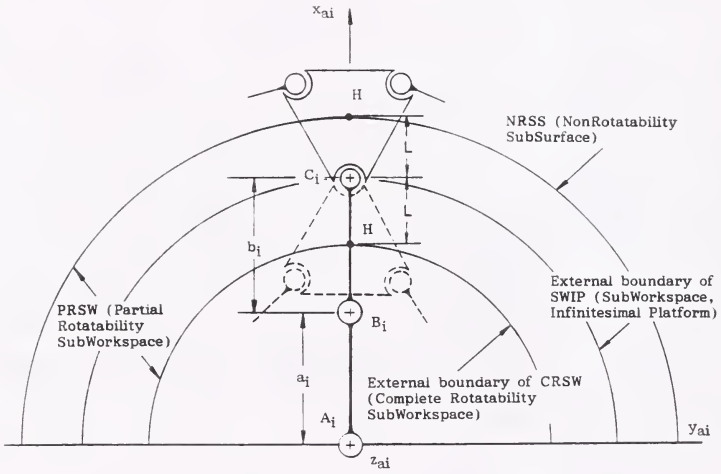

Figure 4.1 The relationships between the external boundaries of CRSW and NRSS of subchain i as $a_i = b_i$ (i = 1, 2 and 3)

$$F_{Ei}(X_m, Y_m, Z_m) \leq 0 \tag{4.1}$$

$$F_{Ii}(X_m, Y_m, Z_m) \geq 0 \tag{4.2}$$

Here the subscripts E and I denote respectively the external and internal boundaries. For distinction of the coordinates of the points on the boundaries of SWIP (SubWorkspace, Infinitesimal Platform) from those of the points inside the subworkspace of H, we use X_m, Y_m and Z_m to denote the coordinates derived in Chapter 3 for infinitesimal platform, and X, Y and Z are used in the following sections to denote the coordinates when a finite size platform is considered. The boundaries of the SWIP can then be respectively expressed symbolically by the corresponding equalities as

$$F_{Ei}(X_m, Y_m, Z_m) = 0 \tag{4.3}$$

$$F_{Ii}(X_m, Y_m, Z_m) = 0 \tag{4.4}$$

4.3 The Complete Rotatability Workspace (CRW) and the Partial Rotatability Workspace (PRW)

The platform can rotate about point C_i describing a whole sphere as the locus of point H, if we disregard link interferences and the constraints imposed by the other two subchains, even when point C_i is already on the external boundary of the i-th SWIP. This situation, with the finite dimensions of the platform, is depicted in Fig. 4.2, where C_i are at the vertices of an equilateral triangle with H at

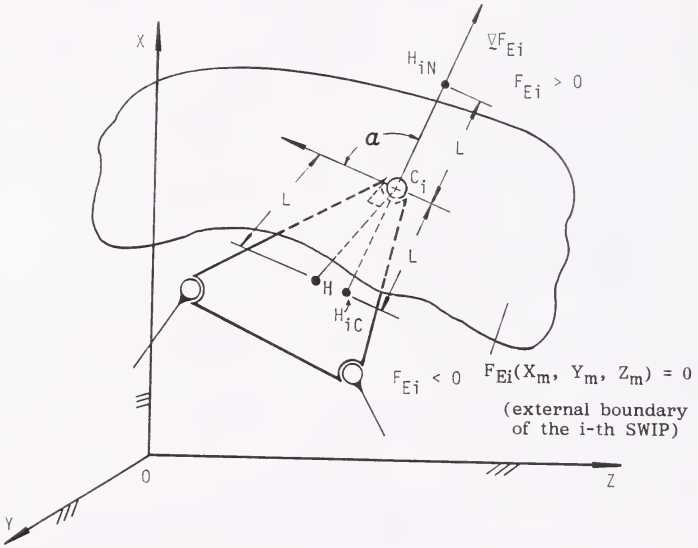

Figure 4.2 Rotatability of the finite size platform

its geometric center. Considering point H as the center of the rotation of the platform, however, the platform can usually rotate about it only in a portion of a sphere. The platform can rotate about H only in such a direction that the angle α between the velocity of point C_i moving with the rotating platform and the gradient ∇F_{Ei}, which points towards the outside of the SWIP, is greater than $\pi/2$. When the platform rotates so that $\overrightarrow{HC}_i$ approaches the direction of the gradient, then C_i moves inside the SWIP. Therefore, it does not prevent the platform from rotating. But in the opposite direction, C_i would move outside the SWIP, and therefore, it prevents the platform from rotating. This means that at this position of H, the platform has partial rotatability about the center H.

Referring to Fig. 4.2, let H_{iC} denote the point which is on the internal extension of the line of the gradient ∇F_{Ei}, and the distance from H_{iC} to the boundary equals the length of $\overline{C_iH}$ of the platform. The sense of $\overrightarrow{C_iH_{iC}}$ is opposite to that of the gradient. If the point H takes the place of H_{iC}, the instantaneous velocity of C_i, when the platform starts to rotate in any arbitrary direction, is perpendicular to ∇F_{Ei}. In this case point C_i moves either on the boundary or toward the inside of the SWIP. Disregarding link interference, the subchain i does not prevent the platform from rotating about point H, and therefore, the platform is said to have complete rotatability, so far as the i-th subchain is concerned. The

locus of all points H_{iC} constitutes the external boundary of the so called complete rotatability subworkspace (CRSW) determined by the subchain i. The CRW (Complete Rotatability Workspace) of the manipulator is the common region of the three CRSWs. Moreover, let us consider the other point H_{iN} on the line of the gradient ∇F_{Ei}, and with the same distance outside of the boundary as H_{iC} on the inside. The sense of $\overrightarrow{C_iH_{iN}}$ is the same as that of the gradient. One can easily verify that the locus of these H_{iN} points constitutes the so-called nonrotatability subsurface (NRSS). The region between the CRSW and NRSS is called the partial rotatability subworkspace (PRSW). After the three PRSWs of each of the three subchains have been obtained, one can find the manipulator's PRW (Partial Rotatability Workspace) as the common regions of the three PRSWs.

It should be noticed that for the complete rotatability subworkspace to exist, the short principal radius of curvature of the surface of the external boundary should be longer than L, the length of $\overline{C_iH}$ of the platform. Otherwise the arc drawn by point C_i centered at H_{iC} is on the outside of the SWIP as shown in Fig. 4.3, and therefore, point C_i would prevent the platform from rotating about H. For the manipulator with the R-L actuators with offset $s_{bi} = 0$, the external boundary of the SWIP is the cylinder of radius $(a_i + b_i)$ (see Fig. 3.21). Since the short principal radius of curvature of a cylinder is the radius of the cylinder

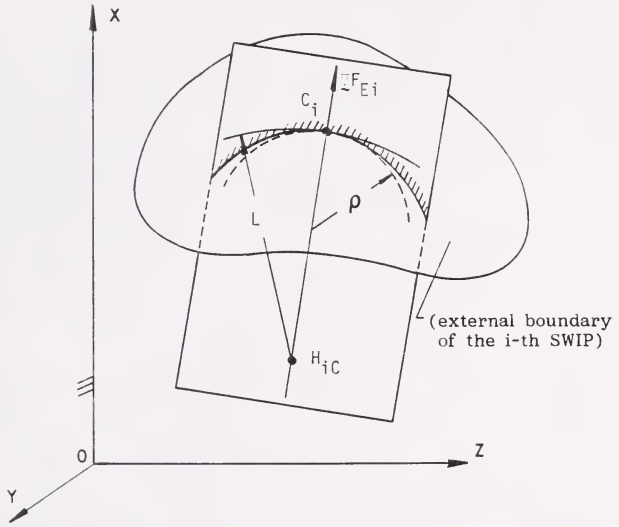

Figure 4.3 Radius of curvature of the external boundary of SWIP (SubWorkspace, Infinitesimal Platform)

itself, it is important to design the manipulator so that the condition $a_i + b_i > L$ be satisfied. Otherwise, the complete rotatability subworkspace does not exist. In fact, to make the CRSW as large as possible, the length of $\overline{C_iH}$, and thus the size of the platform, ought to be as small as possible. Mathematically, the coordinates of the point on the CRSW and the NRSS can be expressed respectively as

$$\begin{bmatrix} X \\ Y \\ Z \end{bmatrix}_{(CRSW)} = \begin{bmatrix} X_m \\ Y_m \\ Z_m \end{bmatrix} - \frac{\nabla F_{Ei}}{|\nabla F_{Ei}|} L \tag{4.5}$$

and

$$\begin{bmatrix} X \\ Y \\ Z \end{bmatrix}_{(NRSS)} = \begin{bmatrix} X_m \\ Y_m \\ Z_m \end{bmatrix} + \frac{\nabla F_{Ei}}{|\nabla F_{Ei}|} L \tag{4.6}$$

Generally the simultaneous solution of Eqs. (4.5) and (4.3) represents the equation of the external boundary of the CRSW, and the simultaneous solution of the Eqs. (4.6) and (4.3) represents the equation of the NRSS, where both are expressed in two of the three variables, X_m, Y_m and Z_m. For obtaining the implicit equations of the boundaries of the CRSW and NRSS correlating X, Y and Z, one can derive the expressions of X_m, Y_m and Z_m in terms of X, Y and Z from Eqs. (4.5) and (4.6), respectively, and then substitute the resulting expressions into Eq. (4.3).

For the manipulator shown in Fig. 3.19 and with the base arrangement in equilateral triangle form (see Fig. 3.37), Eqs. (4.3) for subchains 1, 2 and 3 have the following forms (see Eq. (3.25) - (3.27))

$$F_{E1} = X_m^2 + (Y_m + h)^2 - (a_1 + b_1)^2 = 0 \tag{4.7}$$

$$F_{E2} = X_m^2 + (-Y_m/2 + \sqrt{3}Z_m/2 + h)^2 - (a_2 + b_2)^2 = 0 \tag{4.8}$$

$$F_{E3} = X_m^2 + (-Y_m/2 - \sqrt{3}Z_m/2 + h)^2 - (a_3 + b_3)^2 = 0 \tag{4.9}$$

We now calculate the gradient of the first equation $F_{E1} = 0$, $\underset{\sim}{\nabla}F_{E1}$ as

$$\underset{\sim}{\nabla}F_{E1} = \begin{bmatrix} \partial F_{E1}/\partial X_m \\ \partial F_{E1}/\partial Y_m \\ \partial F_{E1}/\partial Z_m \end{bmatrix} = \begin{bmatrix} 2X_m \\ 2(Y_m + h) \\ 0 \end{bmatrix} \tag{4.10}$$

$$\begin{aligned} |\underset{\sim}{\nabla}F_{E1}| &= \sqrt{(\partial F_{E1}/\partial X_m)^2 + (\partial F_{E1}/\partial Y_m)^2 + (\partial F_{E1}/\partial Z_m)^2} \\ &= 2\sqrt{X_m^2 + (Y_m + h)^2} \\ &= 2(a_1 + b_1) \end{aligned} \tag{4.11}$$

Substituting expressions (4.10) and (4.11) into Eq. (4.5), we obtain

$$X = X_m - \frac{X_m L}{a_1 + b_1} \tag{4.12}$$

$$Y = Y_m - \frac{(Y_m + h)L}{a_1 + b_1} \tag{4.13}$$

$$Z = Z_m \tag{4.14}$$

Solving Eq. (4.12) - (4.14) for X_m, Y_m and Z_m in terms of X, Y and Z yields

$$X_m = \frac{X(a_1 + b_1)}{a_1 + b_1 - L} \tag{4.15}$$

$$Y_m = \frac{Y(a_1 + b_1) + hL}{a_1 + b_1 - L} \tag{4.16}$$

$$Z_m = Z \tag{4.17}$$

Finally, substituting expressions (4.15) - (4.17) into Eq. (4.7) yields the equation of the external boundary of the CRSW of the first subchain as

$$F_{EC1} = X^2 + (Y + h)^2 - (a_1 + b_1 - L)^2 = 0 \tag{4.18}$$

where the subscript C denotes complete rotatability.

Similarly, the equations of the external boundaries of the CRSW of the second and third subchains are found to be as follows:

$$F_{EC2} = X^2 + (-Y/2 + \sqrt{3}Z/2 + h)^2 - (a_2 + b_2 - L)^2 = 0 \tag{4.19}$$

$$F_{EC3} = X^2 + (-Y/2 - \sqrt{3}Z/2 + h)^2 - (a_3 + b_3 - L)^2 = 0 \tag{4.20}$$

In fact, the SWIP represented by Eq. (4.3) is a cylinder of radius $(a_i + b_i)$, and the CRSW is a coaxial cylinder of radius $(a_i + b_i - L)$. Therefore one can easily

write Eqs. (4.21) - (4.23) for the NRSS (NonRotatability SubSurface) directly by referring to Eqs. (4.18 - 4.20) as follows:

$$F_{SN1} = X^2 + (Y + h)^2 - (a_1 + b_1 + L)^2 = 0 \qquad (4.21)$$

$$F_{SN2} = X^2 + (-Y/2 + \sqrt{3}Z/2 + h)^2 - (a_2 + b_2 + L)^2 = 0 \qquad (4.22)$$

$$F_{SN3} = X^2 + (-Y/2 - \sqrt{3}Z/2 + h)^2 - (a_3 + b_3 + L)^2 = 0 \qquad (4.23)$$

where the subscripts S and N denote surface and nonrotatability, respectively.

Then we can obtain the external boundaries of the CRW of the manipulator by solving Eqs. (4.18) - (4.20) simultaneously. The PRW (Partial Rotatability Workspace) can be obtained as the following inequalities are satisfied:

$$F_{ECi}(X, Y, Z) > 0 \qquad (4.24)$$

and

$$F_{SNi}(X, Y, Z) < 0 \qquad (4.25)$$

where i = 1, 2 and 3.

The equations of the internal boundary of the CRSW of subchains 1, 2, and 3, which can be derived in a similar way, are expressed as follows:

$$F_{IC1} = X^2 + (Y + h)^2 - (r_{Ii} + L)^2 \geq 0 \qquad (4.26)$$

$$F_{IC2} = X^2 + [-Y/2 + (\sqrt{3}/2)Z + h]^2 - (r_{Ii} + L)^2 \geq 0 \quad (4.27)$$

$$F_{IC3} = X^2 + [-Y/2 - (\sqrt{3}/2)Z + h]^2 - (r_{Ii} + L)^2 \geq 0 \quad (4.28)$$

where r_{Ii} denotes r_{2i} or r_{3i} (see Fig. 3.36) and i = 1, 2 and 3. Once the internal boundaries of the three CRSWs have been obtained, the internal boundary of the CRW can be found as the common areas of the three CRSWs.

Numerical example. The given parameters are as follows:

$a_1 = a_2 = a_3 = 3"$, $b_1 = b_2 = b_3 = 3"$, $h = 2"$, $L = 1"$ and $X = 4"$

In Fig. 4.4, a cross section of the workspace of the manipulator is plotted on the plane OYZ, with X = 4. It is noticed that the complete rotatability workspace is very limited for this kind of manipulator, especially when the size of the platform is not small compared to the length of the links.

4.4 The Workspace of the Platform with Given Orientation

The workspace of the platform with given orientation on a plane is defined here as the reachable region on a plane of the center H of the platform, while the platform keeps moving with a given orientation. The simplest case is that the plane is perpendicular to one of the coordinate axes, X,

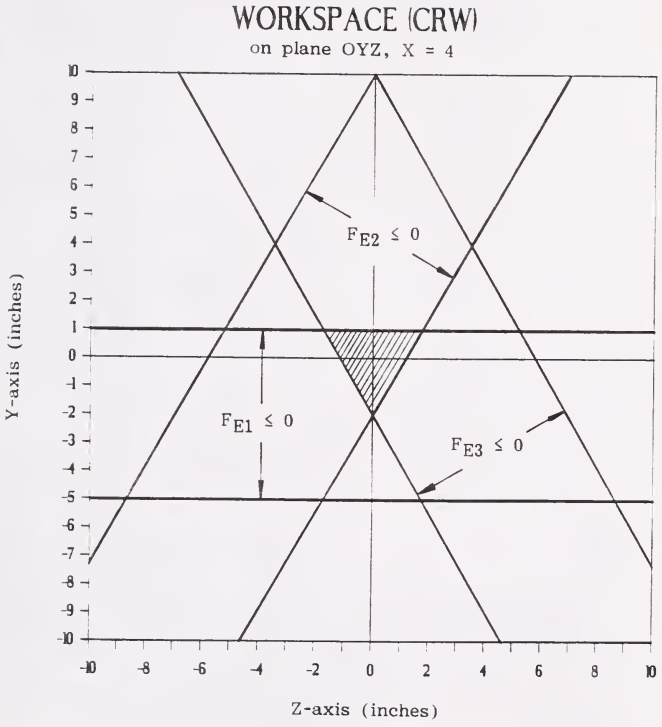

Figure 4.4 Complete rotatability workspace of the manipulator on plane OYZ, with X = 4

Y or Z of the fixed global system. All the points C_i are in that same plane.

When the point C_i of subchain i is on the intersection of the boundary of the SWIP with the plane, which plane is, for example, perpendicular to the X axis as shown in Fig. 4.5, the platform can rotate in the plane about the axis through H and normal to the plane in a portion of a circle. The platform can rotate only in such a direction that the point C_i moves inside the SWIP.

In general, the intersection of the SWIP with the plane are lines. They can be symbolically expressed as

$$F_{Ei}^{x}(X_m, Y_m, Z_m) = 0 \tag{4.29}$$

and

$$X_m = d \tag{4.30}$$

where the superscript x denotes the normal of the plane, the subscript E implies the external boundary, d is a constant distance from the origin and i = 1, 2 and 3. Since the procedures of the analysis for the external and internal boundaries are similar to each other, we discuss only positions on the external boundary in the following section. The workspace inside the external boundary is expressed by inequality (one for each subchain):

$$F_{Ei}^{x}(X_m, Y_m, Z_m) < 0, \quad i = 1, 2, 3 \tag{4.31}$$

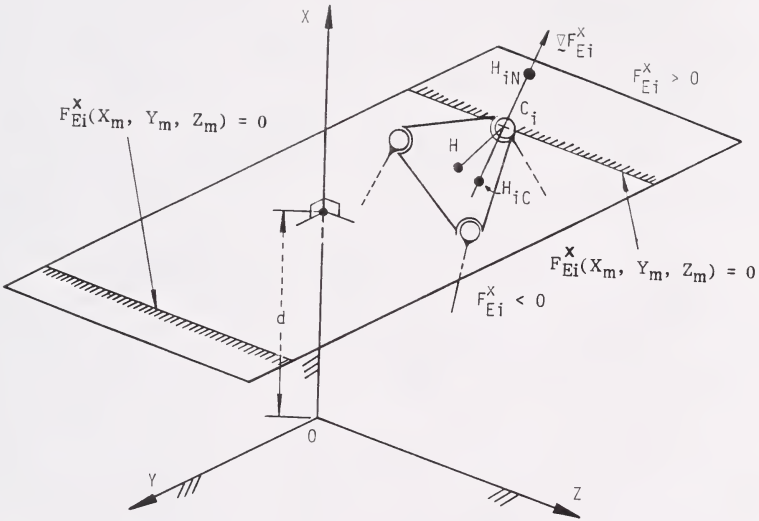

Figure 4.5 Schematic drawing of the positions of points H_{iC} and H_{iN} when the platform keeps moving in a plane perpendicular to the X axis of the global coordinate system (no scale)

The gradient of $F_{Ei}{}^{X}$ can be expressed as follow:

$$\nabla F_{Ei}{}^{X} = [0,\ \partial F_{Ei}{}^{X}/\partial Y_m,\ \partial F_{Ei}{}^{X}/\partial Z_m]^T \tag{4.32}$$

and points toward the outside of the boundary.

Let H_{iC} and H_{iN} be the points on the line of the gradient such that the distance from these two points to the boundary is L (the same as $\overline{C_iH}$), and the sense of $\overrightarrow{C_iH_{iC}}$ is opposite to that of the gradient and the sense of $\overrightarrow{C_iH_{iN}}$ is the same as that of gradient. It is seen that when the center H takes the position of H_{iC}, the platform reaches a limiting position in the direction of the gradient with complete rotatability about H, provided we disregard link interference and the constraints imposed by the other two subchains. This means that the locus of points H_{iC} constitutes the external boundary of the CRSW with the platform remaining in the given plane. Similarly, one can see that the locus of points H_{iN} constitutes the intersection of the NRSS with the plane.

The coordinates of the points H_{iC} and H_{iN} when H is on the plane can be expressed by Eq. (4.5) and (4.6) with X = d. The simultaneous solution of Eqs. (4.5) and (4.29), therefore, represents the intersection of the external boundary of the CRSW with the plane X = d, and the simultaneous solution of Eqs. (4.6) and (4.29) represents the intersection of the NRSS with the plane X = d. Having the equations of the intersection lines of the boundaries of

the three CRSWs and the three NRSSs of the three subchains with the plane X = d, the intersections of the CRW and PRW of the manipulator with the plane X = d are the common regions of the former intersections.

For the manipulator shown in Fig. 3.19 and, with the base arrangement in equilateral triangle form (Fig. 3.37), for example, the intersection of the SWIP determined by the first subchain with the YZ plane (X = d) is described as (see Eq. 3.31)

$$Y_m = -h \pm \sqrt{(a_1 + b_1)^2 - X_m^2} \tag{4.33}$$

where X_m is a constant, and therefore this equation represents two straight lines parallel to the Z axis. To express the subworkspace, Eq. (4.33) ought to be written individually for these two lines, two branches of the intersections of the boundary with plane X = constant, as

$$F_{E1}{}^X(X_m, Y_m, Z_m) = Y_m + h - \sqrt{(a_1 + b_1)^2 - X_m^2} \leq 0 \tag{4.34}$$

and

$$F_{E1}{}^X(X_m, Y_m, Z_m) = -(Y_m + h) - \sqrt{(a_1 + b_1)^2 - X_m^2} \leq 0 \tag{4.35}$$

The gradients of the two half-planes defined by these two inequalities are

$$\nabla F_{E1}{}^X = (0, 1, 0)^T \tag{4.36}$$

and

$$\nabla F_{E1}{}^X = (0, -1, 0)^T \tag{4.37}$$

Substituting the expressions (4.36) and (4.37) into Eq. (4.5), the boundary of the CRW becomes these two lines:

$$X = X_m$$
$$Y = Y_m - L \tag{4.38}$$
$$Z = Z_m$$

and

$$X = X_m$$
$$Y = Y_m + L \tag{4.39}$$
$$Z = Z_m$$

Furthermore, substituting Eqs. (4.38) and (4.39) into (4.34) and (4.35) respectively, we obtain the two corresponding lines of the intersections of the CRSW with the plane X = constant expressed in X, Y and Z as

$$Y + L + h - \sqrt{(a_1 + b_1)^2 - X^2} \leq 0 \tag{4.40}$$

and

$$-(Y - L + h) - \sqrt{(a_1 + b_1)^2 - X^2} \leq 0 \tag{4.41}$$

where X is a constant.

The intersection with the plane can be expressed in one equation which has a form similar to Eq. (4.33) as

$$Y = -h \pm \sqrt{(a_1 + b_1)^2 - X^2} \pm (-L) \tag{4.42}$$

where X is a constant and therefore Eq. (4.42) also represents two straight lines parallel to the Z axis.

Similarly, the equations of the external boundaries of the CRSW of the second and third subchains are found to be as follows:

$$F_{E2C}{}^{X} = X^2 + (-Y/2 + \sqrt{3}Z/2 + h + L)^2 - (a_2 + b_2)^2 = 0 \tag{4.43}$$

$$F_{E3C}{}^{X} = X^2 + (-Y/2 - \sqrt{3}Z/2 + h + L)^2 - (a_3 + b_3)^2 = 0 \tag{4.44}$$

Numerical example. The given parameters are as follows:

$a_1 = a_2 = a_3 = 3"$, $b_1 = b_2 = b_3 = 3"$, $h = 2"$, $L = 1"$ and $X = 4"$

In Fig. 4.6, a cross section of the workspace of the manipulator is plotted on the plane $X = 4$. It is noticed that the complete rotatability workspace is larger than the cross section of the workspace as shown in Fig. 4.4. However, the cross section of the workspace of the manipulator is still very limited.

The equations for the NRSSs determined by the corresponding subchains can be derived in a similar way and are therefore not described here.

The foregoing discussion applies to the case where the given plane is perpendicular to one of the axes of the global coordinate system. In a general case, where the plane is inclined to the axes of the system, the gradient of

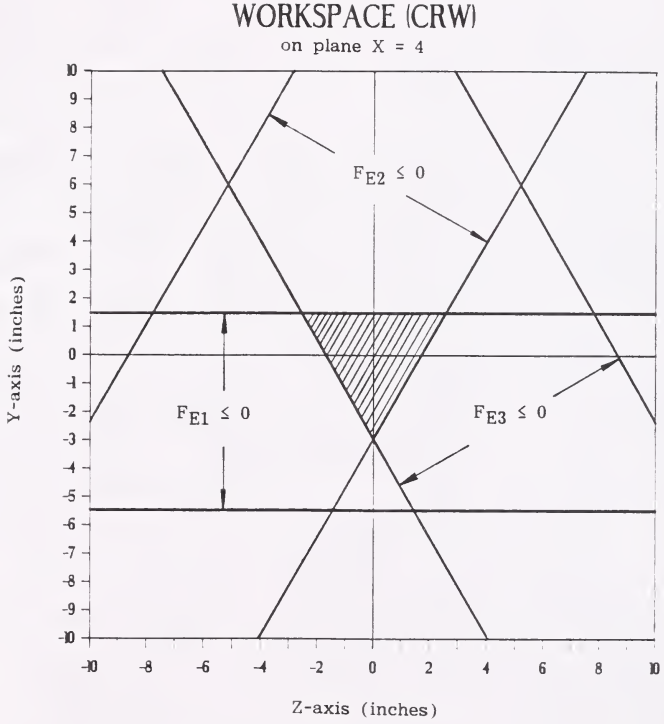

Figure 4.6 Complete rotatability workspace of the manipulator on plane X = 4

the intersection of the SWIP with the given plane can be obtained by coordinate transformation.

The given plane can be specified by its normal $\underset{\sim}{N}$ and the shortest distance to the plane from the origin of the global system, d. We can set a new reference system Oxyz with the x axis coincident with the normal of the plane, and with the origin coincident with the origin of the old system as shown in Fig. 4.7. The axis y is set to be perpendicular to both the axis X of the old system and the normal. Let $\underset{\sim}{n}$, $\underset{\sim}{r}$, and $\underset{\sim}{s}$ now be unit vectors on the three new axes of x, y and z, respectively. The unit vector $\underset{\sim}{n}$ is given as

$$\underset{\sim}{n} = (n_x, n_y, n_z)^T$$

Then

$$\underset{\sim}{r} = \underset{\sim}{i} \times \underset{\sim}{n} = \begin{bmatrix} i & j & k \\ 1 & 0 & 0 \\ n_x & n_y & n_z \end{bmatrix} = (0, -n_z, n_y)^T$$

$$\underset{\sim}{s} = \underset{\sim}{n} \times \underset{\sim}{r} = \begin{bmatrix} i & j & k \\ n_x & n_y & n_z \\ 0 & -n_z & n_y \end{bmatrix} = (n_y^2 + n_z^2, -n_x n_y, -n_x n_z)^T$$

The transformation matrix from the new system to the old one can be written as

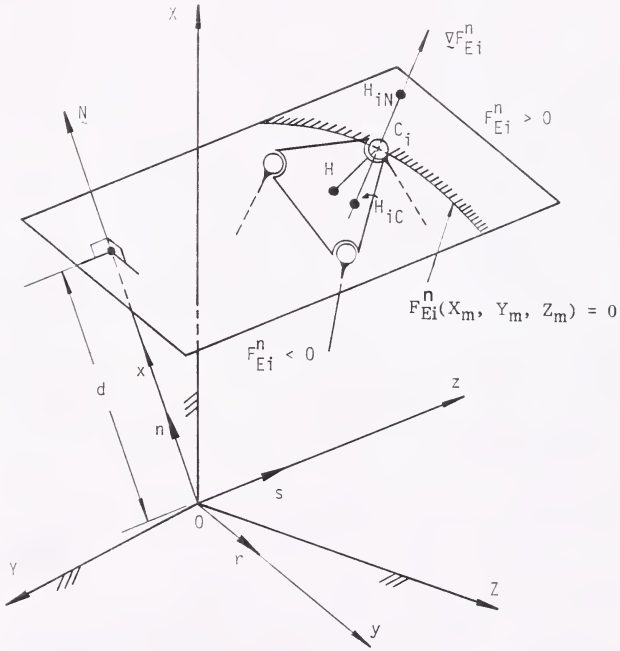

Figure 4.7 The positions of points H_{iC} and H_{iN} when the platform keeps moving in a plane inclined to the axes of the global coordinate system

$$A = \begin{bmatrix} n_x & r_x & s_x & 0 \\ n_y & r_y & s_y & 0 \\ n_z & r_z & s_z & 0 \\ 0 & 0 & 0 & 1 \end{bmatrix} = \begin{bmatrix} n_x & 0 & n_y^2 + n_z^2 & 0 \\ n_y & -n_z & -n_x n_y & 0 \\ n_z & n_y & -n_x n_z & 0 \\ 0 & 0 & 0 & 1 \end{bmatrix}$$

Using the transformation of

$$\begin{bmatrix} X \\ Y \\ Z \\ 1 \end{bmatrix} = A \begin{bmatrix} x \\ y \\ z \\ 1 \end{bmatrix} = \begin{bmatrix} xn_x + z(n_y^2 + n_z^2) \\ xn_y - yn_z - zn_x n_y \\ xn_z + yn_y - zn_x n_z \\ 1 \end{bmatrix}$$

the equation of the boundary of the SWIP originally expressed with respect to the global system OXYZ can be transformed to be expressed with respect to the new system Oxyz. For example, Eq. (4.7) of the external boundary of the SWIP of the first subchain can be transformed to be expressed with respect to the new system as

$$F_{E1} = [X_m n_x + Z_m(n_y^2 + n_z^2)]^2 + [X_m n_y - Y_m n_z - Z_m n_x n_z + h]^2 - (a_1 + b_1)^2 = 0 \qquad (4.45)$$

where X_m is a constant.

Eq. (4.45) represents the intersection of the boundary with the given plane with respect to the new system Oxyz. In the above equations the subscript m denotes that the

corresponding coordinates are of the point on the SWIP. The gradient of the intersection expressed with respect to the new system can be obtained as

$$\underset{\sim}{\nabla} F_{E1}{}^{n} = (0,\ \partial F_{E1}/\partial Y_m,\ \partial F_{E1}/\partial Z_m) \tag{4.46}$$

where the superscript n denotes that the gradient is on the plane whose normal is $\underset{\sim}{N}$, and from Eq. (4.45) one can obtain

$$\partial F_{E1}/\partial Y_m = 2(X_m n_Y - Y_m n_Z - Z_m n_X n_Z + h)(-n_Z) \tag{4.47}$$

and

$$\partial F_{E1}/\partial Z_m = 2[X_m n_X + Z_m(n_Y{}^2 + n_Z{}^2)](n_Y{}^2 + n_Z{}^2) + 2(X_m n_Y - Y_m n_Z - Z_m n_X n_Z + h)(-n_X n_Z) \tag{4.48}$$

Let G_Y and G_Z denote respectively $\partial F_{E1}/\partial Y_m$ and $\partial F_{E1}/\partial Z_m$ expressed by Eqs. (4.47) and (4.48). Then we can obtain

$$|\underset{\sim}{\nabla} F_{E1}{}^{n}| = \sqrt{G_Y{}^2 + G_Z{}^2} \tag{4.49}$$

Substituting Eqs. (4.46), (4.47), (4.48) and (4.49) into Eq. (4.5), we obtain the coordinates of point H_{1C}, the limiting position of point H where the platform has complete rotatability in the given plane, as follows:

$$x = X_m \tag{4.50}$$

$$y = Y_m - G_Y L/\sqrt{G_Y{}^2 + G_Z{}^2} \tag{4.51}$$

$$z = Z_m - G_z L/\sqrt{G_y^2 + G_z^2} \qquad (4.52)$$

The simultaneous solution of Eqs. (4.50) - (4.52) and (4.45) represents the equation of the external boundary of the CRSW of the first subchain on the plane, correlating Y_m and Z_m expressed in the new system Oxyz.

Finally we can use the inverse transformation A^{-1}

$$\begin{bmatrix} x \\ y \\ z \\ 1 \end{bmatrix} = A^{-1} \begin{bmatrix} X \\ Y \\ Z \\ 1 \end{bmatrix}$$

and transform the coordinates of the point on the boundary defined by Eq. (4.50) - (4.52) combined with Eq. (4.45) to be expressed with respect to the global system OXYZ.

That is the method of transforming the SWIP in the plane to be expressed with respect to a new reference where the given plane is perpendicular to one of the axes. Then in the new reference the gradient of the boundary in the given plane and the coordinates of the point on the CRSW or NRSS are respectively calculated. Finally, the results are transformed back to be expressed with respect to the global system using inverse transformation. This procedure will be taken for the three subworkspaces with complete rotatability or nonrotatability of the platform, and the corresponding workspace of the manipulator is obtained as the common region of these three subworkspaces.

4.5 Summary

Two sorts of the workspace, the complete rotatability workspace (CRW) and partial rotatability workspace (PRW), of the parallel manipulator with finite size platform are studied in this chapter. The nonrotatability surface (NRS) and the boundaries of the complete rotatability workspace are parallel to the boundary of the workspace of the manipulator with infinitesimal platform (WIP). The complete rotatability workspace is inside, and the nonrotatability surface is outside of the WIP.

The cross sections of the CRW of the manipulator are plotted on the plane OYZ, with X = constant and on the plane, X = constant, where the platform can only move around, respectively. The workspace of this type of manipulator is limited.

For a workspace with complete rotatability to be as large as possible, the size of the platform should be as small as possible. For a large partial rotatability workspace, the size of the platform should be as large as possible.

CHAPTER 5
MECHANICAL ERROR ANALYSIS OF THE MANIPULATOR

5.1 Introduction

In the control of robotic manipulators, the primary task is to drive the links to their desired positions corresponding to a given input. Actuators are the devices that make the robot move. The mechanical error is defined as the minor inaccuracies in displacements (translation and rotation) of the actuators for a certain specified hand position. In order to increase the accuracy of the desired hand position, we must reduce all errors as far as possible.

In this chapter, a six-degree-of-freedom parallel manipulator with ground-mounted actuators, as shown in Fig. 3.1, has been studied from the viewpoint of mechanical error analysis. Ground-mounted actuators in parallel manipulators avoid the dynamic errors caused in serial manipulators by those actuators mounted on the movable links, away from the ground. Therefore, the mechanical errors of parallel manipulators with ground-mounted actuators are due to the input angle and translation errors of the actuators, if the tolerances of the link lengths are not considered. In the study of position and orientation of the hand (end-effector) embedded in the platform, we may use inverse kinematics to transform the pose (position and

orientation) of the hand to a global coordinate system by homogeneous transformation matrices. The determination of joint velocities using screws, presented by Mohamed and Duffy [46] and Sugimoto [47], is adapted in this chapter to describe the velocities and small displacements.

With consideration of input errors as differential motions, we will obtain the corresponding error movement of the platform, in which the hand is embedded, due to the inaccuracies of the actuators.

5.2 Position Analysis

A subchain of a six-degree-of-freedom parallel manipulator, where all the actuators are ground-mounted, is shown schematically in Fig. 5.1. Let $\underline{H}$ denote the position vector of the hand which is embedded on the platform, and $\underline{l}$, $\underline{m}$ and $\underline{n}$ denote the unit vectors describing the hand orientation of the moving system. By using homogeneous transformation, we can describe the relative position and orientation between any two coordinate frames. Therefore, we can have the coordinate transformation matrix T_p as follow:

$$T_p = \begin{bmatrix} l_x & m_x & n_x & H_x \\ l_y & m_y & n_y & H_y \\ l_z & m_z & n_z & H_z \\ 0 & 0 & 0 & 1 \end{bmatrix} \tag{5.1}$$

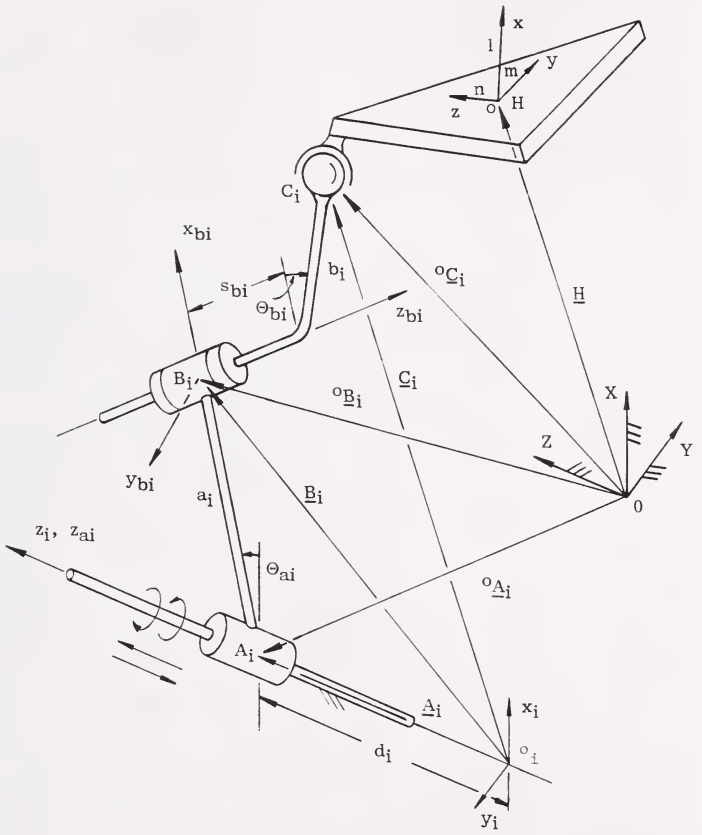

Figure 5.1 The i-th subchain of the manipulator, with R-L actuator at A_i

where $\underline{l}_i$, $\underline{m}_i$ and $\underline{n}_i$ are the components of the basis unit vectors of the hand coordinate system, H_i are the components of the hand position vector and i = x, y and z. The position vector of point C_i with respect to OXYZ then can be calculated from the following equation:

$$^{o}\underline{C}_i = T_p \, ^{m}(\overrightarrow{HC}_i) \tag{5.2}$$

where $^{m}(\overrightarrow{HC}_i)$ denotes the vector $\overrightarrow{HC}_i$ with respect to the moving coordinate system Hxyz. We can also find another coordinate transformation matrix T_i, from $o_i x_i y_i z_i$ to OXYZ, which can be expressed as

$$T_i = \begin{bmatrix} x_{ix} & y_{ix} & z_{ix} & Oo_{ix} \\ x_{iy} & y_{iy} & z_{iy} & Oo_{iy} \\ x_{iz} & y_{iz} & z_{iz} & Oo_{iz} \\ 0 & 0 & 0 & 1 \end{bmatrix} \tag{5.3}$$

According to the relationship between the coordinate systems, we can have the following equations:

$$^{o}\underline{C}_i = T_i \underline{C}_i \tag{5.4}$$

or

$$\underline{C}_i = (T_i)^{-1} \, ^{o}\underline{C}_i \tag{5.5}$$

where

$$(T_i)^{-1} = \begin{bmatrix} x_{ix} & x_{iy} & x_{iz} & -Oo_i \cdot x_i \\ y_{ix} & y_{iy} & y_{iz} & -Oo_i \cdot y_i \\ z_{ix} & z_{iy} & ziz & -Oo_i \cdot z_i \\ 0 & 0 & 0 & 1 \end{bmatrix} \tag{5.6}$$

and $\underline{x}_i$, $\underline{y}_i$ and $\underline{z}_i$ are unit vectors along the axes of $^{o_i}x_iy_iz_i$.

The coordinates of point C_i with respect to the system $^{o_i}x_iy_iz_i$ can be used to determine the necessary joint displacements by inverse kinematics, which is described in detail in Chapter 2.5.1. It is noted that there are four possible sets of solutions for a given location and orientation of the hand. Each set of solutions corresponds to a specific configuration of branches of the subchains. Calculation of Jacobian and error analyses should be performed in the same branch.

In Fig. 5.1, the position vectors $^{o}\underline{A}_i$, $^{o}\underline{B}_i$ and unit vectors $^{o}\underline{z}_{ai}$ and $^{o}\underline{z}_{bi}$ with respect to the global coordinate system OXYZ can be calculated respectively by coordinate transformation, and can be expressed as follows:

$$^{o}\underline{A}_i = T_i\underline{A}_i \tag{5.7}$$

$$^{o}\underline{B}_i = T_i\underline{B}_i \tag{5.8}$$

$$^{o}\underline{z}_{ai} = T_i\underline{z}_{ai} \tag{5.9}$$

$$^{o}\underline{z}_{bi} = T_i\underline{z}_{bi} \tag{5.10}$$

5.3 Reciprocal Screws

A screw is defined by Ball [54] as a straight line with which a definite linear magnitude termed the pitch is associated. If (L, M, N; P, Q, R) are the Plücker coordinates, as shown in Fig. 5.2, of the screw axis, (L, M,

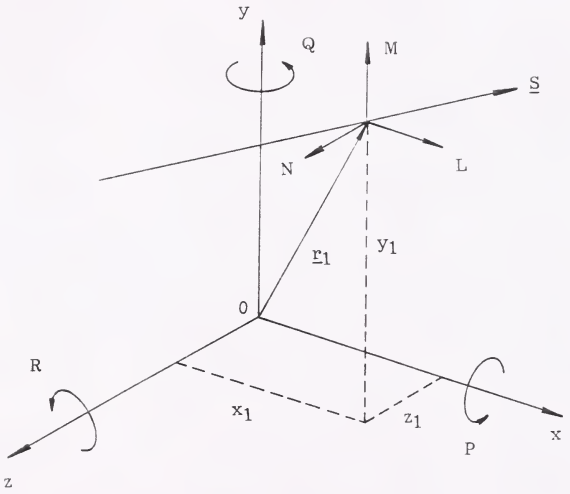

Figure 5.2 Plücker line coordinates

N) are the direction ratios of the line and (P, Q, R) are the x, y and z components of the moment of the line about the origin, then we can express the screw coordinates as $(\underline{S} ; \underline{S}_o)$ where

$$\underline{S} = L\underline{i} + M\underline{j} + N\underline{k} \tag{5.11}$$

$$\underline{S}_o = P\underline{i} + Q\underline{j} + R\underline{k} \tag{5.12}$$

and

$$L = x_2 - x_1$$

$$M = y_2 - y_1$$

$$N = z_2 - z_1$$

$$P = y_1N - z_1M$$

$$Q = -x_1N + z_1L$$

$$R = x_1M - y_1L$$

Figure 5.3 shows a rigid body which is constrained to move on a screw $\$_2 = (\underline{S}_2; \underline{S}_{o2})$. A wrench $(\underline{f}_1; \underline{C}_1)$ of intensity f_1 is applied to the body on a screw $\$_1 = (\underline{S}_1; \underline{S}_{o1})$ and it produces a twist $(\underline{\omega}_2; \underline{v}_2)$ of amplitude ω_2 on the screw $\$_2$. Thus the moment of the force $\underline{f}_1$ about the point A is $a_{12}\underline{a}_{12} \times \underline{f}_1$, and the virtual work produced by the wrench can be expressed as follow:

$$U = \underline{f}_1 \cdot \underline{v}_2 + \underline{C}_1 \cdot \underline{\omega}_2 - a_{12}\underline{a}_{12} \times \underline{f}_1 \cdot \underline{\omega}_2 \tag{5.13}$$

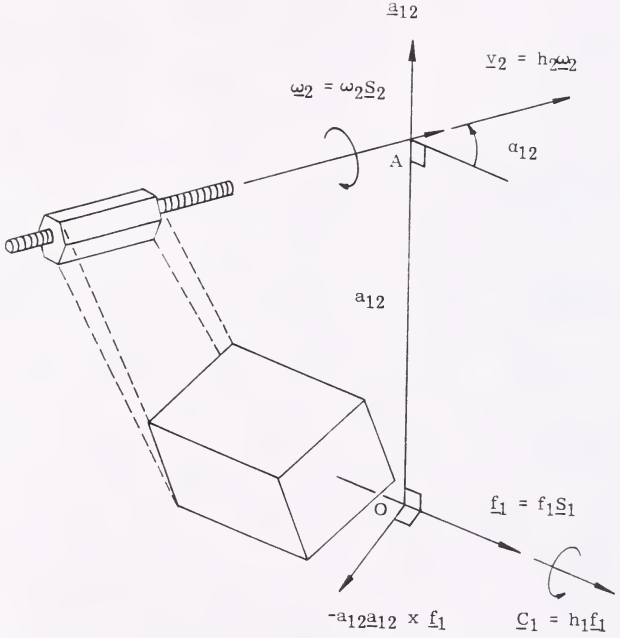

Figure 5.3 A wrench on a screw

Substituting $\underline{f}_1 = f_1\underline{S}_1$, $\underline{C}_1 = h_1 f_1 \underline{S}_1$, $\underline{\omega}_2 = \omega_2\underline{S}_2$ and $\underline{v}_2 = h_2\omega_2\underline{S}_2$ into Eq. (5.13), the virtual work produced by the wrench can thus be expressed as

$$U = f_1\omega_2 \{(h_1 + h_2)\cos\alpha_{12} - a_{12}\sin\alpha_{12}\} \tag{5.14}$$

If the pitches h_1 and h_2, the twist angle α_{12}, and mutual perpendicular distance a_{12} between the axes $\underline{S}_1$ and $\underline{S}_2$ of the two screws are chosen such that

$$(h_1 + h_2)\cos\alpha_{12} - a_{12}\sin\alpha_{12} = 0 \tag{5.15}$$

then the wrench cannot produce motion on the screw $\underline{\$}_2$ no matter how large is the intensity f_1. The screws $\underline{\$}_1$ and $\underline{\$}_2$ are then said to be reciprocal. It is noted that Eq. (5.15) is symmetrical, and a wrench on the screw $\underline{\$}_2$ cannot produce motion on the screw $\underline{\$}_1$.

Hunt [49] shows that, when the line of action of a force passes through an axis of an revolute pair, the force does not affect the rotation around the revolute pair because it cannot exert any moment about it. Reciprocity between a force $\underline{F}$ and an angular velocity $\underline{\omega}$ about an revolute pair axis means that when a body is attached to a base through a single revolute pair about which it can turn at an angular velocity $\underline{\omega}$ at any instant, a force $\underline{F}$ is reciprocal to $\underline{\omega}$ when its contribution to the rate of working is zero. For the prismatic pair, when the line of action of

a force is perpendicular to the direction of the prismatic pair, there is no contribution by this force to the rate of working. Also, an revolute pair perpendicular to the direction of a couple also satisfies the condition of reciprocity. All couples, no matter how they are oriented, are reciprocal to a pure translation in a direction parallel to a prismatic pair. Therefore, if a body is constrained to move about an ISA (Instantaneous Screw Axis), ζ, a wrench acting on a screw ζ' can contribute nothing to the rate at which work is being done on the body. In such a circumstance ζ and ζ' are said to be reciprocal screws.

The necessary and sufficient condition for a pair of screws, $\underline{\$}_1 = \underline{S}_1 + \varepsilon\underline{S}_{o1}$ and $\underline{\$}_2 = \underline{S}_2 + \varepsilon\underline{S}_{o2}$, to be reciprocal can thus be expressed as

$$\underline{\$}_1 \circ \underline{\$}_2 = \underline{S}_1 \cdot \underline{S}_{o2} + \underline{S}_2 \cdot \underline{S}_{o1} = 0 \qquad (5.16)$$

where the symbol $\circ$ denotes the reciprocal product of a pair of screws.

5.4 Screws of the Relative Motion of the Joints

In order to calculate the screws representing the relative motion of the joints, we would like to have each joint expressed with respect to the global system OXYZ.

Let $\omega_{ji}(\underline{S}_{ji}, \underline{S}_{oji})$ denote the motion screws of the joints with respect to the OXYZ system, where $j = 1, 2, \ldots,$ 6 denote the joints and $i = 1, 2$ and 3 denote the subchain. Thus, representations of the screws are

Cylindric joint A_i $\quad \$_{1i} = \omega_{1i}(\underline{S}_{1i}, {}^{O}\underline{A}_i \times \underline{S}_{1i})$

$\$_{2i} = v_{2i}(0, \underline{S}_{1i})$

Revolute joint B_i $\quad \$_{3i} = \omega_{3i}(\underline{S}_{3i}, {}^{O}\underline{B}_i \times \underline{S}_{3i})$

Spherical joint C_i $\quad \$_{4i} = \omega_{4i}(\underline{i}, {}^{O}\underline{C}_i \times \underline{i})$

$\$_{5i} = \omega_{5i}(\underline{j}, {}^{O}\underline{C}_i \times \underline{j})$

$\$_{6i} = \omega_{6i}(\underline{k}, {}^{O}\underline{C}_i \times \underline{k})$

where $\underline{S}_{1i} = {}^{O}\underline{z}_{ai}$ and $\underline{S}_{3i} = {}^{O}\underline{z}_{bi}$.

Since we deal with instantaneous kinematics, the spherical joint C_i may be considered as a combination of three revolute joints whose concurrent axes are parallel to the axes of the OXYZ system.

Mohamed and Duffy [46] used orthogonal screws to study the instantaneous kinematics of the end-effector platform of fully parallel robot type devices. They demonstrated that for any parallel device the twist representing the instantaneous motion of the end-effector platform is equal to the sum of its partial twists. A partial twist is defined as the twist representing the instantaneous motion of the end-effector when all actuators other than the input actuator are locked.

We can find the reciprocal screws, ${}^{r}\$_{1i}$ and ${}^{r}\$_{2i}$, reciprocal to all other screws in subchain i but $\$_{1i}$ and $\$_{2i}$, respectively. As shown in Fig. 5.4, the reciprocal screw ${}^{r}\$_{1i}$ passes through the center of spherical joint C_i, intersects the axis of revolute joint B_i and also lies on the plane P which is perpendicular to the axis of cylindric joint A_i. In Fig. 5.5, the reciprocal screw ${}^{r}\$_{2i}$ passes

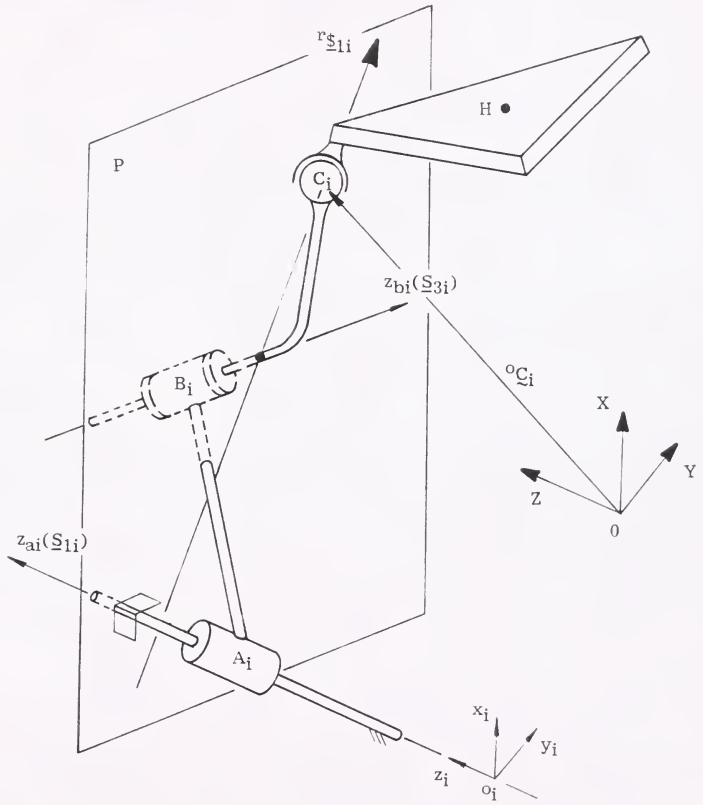

Figure 5.4 Reciprocal screw $^{r}\underline{\$}_{1i}$ reciprocal to all other screws in subchain i but $\underline{\$}_{1i}$

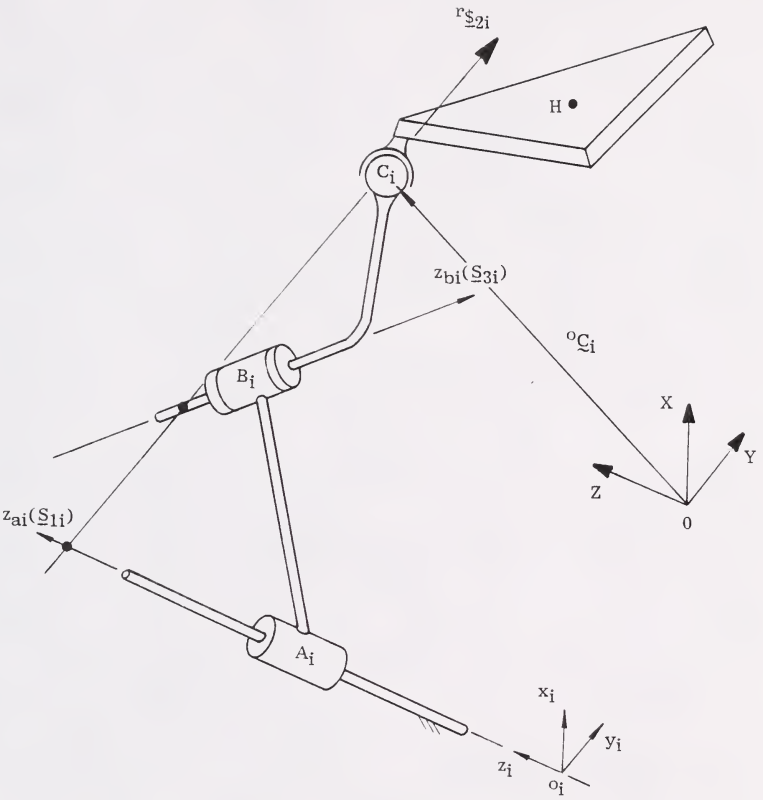

Figure 5.5 Reciprocal screw $^{r}\underline{\$}_{2i}$ reciprocal to all other screws in subchain i but $\underline{\$}_{2i}$

through the center of spherical joint C_i and intersects both the axes of joints A_i and B_i. A numerical example is given to illustrate how to obtain such reciprocal screws as follow:

Numerical example. With the base arrangement of the manipulator shown in Fig. 3.37 and the dimensions of the first subchain given as follows:

$a_1 = 3$, $b_1 = 2$, $s_{b1} = 1$, $h = 1$, $\alpha_{b1} = -90°$ and ${}^{o}\underline{C}_1 = [4.000, 0.000, 2.732]^T$,

one set of the four possible solutions can be obtained as $d_1 = 1$, $\theta_{a1} = 0°$ and $\theta_{b1} = -60°$ (see Section 2.5.1). Therefore, the position vectors of joints A_1 and B_1 with respect to the global coordinate system OXYZ can be calculated as

$$ {}^{o}\underline{A}_1 = \begin{bmatrix} 0.000 \\ -1.000 \\ 1.000 \end{bmatrix} \text{ and } {}^{o}\underline{B}_1 = \begin{bmatrix} 3.000 \\ -1.000 \\ 1.000 \end{bmatrix} $$

Therefore, the motion screws of the joints with respect to the global coordinate system OXYZ system can be expressed as

$$\underline{\$}_{11} = (0, 0, 1; \quad -1, \quad 0, 0)$$
$$\underline{\$}_{21} = (0, 0, 0; \quad 0, \quad 0, 1)$$
$$\underline{\$}_{31} = (0, 1, 0; \quad -1, \quad 0, 3)$$
$$\underline{\$}_{41} = (1, 0, 0; \quad 0, \quad 2.732, 0)$$
$$\underline{\$}_{51} = (0, 1, 0; -2.732, \quad 0, 4)$$
$$\underline{\$}_{61} = (0, 0, 1; \quad 0, \quad -4, 0)$$

In order to find ${}^{r}\underline{\$}_{11}$, which is reciprocal to all other screws in first subchain but $\underline{\$}_{11}$, the following equations must be satisfied:

$$L_{21}P_{r1} + M_{21}Q_{r1} + N_{21}R_{r1} + L_{r1}P_{21} + M_{r1}Q_{21} + N_{r1}R_{21} = 0 \quad (5.17)$$

$$L_{31}P_{r1} + M_{31}Q_{r1} + N_{31}R_{r1} + L_{r1}P_{31} + M_{r1}Q_{31} + N_{r1}R_{31} = 0 \quad (5.18)$$

$$L_{41}P_{r1} + M_{41}Q_{r1} + N_{41}R_{r1} + L_{r1}P_{41} + M_{r1}Q_{41} + N_{r1}R_{41} = 0 \quad (5.19)$$

$$L_{51}P_{r1} + M_{51}Q_{r1} + N_{51}R_{r1} + L_{r1}P_{51} + M_{r1}Q_{51} + N_{r1}R_{51} = 0 \quad (5.20)$$

$$L_{61}P_{r1} + M_{61}Q_{r1} + N_{61}R_{r1} + L_{r1}P_{61} + M_{r1}Q_{61} + N_{r1}R_{61} = 0 \quad (5.21)$$

Therefore, ${}^{r}\underline{\$}_{11}$ is obtained by selecting the ratio $R_{r1}/M_{r1} = 4$ and solving Eqs. (5.17) - (5.21) simultaneously, which yields

$${}^{r}\underline{\$}_{11} = (0, 1, 0; -2.732, 0, 4)$$

Similarly, ${}^{r}\underline{\$}_{21}$ can be obtained by selecting the ratio $R_{r1}/M_{r1} = 4$ and solving the Eqs. (5.18) -(5.22) simultaneously, which yields

$${}^{r}\underline{\$}_{21} = (4, 1, 6.928; -2.732, -16.784, 4)$$

where

$$L_{11}P_{r1} + M_{11}Q_{r1} + N_{11}R_{r1} + L_{r1}P_{11} + M_{r1}Q_{11} + N_{r1}R_{11} = 0 \quad (5.22)$$

Similarly, the reciprocal screws ${}^{r}\underline{\$}_{1i}$ and ${}^{r}\underline{\$}_{2i}$, reciprocal to all other screws in subchain i (i = 2 and 3) but $\underline{\$}_{1i}$ and $\underline{\$}_{2i}$, respectively, can be found as the positions and orientations of joint C_i are given and therefore are not listed here.

It is noted that a force dose not affect the rotation around a revolute joint when its line of action is parallel to or along the axis of revolute joint. This is also the reciprocity condition.

5.5 Jacobian Matrix

Let ${}^{\omega}\underline{\$}$ represent the motion screw of the platform with respect to the global system OXYZ, which can be expressed as

$$ {}^{\omega}\underline{\$} = \sum_{j=1}^{6} \sum_{i=1}^{3} \omega_{ji}\underline{\$}_{ji} \tag{5.23} $$

Taking reciprocal products with reciprocal screws ${}^{r}\underline{\$}_{1i}$ and ${}^{r}\underline{\$}_{2i}$ of Eq. (5.23) respectively yields

$$ {}^{\omega}\underline{\$} \circ {}^{r}\underline{\$}_{1i} = \omega_{1i}\underline{\$}_{1i} \circ {}^{r}\underline{\$}_{1i} \tag{5.24} $$

and

$$ {}^{\omega}\underline{\$} \circ {}^{r}\underline{\$}_{2i} = \omega_{2i}\underline{\$}_{2i} \circ {}^{r}\underline{\$}_{2i} \tag{5.25} $$

where the symbol $\circ$ denotes the reciprocal product of a pair of screws and i = 1, 2 and 3. Thus, we can obtain the following equation:

$$\begin{bmatrix} {}^{r}\underline{\$}_{11}{}^{T} \\ {}^{r}\underline{\$}_{21}{}^{T} \\ {}^{r}\underline{\$}_{12}{}^{T} \\ {}^{r}\underline{\$}_{22}{}^{T} \\ {}^{r}\underline{\$}_{13}{}^{T} \\ {}^{r}\underline{\$}_{23}{}^{T} \end{bmatrix} \omega[\underline{\$}] = \begin{bmatrix} \underline{\$}_{11}\circ{}^{r}\underline{\$}_{11} & 0 & 0 & 0 & 0 & 0 \\ 0 & \underline{\$}_{21}\circ{}^{r}\underline{\$}_{21} & 0 & 0 & 0 & 0 \\ 0 & 0 & \underline{\$}_{12}\circ{}^{r}\underline{\$}_{12} & 0 & 0 & 0 \\ 0 & 0 & 0 & \underline{\$}_{22}\circ{}^{r}\underline{\$}_{22} & 0 & 0 \\ 0 & 0 & 0 & 0 & \underline{\$}_{13}\circ{}^{r}\underline{\$}_{13} & 0 \\ 0 & 0 & 0 & 0 & 0 & \underline{\$}_{23}\circ{}^{r}\underline{\$}_{23} \end{bmatrix} \begin{bmatrix} \omega_{11} \\ \omega_{21} \\ \omega_{12} \\ \omega_{22} \\ \omega_{13} \\ \omega_{23} \end{bmatrix} \tag{5.26}$$

or

$$[A]\omega[\underline{\$}] = [B][\omega_a] \tag{5.27}$$

where the components of $[\omega_a] = (\omega_{11}, \omega_{21}, \omega_{12}, \omega_{22}, \omega_{13}, \omega_{23})^T$ are the intensities of the motion screws of the actuators, and for the linear actuators of the A_i joints, $\omega_{21} = v_{21}$, $\omega_{22} = v_{22}$ and $\omega_{23} = v_{23}$.

If [A] is nonsingular, we can write

$$\omega[\underline{\$}] = [A]^{-1}[B][\omega_a] = [J][\omega_a] \tag{5.28}$$

where $[J] = [A]^{-1}[B]$ may be called a Jacobian matrix.

5.6 Mechanical Error Analysis of the Platform

The term of mechanical error defined here means the minor movements of the platform due to the inaccuracies in displacements (rotation and translation) of the actuators for a certain specified position and orientation of the platform. Let the errors of the displacements of the actuators, $[\delta\Theta_a]$, be expressed as

$$[\delta\Theta_a] = [\omega_a]\delta t, \tag{5.29}$$

where δt denotes a very short period of time.

Then we have

$$\omega\delta t[\underline{\$}] = [J][\omega_a]\delta t \tag{5.30}$$

or

$$\delta\Theta[\underline{\$}] = [J][\delta\Theta_a] \tag{5.31}$$

where $\delta\Theta$ denotes the minor angular displacement of the platform about its axis due to the error input, $\delta\Theta_a$, of the actuators.

The movement of the platform is generally specified by the linear displacement of the center, H, and the angular displacements of the hand coordinate system embedded in the platform about the axes of the global coordinate system OXYZ. In order to calculate the components of the minor movements of the platform, the motion screws of the platform may be expressed as

$$\omega\underline{\$} = \omega[\underline{S} + \underline{S}_o] = \omega[\underline{S} + \varepsilon(\underline{r} \times \underline{S} + h\underline{S})] \tag{5.32}$$

where $\underline{r}$ is the global position vector of an arbitrary point on the axis of the motion screw of the platform, ε denotes the dual part of a vector and h is the pitch; this screw is shown in Fig. 5.6.

Now, we have

$$h = \underline{S} \cdot \underline{S}_o \tag{5.33}$$

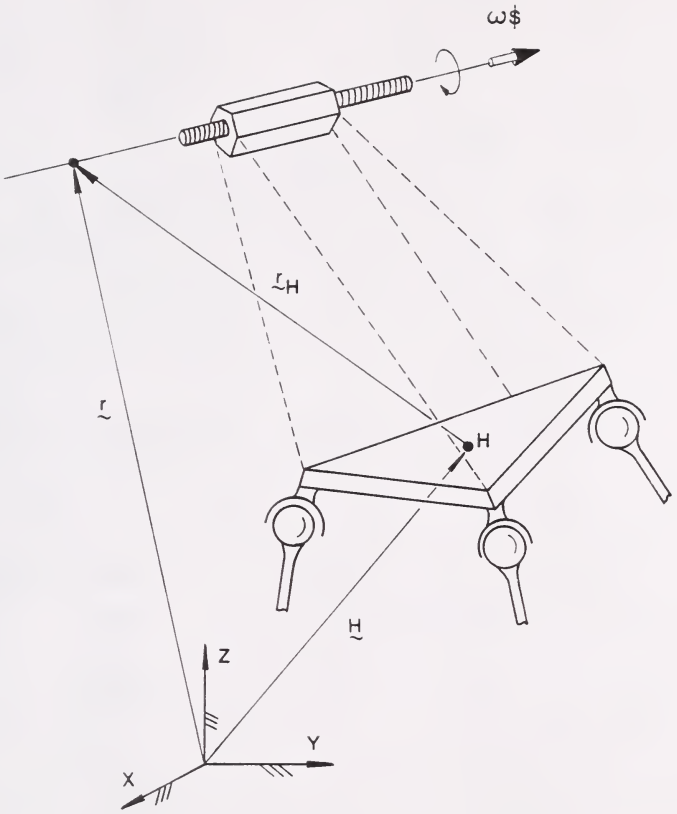

Figure 5.6 Screw representing the motion of the platform with respect to the global system OXYZ

and

$$\underline{r} \times \underline{S} = \underline{S}_O - h\underline{S} \tag{5.34}$$

Since $\underline{r} = \underline{H} + \underline{r}_H$, we can have the following equations:

$$(\underline{H} + \underline{r}_H) \times \underline{S} = \underline{S}_O - h\underline{S} \tag{5.35}$$

or

$$\underline{r}_H \times \underline{S} + h\underline{S} = \underline{S}_O - \underline{H} \times \underline{S} \tag{5.36}$$

The velocity of the center H of the platform can be obtained as

$$\underline{v}_H = \omega(\underline{r}_H \times \underline{S} + h\underline{S}) \tag{5.37}$$

or

$$\underline{v}_H = \omega(\underline{S}_O - \underline{H} \times \underline{S}) \tag{5.38}$$

Then the linear displacement of H can be obtained as

$$\delta\underline{d}_H = \delta\Theta(\underline{S}_O - \underline{H} \times \underline{S}) \tag{5.39}$$

As we consider differential motions, let us define the rotation matrix of a small rotation angle $\delta\Theta$ about unit vector $\underline{S}$. For small angles, $\sin\delta\Theta \approx \delta\Theta$, $\cos\delta\Theta \approx 1$ and $V\delta\Theta = \cos\delta\Theta - 1 \approx 0$. Thus, we can have the rotation matrix with small $\delta\Theta$ as

$$R[\delta\Theta, \underline{S}] = \begin{bmatrix} S_x{}^2V\delta\Theta+C\delta\Theta & S_xS_yV\delta\Theta-S_zS\delta\Theta & S_xS_zV\delta\Theta+S_yS\delta\Theta & 0 \\ S_xS_yV\delta\Theta+S_zS\delta\Theta & S_y{}^2V\delta\Theta+C\delta\Theta & S_yS_zV\delta\Theta-S_xS\delta\Theta & 0 \\ S_xS_zV\delta\Theta-S_yS\delta\Theta & S_yS_zV\delta\Theta+S_xS\delta\Theta & S_z{}^2V\delta\Theta+C\delta\Theta & 0 \\ 0 & 0 & 0 & 1 \end{bmatrix}$$

(continued)

$$= \begin{bmatrix} 1 & -S_z\delta\Theta & S_y\delta\Theta & 0 \\ S_z\delta\Theta & 1 & -S_x\delta\Theta & 0 \\ -S_y\delta\Theta & S_x\delta\Theta & 1 & 0 \\ 0 & 0 & 0 & 1 \end{bmatrix} \tag{5.40}$$

Dividing the small rotation angles, $\delta\Theta$, about $\underline{S}$ into three components $\delta\Theta_X$, $\delta\Theta_Y$ and $\delta\Theta_Z$ about the axes of the global system OXYZ, the rotation matrix can be expressed as

$$\text{Rot}(\delta\Theta_X, X)\ \text{Rot}(\delta\Theta_Y, Y)\ \text{Rot}(\delta\Theta_Z, Z)$$

$$= \begin{bmatrix} 1 & 0 & 0 & 0 \\ 0 & 1 & -\delta\Theta_X & 0 \\ 0 & \delta\Theta_X & 1 & 0 \\ 0 & 0 & 0 & 1 \end{bmatrix} \begin{bmatrix} 1 & 0 & \delta\Theta_Y & 0 \\ 0 & 1 & 0 & 0 \\ -\delta\Theta_Y & 0 & 1 & 0 \\ 0 & 0 & 0 & 1 \end{bmatrix} \begin{bmatrix} 1 & -\delta\Theta_Z & 0 & 0 \\ \delta\Theta_Z & 1 & 0 & 0 \\ 0 & 0 & 1 & 0 \\ 0 & 0 & 0 & 1 \end{bmatrix}$$

$$= \begin{bmatrix} 1 & -\delta\Theta_Z & \delta\Theta y & 0 \\ \delta\Theta z & 1 & -\delta\Theta x & 0 \\ -\delta\Theta_Y & \delta\Theta_X & 1 & 0 \\ 0 & 0 & 0 & 1 \end{bmatrix} \tag{5.41}$$

where $\delta\Theta_X$, $\delta\Theta_Y$ and $\delta\Theta_Z$ are all small angles. We therefore simplify by neglecting the second and third order terms. Comparing Eqs. (5.40) and (5.41), we obtain

$$\begin{aligned} \delta\Theta_X &= S_x\delta\Theta \\ \delta\Theta_Y &= S_y\delta\Theta \\ \delta\Theta_Z &= S_z\delta\Theta \end{aligned} \tag{5.42}$$

It is noted that a differential rotation $\delta\Theta$ about an arbitrary unit vector $\underline{S}$ is equivalent to three differential rotations, $\delta\Theta_X$, $\delta\Theta_Y$ and $\delta\Theta_Z$, about the X, Y and Z axes. Finally, the error movement of the platform may be expressed as a vector as follow:

$$\begin{bmatrix} \delta\Theta\underline{S} \\ \delta\underline{d}_H \end{bmatrix} = \begin{bmatrix} \underline{S} \\ \underline{S}_O - \underline{H} \times \underline{S} \end{bmatrix} \delta\Theta \tag{5.43}$$

The range of uncertainty of the position of any point in the end-effector body, say, the point H, is shown in Fig. 5.7. Such uncertainty in space can be approximated by a small parallelepiped, whose three edges are δh, $\rho\delta\Theta$ and $\delta\rho$. Here, δh is the axial position error, ρ is the distance of point H from the error screw axis $\underline{\$}$, $\delta\Theta$ is the angular error range and $\delta\rho$ is due to the uncertainty of position of the screw axis.

5.7 Summary

The mechanical error analysis of a six degree-of-freedom parallel manipulator has been studied in this chapter. Matrix transformations, widely used in spatial mechanisms, are applied. The screw theory, as applied to determine the instantaneous kinematics of fully parallel manipulators, is utilized. Numerical example is presented to show how to determine the reciprocal screws in each subchain. Velocities and small displacements of the joints

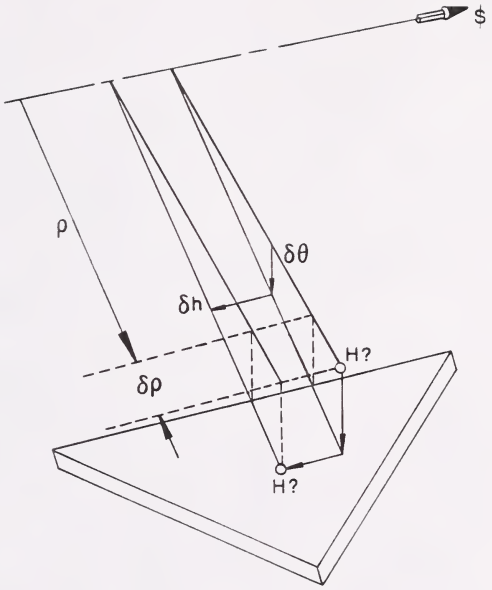

Figure 5.7 Range of uncertainty of the position of point H on the end-effector

as well as the region of uncertainty of hand position due to actuator errors are described.

The interferences between links, which affect the working space and are related to the mechanical error of the hand, are not considered in this chapter. The effect of clearances in the joints and tolerances on link lengths and the resulting uncertainty of the hand position in parallel manipulators are not considered in this chapter either. These are some of the subjects recommended for further study.

CHAPTER 6
CONCLUSIONS AND RECOMMENDATIONS FOR FURTHER RESEARCH

6.1 Conclusions

An industrial robot is defined by the U.S. Robot Industries Association (RIA) as a "reprogrammable, multifunctional manipulator designed to move material, parts, tools, or specialized devices through variable programmed motions for the performance of a variety of tasks". In the early development of industrial robots, they operated in a fixed sequence and could repeat a sequence of operations once they have been programmed. Later, the robots were equipped with sensory devices that allowed them to act in a not-completely defined environment. Now some industrial robots have the intelligence to allow them to make decisions.

It has been well recognized that, by using multi-degree-of-freedom robot manipulators with multiple actuators and automatic control systems, we can achieve the goal of improving efficiency, accuracy, reliability and reducing energy consumptions and cost of production in a flexible manufacturing system.

Robot applications are continuously widening, their functions are becoming more and more complicated and the optimal designs are not yet established. Therefore, some

basic parameters of robots should be considered before the applications to robotics, and they are listed as follows:

1. Mobility (degrees of freedom)
2. Workspace (volume, shape and degrees of redundancy)
3. Agility (effective speeds of execution of prescribed motions)
4. Positioning (accuracy and repeatability)
5. Dynamics behavior (structural stiffness, masses, payload, damping coefficients and natural frequencies)
6. Economics (cost, reliability, maintainability, etc.)

In recent years, there has been considerable increase in research in the area of robotics and multi-degree-of-freedom programmable automation devices. Almost all the industrial robots in use now are open-loop serial-link manipulators with up to six degrees of freedom. Research in the field of parallel manipulators is still in the infancy of development. Therefore, the aim of this study is to investigate and develop the theoretical background in the kinematics of parallel robots. One of these kinds of manipulators has been shown in Fig. 3.1.

The special feature of the proposed parallel manipulator is that the novel geometry of a two-degree-of-freedom self-actuated joint which combines a rotary actuator

and a linear actuator, is introduced. It imparts cylindric, two-degree-of-freedom, combined rotational and translational relative motion to the link with respect to ground. The distinct advantage of using this kind of actuator, called R-L (Rotary-Linear) actuator, is that the inertias of the rotary and linear actuators are independent of each other. In other words, the inertia of the rotary actuator is not seen by the linear actuator and vice versa. Furthermore, in case of parallel manipulators, all such R-L actuators can be ground-mounted. Thus, the linkage itself can be made lighter, and better dynamic performance can be achieved. It is noted that one of the attractive utilizations of the R-L actuator is that they can also be used in the military. Since the actuators and their microprocessors are the most sensitive parts of manipulators, they can be shielded from external hazards as shown in Fig. 6.1. Therefore, only the bare moving links with unpowered passive joints are exposed and they can be quickly and easily replaced once they suffer environmental or battle damage. Another attractive utilization, as shown in Fig. 6.2, is that the manipulator can be in an overhead, upside-down position for high-precision micro-manipulation.

The use of ground-mounted R-L actuators in conjunction with a parallel manipulator configuration promises to provide some unique features which can be expected as follows:

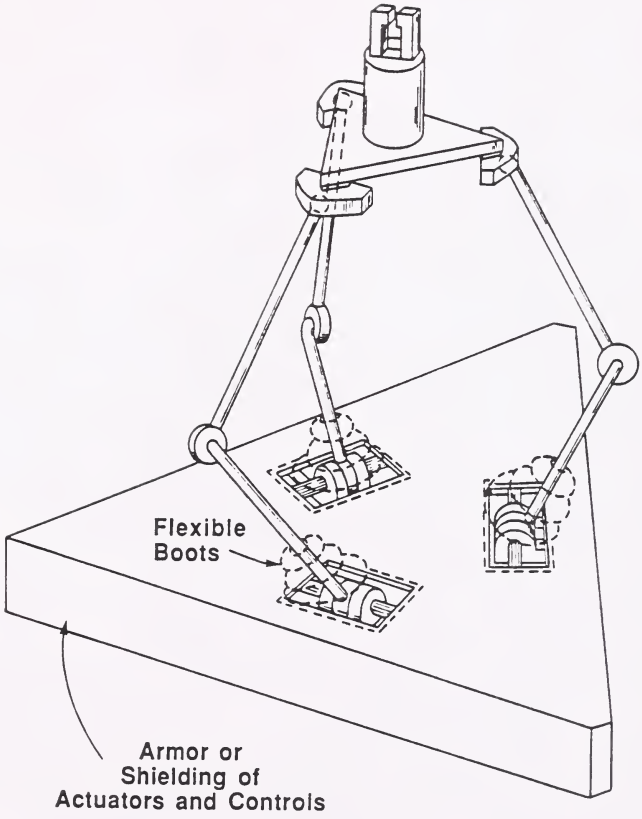

Figure 6.1 Shielded R-L actuators

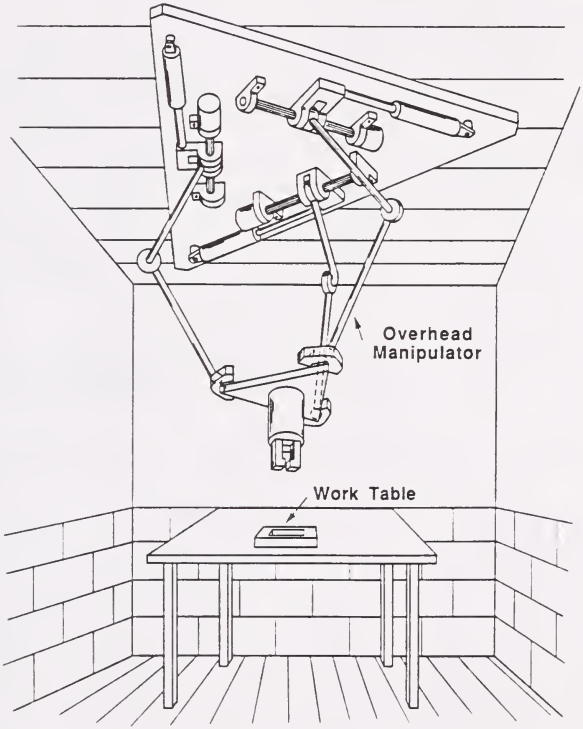

Figure 6.2 Overhead Micro-manipulator

1. increased payload capacities with ground-mounted actuators
2. increased positioning accuracy supported by the parallel subchains (legs)
3. increased speed with lighter construction
4. better dynamic performance
5. greater economy in energy consumption and reduced first cost
6. reduced computation time with parallel processing
7. restricted workspace
8. increased link interference

where items 1 to 6 are advantages, 7 and 8 are disadvantages.

In this research, the type synthesis and inverse kinematics of some possible subchains with six degrees of freedom are covered. Workspace analysis of the parallel, platform-type manipulator is presented, by determining the shapes of the subworkspace and the boundaries of the subworkspace. The root regions in the subworkspace is also investigated. The workspace of the manipulator is then the common reachable region of the three subworkspaces determined by the corresponding subchain. In order to study the positioning error of the hand (or end effector) of the manipulator, the theory of screws is applied to determine the instantaneous kinematics of the manipulator. The hand position errors due to linear and angular inaccuracies in the motions of the actuated joints are prescribed.

6.2 Recommendations for Further Research

One of the major difficulties in parallel manipulators is the problem of link interference. Once the link interference problem can be solved, the generalized workspace can be found meaningfully.

It is recommended to simulate the motions of parallel manipulators by computer graphics, since it will facilitate understanding the geometry of the manipulators.

This study is concerned only with a kinematic viewpoint. For the practical application of these types of manipulators, studies of statics and dynamics should follow.

It is hoped that the results of this work will contribute towards a basic understanding of the limitations as well as the potential usefulness of parallel, platform-type manipulators with ground-mounted actuators.

APPENDIX A
ALTERNATIVE METHOD OF FINDING THE COORDINATES OF JOINT C

A.1 Subchain (R-L)-R-S

By using the notations as shown in Fig. A.1 and the method presented in [44], we can obtain the coordinates of joint C with respect to the local coordinate system as

$$\underline{R} = S_1\underline{S}_1 + a_{12}\underline{a}_{12} + S_{22}\underline{S}_2 + a_{23}\underline{a}_{23} \tag{A.1}$$

where S_1 is the translation along the $\underline{S}_1$ axis, S_{22} is the offset along the $\underline{S}_2$ axis, and a_{12} and a_{23} are the perpendicular distances between successive joint axes.

We can rewrite Eq. (A.1) by using the Table A.1 (set 1 of direction cosines - spatial heptagon) as follows:

$$\underline{R} = \begin{bmatrix} c_1 & -s_1 & 0 \\ s_1 & c_1 & 0 \\ 0 & 0 & 1 \end{bmatrix} \left\{ S_1 \begin{bmatrix} 0 \\ 0 \\ 1 \end{bmatrix} + a_{12} \begin{bmatrix} 1 \\ 0 \\ 0 \end{bmatrix} + S_{22} \begin{bmatrix} 0 \\ -s_{12} \\ c_{12} \end{bmatrix} + a_{23} \begin{bmatrix} c_2 \\ U_{21}^{*} \\ U_{21} \end{bmatrix} \right\} \tag{A.2}$$

where $U_{21}^{*} = s_2c_{12}$ and $U_{21} = s_2s_{12}$.

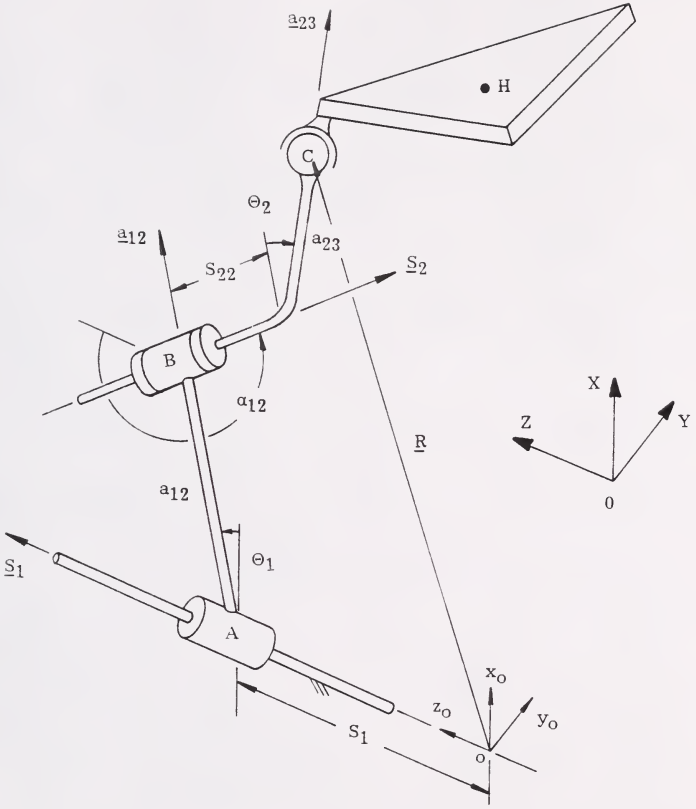

Figure A.1 Subchain (R-L)-R-S

Table A.1 Direction cosines - spatial heptagon (set 1)

$\underline{S}_1(0, 0, 1)$	$\underline{a}_{12}(1, 0, 0)$
$\underline{S}_2(0, -s_{12}, c_{12})$	$\underline{a}_{23}(c_2, U^*_{21}, U_{21})$
$\underline{S}_3(\bar{X}_2, \bar{Y}_2, \bar{Z}_2)$	$\underline{a}_{34}(W_{32}, -U^*_{321}, U_{321})$
$\underline{S}_4(X_{32}, Y_{32}, Z_{32})$	$\underline{a}_{45}(W_{432}, -U^*_{4321}, U_{4321})$
$\underline{S}_5(X_{432}, Y_{432}, Z_{432})$	$\underline{a}_{56}(W_{5432}, -U^*_{54321}, U_{54321})$
$\underline{S}_6(X_{5432}, Y_{5432}, Z_{5432})$	$\underline{a}_{67}(W_{65432}, -U^*_{654321}, U_{654321})$
$\underline{S}_7(X_{65432}, Y_{65432}, Z_{65432})$	$\underline{a}_{71}(c_1, -s_1, 0)$

Therefore, the coordinates of joint C with respect to the local coordinate system can be expressed as follows:

$$C_x = a_{12}c_1 + S_{22}s_{12}s_1 + a_{23}(c_1c_2 - s_1s_2c_{12}) \qquad (A.3)$$

$$C_y = a_{12}s_1 - S_{22}s_{12}c_1 + a_{23}(s_1c_2 + c_1s_2c_{12}) \qquad (A.4)$$

$$C_z = S_1 + S_{22}c_{12} + a_{23}s_2s_{12} \qquad (A.5)$$

The above expression are the same as those in Eq. (2.5) except for different notation for elements of the subchain.

A.2 Subchain (R-L)-P-S

As shown in Fig. A.2, the coordinates of joint C with respect to the local coordinate system can be obtained similarly as

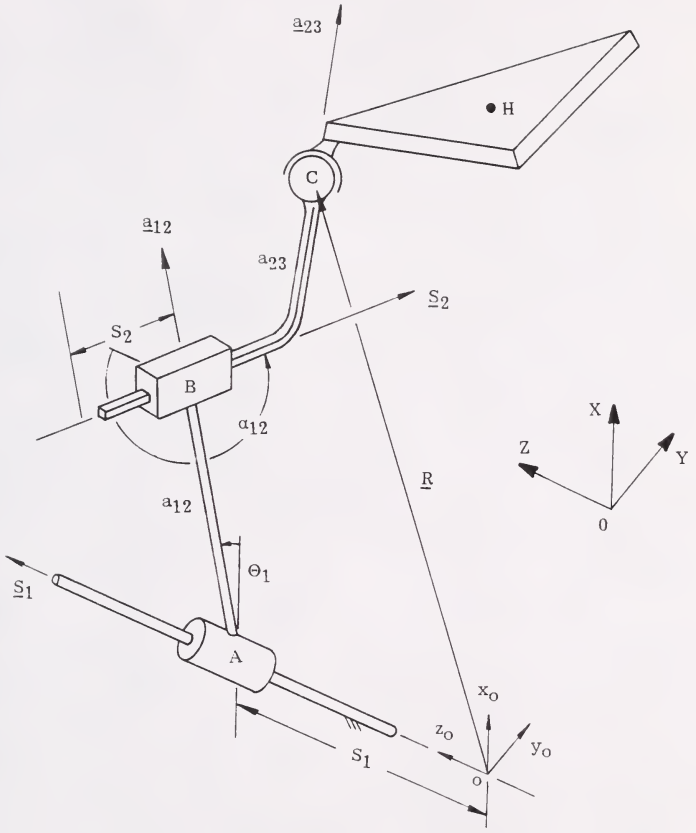

Figure A.2 Subchain (R-L)-P-S

$$\underline{R} = S_1\underline{S}_1 + a_{12}\underline{a}_{12} + S_2\underline{S}_2 + a_{23}\underline{a}_{23} \tag{A.6}$$

where S_1 and S_2 are the translation along the $\underline{S}_1$ and $\underline{S}_2$ axes, respectively, and a_{12} and a_{23} are the perpendicular distances between successive joint axes.

We can rewrite Eq. (A.6) by using the Table A.1 (set 1 of direction cosines - spatial heptagon) as follows:

$$\underline{R} = \begin{bmatrix} c_1 & -s_1 & 0 \\ s_1 & c_1 & 0 \\ 0 & 0 & 1 \end{bmatrix} \{ S_1 \begin{bmatrix} 0 \\ 0 \\ 1 \end{bmatrix} + a_{12} \begin{bmatrix} 1 \\ 0 \\ 0 \end{bmatrix} + S_2 \begin{bmatrix} 0 \\ -s_{12} \\ c_{12} \end{bmatrix} + a_{23} \begin{bmatrix} c_2 \\ U^*_{21} \\ U_{21} \end{bmatrix} \} \tag{A.7}$$

where $U^*_{21} = s_2c_{12}$ and $U_{21} = s_2s_{12}$.

Therefore, the coordinates of joint C with respect to the local coordinate system can be expressed as follows:

$$C_x = a_{12}c_1 + S_2s_{12}s_1 + a_{23}c_1 \tag{A.8}$$

$$C_y = a_{12}s_1 - S_2s_{12}c_1 + a_{23}s_1 \tag{A.9}$$

$$C_z = S_1 + S_2c_{12} \tag{A.10}$$

The above expression are the same as those in Eq. (2.13) except for different notations for the elements of the subchain.

APPENDIX B
EQUATION OF A GENERAL FORM OF TORUS

If the translation d_a along the z axis of the local fixed coordinate system is disregarded in Eq. (2.5), (see Fig. 2.11), we can obtain the following equations:

$$C_x = C\Theta_a(bC\Theta_b + a) - S\Theta_a(bS\Theta_bC\alpha_b - s_bS\alpha_b) \quad (B.1)$$

$$C_y = S\Theta_a(bC\Theta_b + a) + C\Theta_a(bS\Theta_bC\alpha_b - s_bS\alpha_b) \quad (B.2)$$

$$C_z = bS\Theta_bS\alpha_b + s_bC\alpha_b \quad (B.3)$$

Squaring and adding Eqs. (B.1) - (B.3) yields

$$C_x^2 + C_y^2 + C_z^2 = a^2 + b^2 + s_b^2 + 2abC\Theta_b \quad (B.4)$$

Multiplying Eq. (B.4) by $S\alpha_b$ yields

$$S\alpha_b\{(C_x^2 + C_y^2 + C_z^2) - (a^2 + b^2 + s_b^2)\} = 2abC\Theta_bS\alpha_b \quad (B.5)$$

Multiplying Eq. (B.3) by 2a yields

$$2a(C_z - s_bC\alpha_b) = 2abS\Theta_bS\alpha_b \quad (B.6)$$

Finally, squaring and adding Eqs. (B.5) and (B.6) and then rearranging terms yields the following equation:

$$\{(C_x^2 + C_y^2 + C_z^2) - (a^2 + b^2 + s_b^2)\}^2$$

$$= 4a^2\{b^2 - (\frac{C_z - s_b C\alpha_b}{S\alpha_b})^2\} \qquad (B.7)$$

If we replace C_x, C_y and C_z by x, y and z, respectively, s_b by s and α_b by α, we will get the same equation as shown in Eq. (3.1), which represents the general form of torus [51].

REFERENCES

1. Roth, B., "Performance Evaluation of Manipulators from a Kinematic Viewpoint," NBS Special Publication Performance Evaluation of Programmable Robots and Manipulators 459, 1976, pp. 39-61.

2. Shimano, B. E., and Roth, B., "Ranges of Motion of Manipulators," The 3rd CISM-IFTOMM International Symposium on Theory and Practice of Robots and Manipulators, Warsaw, September 1976, pp. 18-27.

3. Sugimoto, K., and Duffy, J., "Determination of Extreme Distances of a Robot Hand. Part 1: A General Theory," ASME Journal of Mechanical Design, Vol. 103, No. 3, 1981, pp. 631-636.

4. Sugimoto, K., and Duffy, J., "Determination of Extreme Distances of a Robot Hand. Part 2: Robot Arms With Special Geometry," ASME Journal of Mechanical Design, Vol. 103, No. 4, 1981, pp. 776-783.

5. Kumar, A., and Waldron, K. J., "The Dexterous Workspace," ASME paper 80-DET-108, 1980.

6. Sugimoto, K., and Duffy, J., "Special Configuration of Industrial Robots," Proceedings of 11th International Symposium on Industrial Robots, 1981.

7. Sugimoto, K., Duffy, J., and Hunt, K. H., "Special Configurations of Spatial Mechanisms and Robot Arms," Journal of Mechanisms and Machine Theory, Vol. 16, No. 2, 1981, pp. 119-132.

8. Kumar, A., and Waldron, K. J., "The Workspace of A Mechanical Manipulator," ASME Journal of Mechanical Design, Vol. 103, No. 3, 1981, pp. 665-672.

9. Tsai, Y. C., and Soni, A. H., "Accessible Region and Synthesis of Robot Arms," ASME Journal of Mechanical Design, Vol. 103, No. 4, 1981, pp. 803-811.

10. Gupta, K. C., and Roth, B., "Design Considerations for Manipulator Workspace," ASME Journal of Mechanical Design, Vol. 104, No. 4, 1982, pp. 704-711.

11. Selfridge, R. G., "The Reachable Workarea of a Manipulator," Journal of Mechanism and Machine Theory, Vol. 18, No. 2, 1983, pp. 131-138.

12. Tsai, Y. C., and Soni, A. H., "An Algorithm for the Workspace of a General n-R Robot," ASME Journal of Mechanisms, Transmissions, and Automation in Design, Vol. 105, No. 1, 1983, pp. 52-57.

13. Yang, D. C. H., and Lee, T. W., "On the Workspace of Mechanical Manipulators," ASME Journal of Mechanisms, Transmissions, and Automation in Design, Vol. 105, No. 1, 1983, pp. 62-69.

14. Lee, T. W., and Yang, D. C. H., "On the Evaluation of Manipulator Workspace," ASME Journal of Mechanisms, Transmissions, and Automation in Design, Vol. 105, No. 1, 1983, pp. 70-77.

15. Hansen, J. A., Gupta, K. C., and Kazerounian, S. M. K., "Generation and Evaluation of the Workspace of a Manipulator," The International Journal of Robotics Research, Vol. 2, No. 3, 1983, pp. 22-31.

16. Freudenstein, F., and Primrose, E. J. F., "On the Analysis and Synthesis of the Workspace of a Three-Link, Turning-Pair Connected Robot Arm," ASME Journal of Mechanisms, Transmissions, and Automation in Design, Vol. 106, No. 3, 1984, pp. 365-370.

17. Kohli, D., and Spanos, J., "Workspace Analysis of Mechanical Manipulators Using Polynomial Discriminants," ASME Journal of Mechanisms, Transmissions, and Automation in Design, Vol. 107, No. 2, 1985, pp. 209-215.

18. Spanos, J., and Kohli, D., "Workspace Analysis of Regional Structures," ASME Journal of Mechanisms, Transmissions, and Automation in Design, Vol. 107, No. 2, 1985, pp. 216-222.

19. Cwiakala, M., and Lee, T.W., "Generation and Evaluation of a Manipulator Workspace Based on Optimum Path Search," ASME Journal of Mechanisms, Transmissions, and Automation in Design, Vol. 107, No. 2, 1985, pp. 245-255.

20. Tsai, Y.C., and Soni, A.H., "Workspace Synthesis of 3R, 4R, 5R and 6R Robots," Journal of Mechanism and Machine Theory, Vol. 20, No. 6, 1985, pp. 555-563.

21. Tsai, Y.C., and Soni, A.H., "The Effect of Link-Parameters on the Workspace of General 3R Robot Arms," Journal of Mechanism and Machine Theory, Vol. 19, No. 1, pp. 9-16.

22. Oblak, D., and Kohli, D., "Boundary Surfaces, Limit Surfaces, Crossable and Noncrossable Surfaces in Workspace of Mechanical Manipulators," ASME paper 86-DET-80.

23. Davidson, J. K., and Hunt, K. H., "Rigid Body Location and Robot Workspace: Some Alternative Manipulator Forms," ASME paper 86-DET-128.

24. Davidson, J. K., and Hunt, K. H., "Robot Workspace of a Tool Plane: Part 1 - A Ruled Surface and Other Geometry," ASME paper 86-DET-126.

25. Davidson, J. K., and Pingail, P., "Robot Workspace of a Tool Plane: Part 2 - Computer Generation and Selected Design Conditions for Dexterity," ASME paper 86-DET-132.

26. Chen, N. X., "Workspace Analysis of Robot Arms Using Differential Geometry. Part 1: A General Theory," ASME paper 86-DET-164.

27. Chen, N. X., "Workspace Analysis of Robot Arms Using Differential Geometry. Part 2: Workspace Analysis of 3R, 4R, 5R and 6R Robot Arms," ASME paper 86-DET-165.

28. Kohli, D., and Hsu, M. S., "The Jacobian Analysis of Workspace of Mechanical Manipulators," accepted for publication in Journal of Mechanism and Machine Theory, 1986.

29. Hsu, M. S., and Kohli, D., "Boundary Surfaces and Accessibility Regions for Regional Structures of Manipulators," accepted for publication in Journal of Mechanism and Machine Theory, 1986.

30. Palmquist, R. D., "Motion Capabilities of Tandem Planar Robots with Computer Graphics Simulation," Master's Thesis, University of Florida, Gainesville, Florida, 1985.

31. Stewart, D., "A Platform with Six Degrees of Freedom," Proceedings of the Institute of Mechanical Engineers, Vol. 180, Part 1, No. 15, 1965-66, pp. 371-386.

32. Asada, H., and Ro, I. H., "A Linkage Design for Direct-Drive Robot Arms," ASME Journal of Mechanisms, Transmissions, and Automation in Design, Vol. 107, 1984, pp. 536-540.

33. Trevelyan, J. P., Kovesi, P. D., and Ong, M. C. H., "Motion Control for a Sheep Shearing Robot," Robotics Research, 1st International Symposium, 1984, pp. 175-190.

34. Bajpai, A., and Roth, B., "Workspace and Mobility of Links of a Closed-loop Manipulator," International Journal of Robotics Research, Vol. 5, No. 2, 1986, pp. 131-142.

35. Yang, D. C. H., and Lee, T. W., "Feasibility Study of A Platform Type of Robotic Manipulators from a Kinematic Viewpoint," ASME Journal of Mechanisms, Transmissions, and Automation in Design, Vol. 106, No. 2, 1984, pp. 191-198.

36. Fichter, E. F., "A Stewart Platform-Based Manipulator: General Theory and Practical Construction," International Journal of Robotics Research, Vol. 5, No. 2, 1986, pp. 157-182.

37. Cwiakala, M., "Workspace of a Closed-Loop Manipulator," ASME paper 86-DET-95.

38. Kohli, D., Lee, S-H., Tsai, K-Y., and Sandor, G. N., "Manipulator Configuration Based on Rotary-Linear (R-L) Actuators and Their Direct and Inverse Kinematics," ASME paper 86-DET-81.

39. Hartenberg, R.S., and Denavit, J., Kinematic Synthesis of Linkages, McGraw-Hill, New York, 1964.

40. Garrett, R.E., and Hall, A.S., "Effects of Tolerance and Clearance in Linkage Design," Trans. ASME, Journal of Engineering for Industry, Vol. 91, 1969, pp. 198-202.

41. Dhande, S.G., and Chakraborty, J., "Analysis and Synthesis of Mechanical Error in Linkages--A Stochastic Approach," Trans ASME, Journal of Engineering for Industry, Vol. 95, 1973, pp. 677-680.

42. Chakraborty, J., "Synthesis of Mechanical Error in Linkages," Journal of Mechanism and Machine Theory, Vol. 10, 1975, pp. 155-165.

43. Dhande, S.G., and Chakraborty, J., "Mechanical Error Analysis of Spatial Linkages," ASME Paper, 77-WA/DE-8, 1977.

44. Duffy, J., Analysis of Mechanisms and Robot Manipulators, Halsted Press, New York, 1980.

45. Hunt, K. H., "Structural Kinematics of In-Parallel-Actuated Robot-Arms," ASME paper 82-DET-105.

46. Mohamed, M. G., and Duffy, J., "A Direct Determination of the Instantaneous Kinematics of Fully Parallel Robot Manipulators," ASME Journal of Mechanisms, Transmissions, and Automation in Design, Vol. 107, No. 2, 1985, pp. 226-229.

47. Sugimoto, K., "Kinematic and Dynamic Analysis of Parallel Manipulators by Means of Motor Algebra," ASME Journal of Mechanisms, Transmissions, and Automation in Design, Vol. 109, No. 1, 1987, pp. 3-7.

48. Cox, D. J., "The Dynamic Modeling and Command Signal Formulation for Parallel Multi-Parameter Robotic Devices," Master's Thesis, University of Florida, Gainesville, Florida, 1981.

49. Hunt, K. H., Kinematic Geometry of Mechanisms, Oxford University Press, London, England, 1978.

50. Freudenstein, F., and Maki, E. R., "The Creation of Mechanisms According to Kinematic Structure and Function," Environment and Planning, B, Vol. 6, 1979, pp. 375-391.

51. Fichter, E. F., and Hunt, K. H., "The Fecund Torus, its Bitangent-Circles and Derived Linkages," Mechanism and Machine Theory, Vol. 10, 1975, pp. 176-176.

52. Torfason, L. E., and Crossley, F. R. E., "Use of the Intersection of Surfaces as a Method for the Design of Spatial Mechanisms," Proceeding of the Third World Congress for the Theory of Machines and Mechanisms, Kupari, Yugoslavia, September 13-20, Vol. B, Paper B-20, 1971, pp. 247-258.

53. Jenkins, E. M., Jr., Crossley, F. R. E., and Hunt, K. H., "Cross Motion Attributes of Certain Spatial Mechanisms," ASME Journal of Engineering for Industry, Trans. Series B, Vol. 91, No. 1, 1969, pp. 83-90.

54. Ball, R. S., A Treaties on the Theory of Screws, Cambridge University Press, Cambridge, 1900.

BIOGRAPHICAL SKETCH

Tzu-Chen Weng was born on September 29, 1956, in Taipei, Taiwan, Republic of China. In 1979, he received a Bachelor of Engineering degree in mechanical engineering from Feng-Chia University in Taiwan. After two years of military service in the Army, he came to the United States and enrolled in graduate school at the University of Florida in Fall 1982. In 1984, he received the degree of Master of Science in mechanical engineering. He is currently pursuing the Doctor of Philosophy in mechanical engineering at the University of Florida.

I certify that I have read this study and that in my opinion it conforms to acceptable standards of scholarly presentation and is fully adequate, in scope and quality, as a dissertation for the degree of Doctor of Philosophy.

George N. Sandor, Chairman
Professor of Mechanical Engineering

I certify that I have read this study and that in my opinion it conforms to acceptable standards of scholarly presentation and is fully adequate, in scope and quality, as a dissertation for the degree of Doctor of Philosophy.

Joseph Duffy
Professor of Mechanical Engineering

I certify that I have read this study and that in my opinion it conforms to acceptable standards of scholarly presentation and is fully adequate, in scope and quality, as a dissertation for the degree of Doctor of Philosophy.

Ali Seireg
Ebaugh Professor of Mechanical Engineering

I certify that I have read this study and that in my opinion it conforms to acceptable standards of scholarly presentation and is fully adequate, in scope and quality, as a dissertation for the degree of Doctor of Philosophy.

Gary K. Matthew
Associate Professor of Mechanical Engineering

I certify that I have read this study and that in my opinion it conforms to acceptable standards of scholarly presentation and is fully adequate, in scope and quality, as a dissertation for the degree of Doctor of Philosophy.

Ralph Selfridge
Professor of Computer and Information Science

This dissertation was submitted to the Graduate Faculty of the College of Engineering and to the Graduate School and was accepted as partial fulfillment of the requirements for the degree of Doctor of Philosophy.

December 1988

Dean, College of Engineering

Dean, Graduate School